Summer 8-15-2015

A Molecular Dynamics Study of the Structure-Dynamics Relationships of Supercooled Liquids and Glasses

Ryan Joseph Soklaski
Washington University in St. Louis

WASHINGTON UNIVERSITY IN ST. LOUIS

Department of Physics

Dissertation Examination Committee:
Li Yang, Chair
Kathy Flores
Erik Henriksen
Kenneth F. Kelton
Cynthia Lo
Zohar Nussinov

A Molecular Dynamics Study of the Structure-Dynamics Relationships of Supercooled Liquids and Glasses

by
Ryan Soklaski

A dissertation presented to the
Graduate School of Arts & Sciences
of Washington University in
partial fulfillment of the
requirements for the degree
of Doctor of Philosophy

August 2015
St. Louis, Missouri

Table of Contents

List of Figures

Acknowledgments

I would first like to acknowledge my advisor Dr. Li Yang, whose path to becoming a tenured professor lined up closely with my own journey through graduate school. During this time I've watched him build a productive, collaborative, and tight-knit group that is already making a strong name for itself in our field. His patience, wisdom, and expert guidance were instrumental to the growth and success that I've enjoyed at Washington University. Above all else, he cared about my well-being and the quality of my future; this has impacted me greatly.

I have had the pleasure of collaborating closely with Dr. Ken Kelton and Dr. Zohar Nussinov for nearly all of my graduate career. My research on supercooled liquids and glasses is inextricably connected to their legacies and is a direct result of their indispensable support. The respect and care with which they received my ideas gave me confidence in my work and allowed me to mature as a physicist. This is a testament to the great character and wisdom of these two men.

Vy Tran is a close friend, climbing partner, coauthor, and an overall brilliant mind. His natural curiosity and drive to learn new skills are truly impressive. Working with him day by day gave me no choice but to reach for such great heights. The growth that I've experienced through our work and conversations together will likely shape the rest of my career.

Lastly, I'd like to acknowledge my other group members of past and present, Shouting Huang, Yufeng, Liang, Ruixiang Fei, and Shiyuan Gao - each of whom is remarkable in his own right. Thank you for your support and friendship.

Ryan Soklaski

Washington University in St. Louis
June 2015

Dedicated to my loving family, whose unending support has affected me immeasurably.

To Kesh, my best friend, who has been there for me through it all.

To Chris Horras, a wonderful teacher who ignited my passion for science during my first day of high school, and fostered it for the following four years.

And to Dr. Leslie Benofy, master educator, who generously showed me so much beauty in mathematics and in the nature of the universe.

ABSTRACT OF THE DISSERTATION

A Molecular Dynamics Study of the Structure-Dynamics Relationships of Supercooled Liquids and Glasses

by

Ryan Soklaski

Doctor of Philosophy in Physics

Condensed Matter and Computational Physics

Washington University in St. Louis, 2015

Professor Li Yang, Chair

Central to the field of condensed matter physics is a decades old outstanding problem in the study of glasses – namely explaining the extreme slowing of dynamics in a liquid as it is supercooled towards the so-called glass transition. Efforts to universally describe the stretched relaxation processes and heterogeneous dynamics that characteristically develop in supercooled liquids remain divided in both their approaches and successes. Towards this end, a consensus on the role that atomic and molecular structures play in the liquid is even more tenuous. However, mounting material science research efforts have culminated to reveal that the vast diversity of metallic glass species and their properties are rooted in an equally-broad set of structural archetypes. Herein lies the motivation of this dissertation: the detailed information available regarding the structure-property relationships of metallic glasses provides a new context in which one can study the evolution of a supercooled liquid by utilizing a structural motif that is known to dominate the glass.

$Cu_{64}Zr_{36}$ is a binary alloy whose good glass-forming ability and simple composition makes it a canonical material to both empirical and numerical studies. Here, we perform classical molecular dynamics simulations and conduct a comprehensive analysis of the dynamical regimes of liquid $Cu_{64}Zr_{36}$, while focusing on the roles played by atomic icosahedral ordering – a structural motif which ultimately percolates the glass' structure. Large data analysis techniques are leveraged to obtain uniquely detailed structural and dynamical information in this context. In doing so, we develop the first account of the origin of icosahedral order in this alloy, revealing deep connections between this incipient structural ordering, frustration-limited domain theory, and recent important empirical findings that are relevant to the nature of metallic liquids at large. Furthermore, important dynamical landmarks such as the breakdown of the Stokes-Einstein relationship, the decoupling of particle diffusivities, and the development of general "glassy" relaxation features are found to coincide with successive manifestation of icosahedral ordering that arise as the liquid is supercooled. Remarkably, we detect critical-like features in the growth of the icosahedron network, with signatures that suggest that a liquid-liquid phase transition may occur in the deeply supercooled regime to precede glass formation. Such a transition is predicted to occur in many supercooled liquids, although explicit evidence of this phenomenon in realistic systems is scarce. Ultimately this work concludes that icosahedral order characterizes all dynamical regimes of $Cu_{64}Zr_{36}$, demonstrating the importance and utility of studying supercooled liquids in the context of locally-preferred structure. More broadly, it serves to confirm and inform recent theoretical and empirical findings that are central to understanding the physics underlying the glass transition.

Chapter 1: Introduction

1.1 An Overview of Supercooling and the Glass Transition

When cooling a liquid at a moderate pressure, one expects that the liquid will freeze and form a solid upon reaching the melting temperature, T_M. The most intuitive example of this, of course, is that of water. At standard atmospheric pressure ($1.01 \times 10^5 Pa$), liquid water can be cooled to $T_M = 273\ K$, where it undergoes a first-order phase transition to form a solid. At T_M, the liquid phase of water possesses a higher free energy than does its solid phase, hence the system will release energy as latent heat in order to occupy the highly ordered, crystalline ground state that we know as ice[*]. It turns out that this freezing process is not guaranteed. Indeed, by cooling water and other liquids rapidly one can obtain a material that persists as a liquid below T_M; this is known as a supercooled liquid. Although supercooled liquids exist in a metastable phase – the crystal does minimize the free energy below T_M, after all – they can persist as ergodic liquids well below T_M[1,2†]. How do supercooled liquids differ from high-temperature liquids? What is the relationship between supercooling and glass formation? Can new phases of matter be accessed from this metastable one? Herein lies a major subfield of condensed matter physics.

[*] Although there are many phases of ice, the single phase that is formed under typical atmospheric conditions consists of crystal possessing a hexagonal symmetry. This phase is known as I_h[64].

[†] The process of avoiding crystallization to obtain a persistent supercooled liquid is neither trivial nor is it guaranteed. A. Cavagna and A. Angell provide important insights regarding the metastability limit in supercooled liquids[7,65].

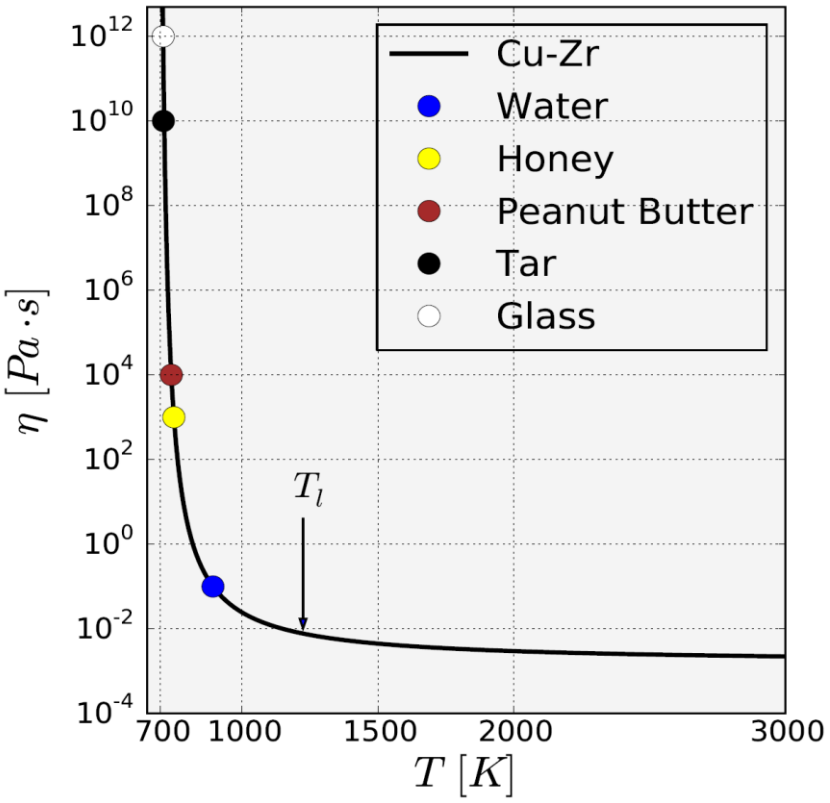

Figure 1.1. A viscosity-temperature curve (VFT-fit) for a binary liquid, $Cu_{64}Zr_{36}$. Approximate viscosity measurements are provided for common materials at room temperature. The liquidus temperature, T_l, is approximately 1230 K[10].

Only a brief discussion of the temperature-dependent behavior of a supercooled liquid is needed to motivate the three afore posed questions. Figure **1.1** depicts the viscosity-temperature curve for a simple binary liquid, $Cu_{64}Zr_{36}$, along with several 'landmark' viscosity values for familiar materials at room temperature[3]. Liquid Cu-Zr experiences a relatively modest growth in viscosity as it is cooled from 3000 K to the liquidus temperature (T_l), which is akin to T_M. Further rapid cooling produces a supercooled liquid, whose viscosity begins to grow rapidly with decreasing temperature. In a narrow range of supercooling, the system goes from being water-like in its ability to flow, to having the consistency of honey, and then to having the consistency of tar. Once the system's viscosity reaches $10^{12} Pa \cdot s$, the material is formally considered to be a glass. The temperature at which this occurs is called the calorimetric glass transition temperature (T_g).

The precise definition of T_g is a purely functional one: the supercooled liquid does not undergo a phase transition here; neither its structure nor its dynamics undergo a drastic change at this temperature[4–7]. This is quite confusing at first glance – if there is no "true" glass transition, then what is a glass anyway[*]? In short, a glass is supercooled liquid that has fallen out of equilibrium (albeit metastable equilibrium) [†]. In a temperature range very close to T_g, the supercooled liquid becomes so viscous that it can no longer ergodically explore phase space in a reasonable amount of time; here, the system's dynamics are so slow that it can no longer flow on a typical laboratory time scale. Let us take a moment to build some intuition for just how sluggish things are at T_g.

The longest running, and perhaps least eventful, experiment in recorded history is an ongoing measurement of the rate of flow of tar[8]. In 1927, Thomas Parnell heated some tar, placed it in a funnel, and let it settle. After allowing the tar to settle for three years, Parnell cut the bottom of the funnel and timed how long it would take for a drop of tar to form and separate from the funnel; the experiment finds that roughly one drop falls every decade. This implies that tar's viscosity is approximately eleven orders of magnitude larger than that of water, and yet is two orders of magnitude smaller than the viscosity of a liquid at T_g (see Figure **1.1**). Thus if the experiment were repeated using a liquid that was supercooled down to T_g, it would take roughly *a millennium* for a drop to form and separate. This is what is meant when one says that a supercooled liquid ceases to flow on a laboratory time scale at T_g. Mind that further cooling beneath T_g will result in continued tremendous growth in the glass' viscosity, so that the

[*] I was told in my middle school science class that a glass is "a solid that flows." That explanation made no sense to me then, and it still makes no sense.

[†] Although the supercooled liquid is, by definition, out of thermodynamic equilibrium, it is ergodic and its dynamical correlation functions obey time translation invariance. This is no longer true below T_g.

millennium needed to form a drop will quickly become millions of years or longer. This immediately dispels the myth that glass flowing over time at room temperature is the mechanism responsible for ancient cathedral windows being thicker at the bottom than at the top[9*]. Indeed, as common experience suggests, glasses well below T_g are truly rigid solids.

1.2 Two-Step Relaxation processes Near T_G

Given the importance of time scales in the classification of glasses, it is natural to ask: are new physical mechanisms at play near T_g? Instead, is a simple physical mechanism responsible for the viscous slowdown beginning at high temperatures, and does this simply lead to a runaway slowdown that inevitably becomes inaccessible by laboratory timescales? Despite the lack of a "fundamental" glass transition temperature, some spectacular physics do appear to be at play in its vicinity[†]. Viewing the temperature dependence of the dynamical correlation functions of a supercooled liquid makes this clear.

[*] Zanotto and Gupta estimate that such a process would require the windows to be far older than they actually are – they would need to be more than a billion times older than the age of the universe.

[†] It has even been suggested that the tremendous viscous slowdown exhibited by supercooled liquids is a signature of a phase transition that resides beneath T_g[6,26]

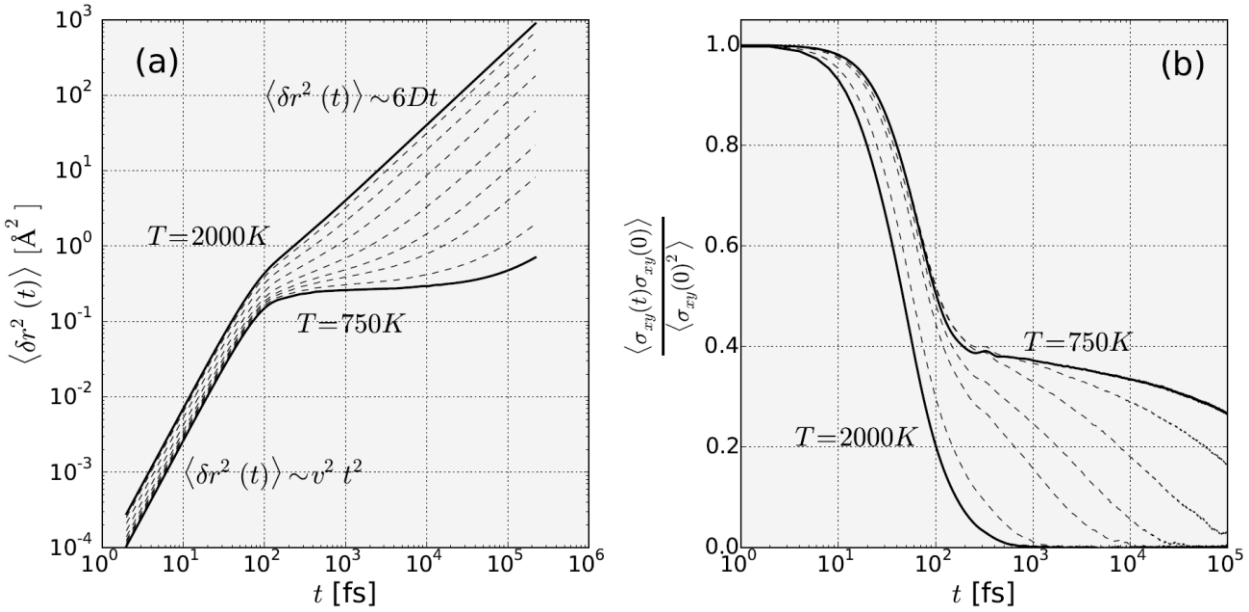

Figure 1.2. Dynamical correlation functions of simulated $Cu_{64}Zr_{36}$ for multiple temperatures. **(a)** The mean-squared displacement trajectory of an ensemble atom in the liquid. **(b)** The time-averaged shear-stress autocorrelation function. Both correlation functions exhibit the development of a distinct plateau feature at low temperatures, which is characteristic of the imminent glass transition.

Figure **1.2** displays dynamical correlation functions for a liquid across a wide range of temperatures. Figure **1.2a** contains, on a log-log scale, the mean-squared displacement (MSD) time trajectory for an average atom in simulated liquid $Cu_{64}Zr_{36}$. For this system, T_l is approximately 1230 K[10] and T_g is near 750 K[11]. At 2000 K, the system is well within its thermodynamic equilibrium liquid phase. Here an atom's MSD trajectory is straightforward: for roughly 100 fs, an atom travels away from its initial position at a constant speed v without experiencing any collisions. Once the atom collides with one of its neighbors, it proceeds to experience uncorrelated collisions in approximately 100 fs intervals, resulting in diffusive motion. Indeed, the long-time asymptote of $\langle \delta r^2(t) \rangle$ is linear in time, which is precisely the behavior one would expect from a particle undergoing a random walk[4]. Upon cooling, one expects a trivial downward shift in $\langle \delta r^2(t) \rangle$ (on the log-log scale) to accompany the kinetic reduction in the atom's speed. This, however, is not the prevailing effect observed when supercooling the liquid well below T_l. At low temperatures, the atom's MSD trajectory is

found to enter a plateau after the first collision. The interpretation of this is that the subsequent collisions experienced by the atom are no longer uncorrelated, rather, the collisions correlate in such a way that the atom remains localized in a narrow region of space for an extended duration of time. Stated more simply, the atom is caged by its neighboring atoms (and those atoms are caged by their neighbors…). The plateau is seen to lengthen with decreasing temperature. At 750 K, this caging effect is long-lived – it takes approximately a nanosecond for the cage to break down, so that the atom can begin to diffuse*.

Figure **1.2b** contains the shear-stress autocorrelation function for liquid $Cu_{64}Zr_{36}$ for multiple temperatures. The behavior of this function reflects the amount of time it takes for the liquid's atoms to rearrange in response to a shear-stress so as to accommodate, and thus dissipate, the stress. That is, it reflects the liquid's ability to flow. A solid's shear-stress autocorrelation function never decays to zero, hence a solid never flows. As seen in the analysis of the MSD trajectories, all of the temperature curves exhibit the same decay behavior within approximately 100 fs of a shear event – this initial relaxation is the result of the ballistic motions of the liquid's atoms. The subsequent behavior of the autocorrelation function depends strongly on temperature. At 2000 K, the function proceeds to exhibit a simple exponential decay to 0:

$$\langle \sigma_{xy}(t)\sigma_{xy}(0)\rangle \propto e^{-t/\tau} \quad (T \gg T_g) \tag{1.1}$$

* Once the atom escapes from a cage, it will soon find itself trapped in another cage. This is not apparent in Figure **1.2a** because time is plotted on a log scale. After the atom leaves the cage, the subsequent ticks on the logarithmic time scale correspond to times greater than that needed for the subsequent cages to break down, hence the atom proceeds to diffuse on this long time scale.

Upon approaching T_g, on the other hand, the initial ballistic decay of the function leads to a sustained plateau. The function's departure from this plateau is non-exponential. Instead, it is well-described by a stretched exponential form*,

$$\langle \sigma_{xy}(t)\sigma_{xy}(0)\rangle \propto e^{-(t/\tau)^{\beta}} \quad (T \approx T_g) \tag{1.2}$$

where $\beta(T) < 1$ and increases monotonically with temperature[12].

The dynamical correlation functions in Figure **1.2** contain essential information about the nature of supercooled liquids and the glass transition. They allow us to understand how liquids in thermodynamic equilibrium are different from supercooled liquids that are ergodic yet only metastable. Furthermore, they reveal that new physical mechanisms do in fact arise near T_g. The most striking feature of both correlation functions near T_g is that they are *characterized by a two-step relaxation process that is separated by a plateau*. The initial, fast decay that leads the correlation function into the plateau is known as the β relaxation process, and the eventual decay from the plateau to zero is the α relaxation process. This is a general feature of dynamical correlation functions of deeply supercooled liquids. A. Cavagna succinctly describes this as being an "equilibrium fingerprint of glassiness."[6] What he means by this is that the plateau feature arises in a supercooled liquid that is still ergodic (and hence in "equilibrium"); thus it is an indicator that the glass transition is imminent, which arises before the supercooled liquid actually falls out of metastable equilibrium. Posed another way, this phenomenon will manifest in a supercooled liquid that is near T_g regardless of the length of the laboratory time scale. This is one of the most resounding pieces of evidence that the glass transition is indeed more than just a runaway timescale dilation.

* This is known as the Kohlrausch-Williams-Watts function.

The discussion of the MSD trajectories in Figure **1.2a** seems to provide a clear interpretation of the physical meaning of the plateau for both dynamical correlation functions. At low temperatures, atoms form cages around one another, and before a given cage breaks apart, an atom within it is temporarily "frozen" in place[*]. It is also natural to assert that, during caging, atoms cannot rearrange to accommodate shear-strains. Once the cage breaks, the supercooled liquid can proceed to flow, and fully relax in response to a shear-strain. Hence the plateau in the shear-stress autocorrelation function appears to be explained by structural caging as well. We seem to be making good progress towards explaining the glass transition: supercooling a liquid leads to the development of stiff but transient cage-like atomic structures. Further supercooling leads to longer-lived cages, and hence an extended plateau that separates the liquid's two-step relaxation processes. The liquid's relaxation time (e.g. the time-integral of the shear-stress autocorrelation function) grows rapidly as the plateau grows; eventually, the plateau becomes so sustained – the atoms remain caged for such extended amounts of time – that the supercooled liquid can no longer explore phase space on the laboratory time scale and it forms a glass.

This synopsis of glass formation does capture many of the important aspects of this process, but provides little explanation of why these things happen. What leads to the initial onset of caging? What is the nature of the structures responsible for caging – are they merely rigid and dense amorphous configurations of atoms? Though we have an equilibrium indicator of impending glassiness, what determines the temperature range where this comes into play? Is caging the only viable explanation for the plateau? To gain insight into these questions and others, we look to the extensive and diverse theoretical works that have been developed in this vein.

[*] The parameter used to characterize the duration of the dynamical plateau is known as the non-ergodicity parameter for this reason. A system cannot ergodically explore phase space while its particles are stuck in cages.

1.3 Theories of Supercooled Liquids and Glasses

When surveying the prominent theories and models that describe supercooled liquids and glasses, it becomes clear that features of rapid viscous slowdown and two-step relaxation are reproduced by many different mathematical systems. It is surprising to find, for instance, that some mean field spin systems exhibit the exact same two-step relaxation processes that are seen in supercooled liquids, while these systems have no real space structures[13]. These spin systems cannot exhibit caging effects, as all of their spins interact with one another without preference, and yet they produce the same plateau features that we ascribed to caged particle dynamics. This example hints at the complexities one faces when searching for a theoretical treatment of the supercooled regime. Although there is no complete theory of supercooled liquids, the prominent theories frequently complement one another – where one theory fails, another holds. Furthermore, these theories generally appear to point in the same direction, though from different starting points. The following are very brief summaries of the theories of supercooled liquids that are most relevant to the content of this dissertation. Naturally, they will be used to provide context for and as points of comparison with the original results that are presented in the following chapters.

1.3.1 Mode-Coupling Theory & p-spin Models

Mode-coupling theory (MCT) stands out amongst supercooled theories as an analytic approach to describing the dynamical slow down and two-step relaxation exhibited by supercooled liquids[14–16]. Starting from the perspective of simple liquid dynamic theory, MCT uses the static structure of a liquid – as described by a two-point spatial correlation function of atomic

positions[*] – and yields a closed set of equations for a dynamical correlation function, $\phi(k,t)$, of the liquid.[†] The triumph of MCT is that $\phi(k,t)$ appropriately develops the two-step relaxation feature as the liquid is supercooled. Moreover, the manner in which $\phi(k,t)$ decays into (β) and from (α) the plateau agrees closely with experimental and numerical measurements. Although MCT correctly captures the early (high-temperature) development of "glassy" features, it suffers from a glaring problem: it predicts that a liquid's viscosity (relaxation time) *diverges at a temperature higher than* T_G. Namely, it predicts that the viscosity grows as a power law:

$$\eta(T) = \frac{m}{(T - T_C)^{\gamma}} \tag{1.3}$$

where $\eta(T)$ is the temperature-dependent liquid viscosity, and T_C, m, and γ are positive-valued fitting parameters. T_C is known as the mode-coupling temperature – this is the temperature where MCT notoriously predicts that the liquid's viscosity diverges. High-temperature fits of liquid viscosity data show that the power law scaling describes well the growth of $\eta(T)$ up until the vicinity of T_C, which is typically larger than T_G by a factor of approximately 1.2. At T_C, the plateau in $\phi(k,t)$ diverges in length, meaning that the system no longer undergoes α relaxations and thus is no longer ergodic.

Given the earlier phenomenological discussion of the glass transition, it is trivial to see that MCT's prediction at T_C is incorrect – one can supercool liquids to this temperature and find that their viscosities remain finite here and below[‡]. It turns out that the premature failure of MCT

[*] Specifically, it uses the static structure factor, $S(q)$, as input. This quantity can be measured directly via x-ray diffraction and neutron scattering experiments.

[†] The dynamical correlation function that is solved for is related to the self-intermediate scattering function. This measures density-density correlations as a function of time.

[‡] It would be far more compelling if MCT fits predicted that $T_C < T_G$. In this case, it is not so obvious that the viscosity doesn't eventually diverge (due to a phase transition), and yet we cannot reach this temperature without forming a glass first. Indeed, this scenario is brought into consideration by the so-called Kauzmann entropy crisis.

indicates that a new liquid relaxation mechanism comes into play near T_C, which is not included in the MCT framework. To identify this mechanism it is fruitful to first briefly turn to p-spin theory to understand the cause of the divergence, but first a certain point must be emphasized. MCT does appropriately capture the onset of two-step relaxation in a liquid, but fails prior to T_G. Whatever new mechanism begins to participate near T_C must (1) prevent the divergence of the liquid's viscosity and (2) contribute to the two-step relaxation that occurs below T_C.

First and foremost, p-spin models are mean-field spin systems that produce dynamical equations that are formally (and coincidentally) equivalent to those in MCT[17,18]. Furthermore, a p-spin model is generally much more transparent than is the MCT framework[19,20]. This explains why it is appropriate to introduce a p-spin model in the context of supercooled liquids to understand the failure of MCT[18,20,21]. The following synopsis follows closely the introduction provided by T. Castellani and A. Cavagna[13]. A simple p-spin Hamiltonian (where $p = 2$) is given by

$$H = -\sum_{\langle i,j \rangle} J_{ij}\sigma_i\sigma_j \tag{1.4}$$

where σ_k is a random spin degree of freedom and J couples the spins. J is given by a probability distribution, hence the system is a mean-field one and has no lattice structure. J is restricted to be constant on the timescale of fluctuations of σ_k – that is, the disorder in the system is "quenched". The first connection between this p-spin model and supercooled liquids can be gleaned from the behavior of the dynamical correlation function

$$\mathrm{C(t)} = \sum_i \sigma_i(t + t_o)\sigma_i(t_o) \tag{1.5}$$

which, at low temperatures, exhibits the telltale two-step relaxation shape.

One can calculate the gradient of the p-spin system's potential energy to find the minima of its energy landscape. The Hessian then provides information about the shape of a given energy minimum in phase space. Specifically, positive eigenvalues indicate a positive energy curvature along the corresponding eigenvectors, whereas a non-positive eigenvalue describes a flat or convex energy curvature. It is found that, for $T > T_C$, the Hessian for an average minimum has multiple non-positive eigenvalues. Thus, above the mode-coupling temperature, the system can freely travel from minimum to minimum in phase space by travelling through the saddle points associated with these eigenvalues. The process of the system dynamically "finding" a saddle point and leaving a minimum via it corresponds to an α relaxation. Decreasing temperature causes a positive shift in the eigenvalue spectrum, reducing the average number of saddle points available to a given energy minimum. At $T = T_C$, the energy landscape undergoes a topological transition – the minima of the energy landscape no longer possess saddle points. At this temperature and below, the system can no longer ergodically explore phase space, as it is trapped in a single energy minimum. This manifests in $C(t)$ as a divergent plateau (the system never α-relaxes), and explains the diverging power-law behavior predicted in Equation 1.3 by MCT.

The satisfactory agreement between MCT and experiment for $T > T_C$, leads one to believe that the energy landscape truly undergoes a topological transition at the mode coupling temperature. If this is the case, then a physical mechanism that is not included in MCT must be responsible for allowing the supercooled liquid to persist ergodically despite the lack of landscape saddle points. The mechanism of activated hopping proposed by Goldstein does just this.

1.3.2 Goldstein Activated Dynamics

Goldstein also makes headway towards understanding supercooled dynamics by considering the role of an energy landscape[22], but his discussion resides in the more familiar phase space of atoms interacting locally in three spatial dimensions. Because the interactions being considered are local in space, it doesn't make sense to think of the entire liquid residing at an energy minimum in phase space at any given time. A local configuration of atoms in one region of the liquid may be rearranging, while other clusters of atoms are in their locally-preferred structures. Indeed, the notion of the system being in a global energy minimum is more cogent when thinking of a crystal. The major point to keep in mind is that any energy minima and relaxation processes (i.e. structural rearrangements) discussed by Goldstein are inherently local in nature.

Goldstein proposed that a local configuration of atoms in an energy minimum can escape from the minimum via activated hopping. That is, thermal energy is utilized to permit local regions of the supercooled liquid to escape from wells in the energy landscape. This interpretation fits naturally into the two-step relaxation scenario: oscillations about energy minima correspond to the short β relaxations leading into the "caged" plateau. Activated hopping then eventually allows the supercooled liquid to leave the minimum (and ergodically explore phase space), which corresponds to an α relaxation. Goldstein made estimates of the temperature dependence of the energy barrier sizes (e.g. the depth of a typical well in the energy landscape) based on the number of atoms involved in a local rearrangement. He argued that the barrier size, $\Delta E(T)$, grows with decreasing temperature, and sought the temperature T_x, below which $\Delta E(T_x) \gg k_B T$. Below T_x, activated hopping is the dominant mechanism for diffusion (α relaxation) in the supercooled liquid.

Remarkably, estimates of T_x are very close to T_C ($T_C \approx T_x \approx 1.2 \times T_G$), meaning that activated hopping begins to dominate the liquid dynamics as MCT breaks down[23–25]. This agreement is extremely fortuitous (and sensible, in hindsight) as it not only rectifies the divergence prescribed by MCT, but it also corrects for oversimplifications made by Goldstein. Recall that MCT predicts a topological transition in the energy landscape at T_C, after which ergodicity is broken because the liquid is trapped in an energy well[*]. This topological transition coincides with the condition that $\Delta E(T) \gg k_B T$, which signals the need for activated hopping to restore ergodicity. On the other hand, Goldstein's approximations provide no explanation for the observed two-step relaxation that occurs above T_x; clearly one then turns to the discussion of MCT and p-spin to understand that for $T > T_x$, the process of finding and travelling between saddle points in the energy landscape leads to a two-step relaxation process.

To summarize the crucial points made by MCT (p-spin) and Goldstein: as a liquid is supercooled, its ergodic exploration of phase eventually becomes impacted by the existence of minima in its energy landscape with β relaxations corresponding to oscillations about these minima. In this temperature regime ($T_m > T > T_C$)[†], local regions of the liquid will remain caged within minima until they can find saddle points to escape their respective energy wells. This α relaxation process crosses over to activated hopping near T_C (T_x), at which the energy landscape has undergone a topological transition so that the minima no longer possess saddle points and the energy barriers have become large compared to $k_B T$.

[*] Activated hopping is impossible for a mean field system, which is why the p-spin system predicts that the liquid is completely trapped in a minimum for $T < T_C$.

[†] Note that signatures of two-step relaxation do not emerge immediately upon supercooling. One may have to supercool significantly below T_m before developing a plateau feature in the liquid's dynamical correlation functions.

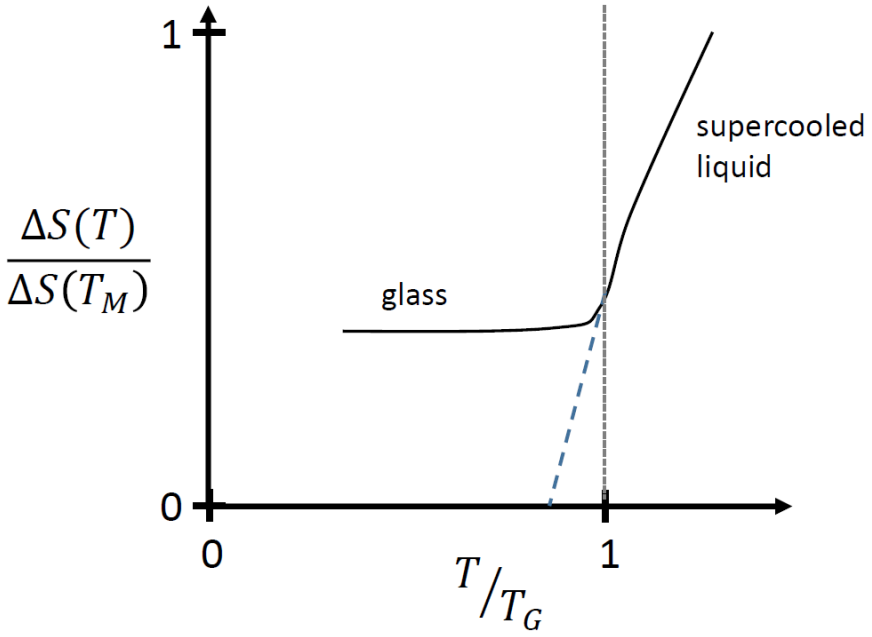

Figure 1.3 A schematic plot of the temperature dependence of a supercooled liquid's excess entropy. At T_G, the supercooled liquid falls out of metastable equilibrium, causing the entropy to level off. A blue dashed line indicates an extrapolation of the supercooled liquid regime.

These two theories make excellent headway towards understanding supercooled liquid dynamics, but they are vague with regards to the roles played by atomic structures. Goldstein's discussion of the energy landscape appeals directly to clusters of atoms purposefully rearranging and notes that the number of atoms involved in such a process ought to increase with decreasing temperature. To this end, several theories address the topic of cooperative structural rearrangements, configurational entropy, and their effects on a supercooled liquid's dynamics.

1.3.3 AGDM Theory & Random First-Order Transition Theory

Figure 1.3 depicts a schematic of the behavior of a supercooled liquid's excess entropy as it is cooled through the glass transition. Here, the excess entropy, $\Delta S(T)$, refers to the difference between the entropy of the liquid and the entropy of the crystal at a given temperature. As explained by Kauzmann[26], as the supercooled liquid falls out of metastable equilibrium, many of

its degrees of freedom "freeze out" and no longer contribute to the material's specific heat (c_p); hence c_p drops rapidly near T_G. This then manifests as a rapid flattening of $\Delta S(T)$ below T_G. A naïve extrapolation of the metastable equilibrium data, shown as a dashed blue line, suggests an interesting phenomenon: at some temperature below T_G, denoted by T_k, the excess entropy of the supercooled liquid (which has hypothetically avoided glass formation) vanishes. This temperature, where the liquid and crystal entropies are the same, marks the occurrence of the so-called Kauzmann entropy crisis*.

Several theories attempt to explain the decrease in entropy that accompanies supercooling in the context of cooperative structural rearrangements within the liquid and the length scales associated with this cooperativity. Adam, Gibbs, and Di Marzio (ADGM) considered a cooperatively rearranging region to be the smallest region of a liquid that can rearrange independently from its surrounding atoms[27,28]. Within this region, then, configurations of atoms are interdependent and, as a whole, only sample a small number of preferred states, Ω†. Taking the number of atoms in the cooperative region to be $n(T)$ and the total number of atoms in the liquid N, then the configurational entropy of the liquid can be calculated by:

$$S_c(T) = \frac{1}{N}\ln\left(\Omega^{N/n(T)}\right) = \frac{1}{n(T)}\ln(\Omega) \tag{1.6}$$

One naturally finds that, as the configurational entropy (which is approximately equal to the liquid's excess entropy) decreases with temperature, the number of particles involved in a

* Kauzmann actually argued that T_k could likely not be reached before a supercooled liquid had first reached an inherent metastability limit, which would force it to crystallize rapidly[26]. Others, however, suspected that the vanishing of ΔS was indicative of a phase transition that would be the true glass transition for which T_G was a mere precursor[66]. Recent experimental evidence suggests that the extrapolated crisis does not actually unfold[1,67].

† That Ω is small and only weakly temperature dependent is a strong assumption made by AGDM.

cooperatively rearranging region must increase. As argued by Goldstein, the hopping activation barrier is expected to scale with $n(T)$ so that

$$\eta(T) = \eta_o e^{\left(\frac{cn(T)}{k_B T}\right)} = \eta_o e^{\left(\frac{c\prime}{S_c(T) k_B T}\right)} \tag{1.7}$$

(c and c' are constants) yields super Arrhenius growth in the liquid viscosity while supercooling, as expected.

The random first order transition (RFOT) theory was developed in the same vein as AGDM, but pays closer attention to the details within the cooperatively rearranging regions of the liquid. It resembles nucleation theory in that it is concerned with the free energy costs associated with creating a droplet of atoms belonging to an amorphous state that differs from its surroundings. That is, it considers the penalty for creating interfaces between amorphous states as well as the entropic gain associated with a rearrangement. Unlike the nucleation process, the supercooled liquid still exhibits time translation invariance during this rearranging, subsequent rearrangements do not decrease the overall free energy of the liquid, and the system is not driven to any particular amorphous state. Thus what is being considered is a steady state balance between surface tension preventing rearrangements and the entropic drive to sample metastable states. RFOT provides an estimate of the length scale of a typical cooperatively rearranging region:

$$\xi \propto \left(\frac{1}{T - T_k}\right)^{(d-\theta)^{-1}} \tag{1.8}$$

where d is the dimensionality of the system and θ is a parameter associated with the geometry of the interfaces formed by cooperative regions. RFOT clearly delineates that metastable states are

inherently local and can only be defined within a region of liquid bounded by $\xi(T)$. Similar to ADGM, RFOT predicts that the number of atoms involved in cooperative rearrangements ($n(T) \propto \xi(T)^d$) grows with decreasing temperature in association with decreasing $\Delta S(T)$. At T_k, this length scale diverges as the entropic difference between the liquid and the solid vanishes (but the difference in their free energies do not vanish[26]). This corresponds to the supercooled liquid occupying a global metastable state, which is possible (i.e. the metastable state is still "local") because $\xi(T)$ diverges at T_k.

Ultimately, the length scale estimations of ADGM and RFOT* provide a measure of the activation barrier associated with hopping dynamics. This leads to an important functional form for liquid viscosity known as the Vogel-Fulcher-Tamman (VFT) law†[29].

$$\eta(T) = \eta_o e^{\left(\frac{\xi^d}{k_B T}\right)} = \eta_o e^{\left(\frac{A}{T - T_k}\right)} \tag{1.9}$$

where A and η_o are constants. Irrespective of AGDM and RFOT, the VFT form is widely used as it tends to fit empirical data well in available temperature ranges; the real success of these theories is that they relate the rapid (super-Arrhenius) growth of a supercooled liquid's viscosity with a growing static length scale associated with cooperative structural rearrangements.

It is interesting to note that both ADGM and RFOT are structure and state agnostic theories. Even though RFOT hinges on the notion of interfaces between local metastable states, it does not discuss the details of these metastable states nor the mismatch that results from a local cooperative rearrangement. This is at significant odds with typical crystal growth in which the

* RFOT's predicted $\xi(T)$ doesn't yield the exact VFT form unless $\theta = {}^{d}/_{2}$.

† Note that $\eta(T)$ diverges at T_k. This feature is inherited from the aforementioned Kauzmann entropy crisis. Recent experiments suggests that VFT does *not* accurately describe $\eta(T)$ below T_G- that is, there is no divergence[1,67].

notion of a mismatch of the nucleating crystal phase with the liquid is quite salient. While there are several methods devised to measure these structure-agnostic static length scales (ξ_s) [30*], the measurements themselves find static length scales that only span a few interparticle distances and grow modestly with decreasing temperature[31–34]. This fails to meet relatively general and rigorous considerations which place lower and upper bounds on the supercooled liquid's viscosity that depend on a growing static length scale[35]. These bounds strongly suggest that a rapidly growing ξ_s should accompany the characteristic growth in viscosity observed near T_G[†]. In light of this, perhaps it is appropriate to make stronger conjectures about the types of structures that participate in and result from cooperative rearrangements. This is the perspective of some more recent theoretical efforts, including those described in the following chapters of this work.

1.3.4 Frustration & Avoided Criticality

Unlike in supercooled liquids and glasses, the structural ordering associated with crystalline solids is unambiguous: the crystal possesses an obvious long-ranged order (LRO). Associated with this LRO is a unit cell containing a locally-preferred structure (LPS) of atoms that can tile three-dimensional space. Thus the short-ranged order (SRO) in an ideal crystal simply tessellates space to produce the crystal's characteristic LRO. By contrast, x-ray diffraction measurements of supercooled liquids and glasses, which reflect spatial correlations between pairs of atoms, reveal a distinct lack of LRO. **Figure 1.4** contains a pair correlation function, $g(r)$, of the real-space atomic structure of simulated $Cu_{64}Zr_{36}$ metallic glass. $g(r)$ is normalized such that a value of unity reflects a random distribution of atoms, thus the solid curve's peaks and valleys convey spatial correlations and anti-correlations between pairs of particles. Unlike what one would find

[*] The methods used to measure static length scales, such as point-to-set measurements, can only be used in numerical studies thus far.

[†] If the viscosity does diverge at some $T < T_G$, then ξ_s must diverge as well.

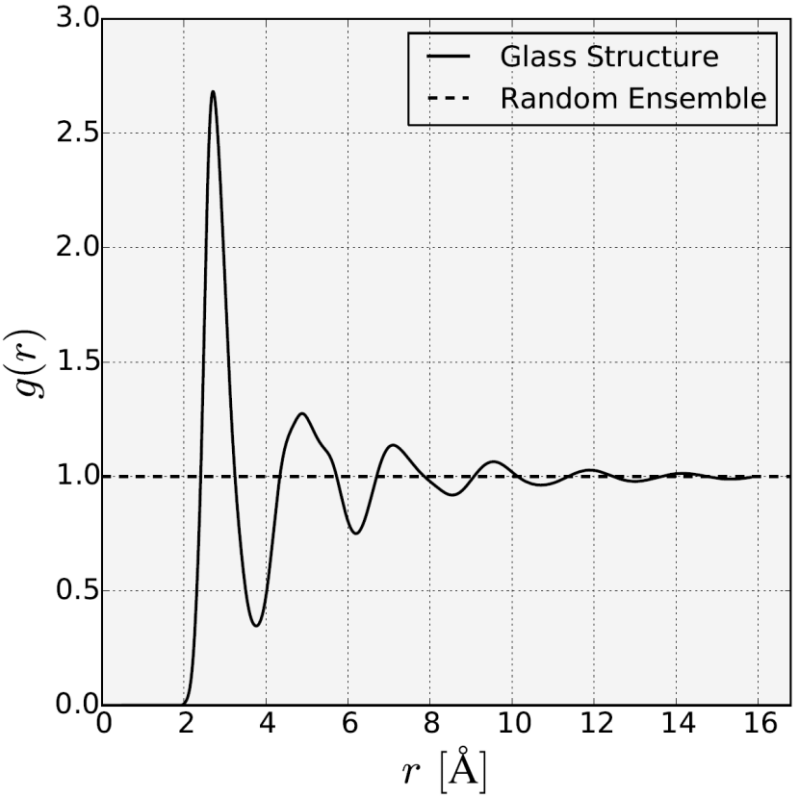

Figure 1.4 A real-space pair correlation function of simulated $Cu_{64}Zr_{36}$ glass. The curve reflects the probability of finding an atom at a distance r from another atom in the glass. The dotted line shows the pair correlation function for an ensemble of random structures.

in a crystal, pairs of atoms in the glass that are separated by more than 14 Å are apparently uncorrelated with one another. Despite the absence of LRO, the structure of the 2nd peak (corresponding to the structure of an atom and its next-nearest neighbors) and beyond indicates that the glass structure does possess SRO as well as medium-range order (MRO). It is natural to investigate the nature of this structural ordering, why it does not lead to a LRO in the glass, and how it might relate to the cooperative structural rearrangements that were considered in **1.3.3**.

In the 1950s, Frank and Kasper considered the LPS of collections of hard spheres and of atoms interacting via Lennard-Jones potentials[36,37]. They found that efficiently packed structures exhibited tetrahedral bonding and culminated in 13-atom clusters that formed icosahedra (consisting of one center atom and 12 vertex atoms). That is, the ground state in this local energy

landscape is a LPS that cannot be tiled in three dimensional Euclidean space due to its fivefold rotational symmetries. This structure can, however, nest with itself to form extended structural domains. Much of Frank and Kasper's work proves to be highly applicable for studying amorphous systems; indeed, icosahedral ordering is found to be prominent in many simple atomic liquids, especially in metallic liquids[38–41]. The inability to tile 3D space with icosahedra immediately brings to the foreground the concept of frustration: locally, atoms want to pack into clusters of icosahedra, but, unlike in crystals, it is impossible for the system to globally exhibit this ordering. Does this frustration manifest in important ways in supercooled liquids? In the following discussion, the phrase locally-preferred structure (LPS) will be used for generality, but one can keep the instance of icosahedral ordering in mind as a precise point of reference.

Similar to RFOT, one can consider the thermodynamics involved when forming a domain of size ξ of a LPS[*]; a major advantage of this approach is that it does away with the vague context of metastable states. One then asks: what is the energetic gain for occupying locally-favored states, what is the cost associated with creating an interface with the bulk liquid, and how much strain is produced due to the degree of frustration that is associated with the LPS? This last notion of frustration-based strain acts to hinder the domain's growth, preventing it from establishing LRO. Hence these domains are deemed frustration-limited domains (FLDs) and the thermodynamic theory describing their growth is known as frustration-limited domain theory (FLDT)[42–44]. FLDT formulates the statistical mechanics of the frustration of liquids in the context of three postulates that are outlined by Tarjus, Kivelson, Nussinov, and Viot[44]: (1) "a liquid is characterized by a LPS which is different than that of the crystalline phase." (2) "The LPS characteristic of a given

[*] Individual LPS clusters can share atoms with one another to create an "extended" structure, which is deemed a domain.

liquid cannot tile the whole space." (3) "It is possible to construct an abstract reference system in which the effect of frustration is turned off. [45,46]"

FLDT argues that the abstract reference system, in which the LPS is not frustrated, exhibits a critical point transition at a temperature T_A*. This critical point separates the high-temperature disordered liquid phase from the lower-temperature frozen phase in which the system ubiquitously conforms to the LPS. In reality, frustration will cause the liquid to avoid this critical point as it is cooled, and will instead yield FLDs that have broken up to a size $\xi(T)$. $\xi(T)$ grows as T is lowered below T_A, and causes a rapid slowing of the liquid dynamics; it is responsible for a crossover from Arrhenius growth of the liquid's viscosity to super-Arrhenius growth. Though avoided, the critical point is predicted to have a major impact on the liquid's structure and dynamics. Specifically FLDT predicts that viscosity grows as:

$$\eta(T) = \eta_o \exp\left(\frac{E^*(T) + E_\infty}{k_B T}\right) \tag{1.10}$$

where $\eta_o \exp\left(\frac{E_\infty}{k_B T}\right)$ is the Arrhenius contribution to the viscosity. $E^*(T)$ vanishes above T_A, but has the form:

$$E^*(T) = k_B T_A \left(1 - \frac{T}{T_A}\right)^{\Psi}, \qquad (T \leq T_A) \tag{1.11}$$

As in RFOT, α-relaxation is still associated with cooperative rearrangements, but in the context of FLDT the rearrangements occur within the FLDs. Thus in order for the liquid to relax, its atoms must cooperate across the length scale $\xi(T)$, whose growth is determined, in large part, by the frustration associated with the liquid's LPS. Impressively, this frustration "degree of

* T_A is predicted to reside above T_m for pure liquids.

freedom" allows FLDT to accurately describe the wide range of non-exponential relaxation behaviors exhibited by different liquids.

It is indeed found that the atoms participating in a liquid's LPS also constitute the population of the slowest moving atoms in the liquid, and that the LPS exhibits an especially long relaxation time[47–51]. The most common criticism of FLDT, however, is that the connection between these local structures and extended FLDs is still not well understood, nor have growing FLDs been directly observed[6,30]. Recently, however, a survey of high temperature metallic liquid viscosity measurements revealed a surprising correlation between T_A and T_G, adding new urgency to understanding the impact of the avoided critical point and the physical processes that become involved nearby.

1.4 Crossover Behavior at T_A & Structural Cooperativity

1.4.1 Solid-like Features of a Liquid Below T_A

In the late 1980's, Chen, Egami, and Vitek noted the importance of T_A in metallic liquids[52]. Their study was based off data from a classical molecular dynamics (MD) simulation of liquid Fe[*]. In this work, T_A was identified as the temperature beneath which the second moments of the liquid pressure and shear-stress fluctuations begin to deviate from a linear temperature dependence[†]. It was found that the liquid's phonon density of states develops a low-frequency transverse phonon peak as the liquid is cooled through T_A. Below T_A, the liquid ceases to behave like a so-called

[*] It is prudent to note that computational limitations restricted this study to consider a system size and timescale that are several orders of magnitude smaller than the current simulation standards. Though the overall results and conclusions of the study have proven to be robust, it is apparent, in light of recent simulations, that some of the observations made were likely affected by these limitations.

[†] The temperature T_A (referred to as T_s in the original paper) found by Chen *et al*. does correspond to the temperature below which the liquid viscosity crosses over from exhibiting Arrhenius growth to super-Arrhenius growth, as identified in FLDT, though the authors did not recognize this in the paper.

"simple liquid", and begins to support shear phonons as well as long-ranged atomic-level shear stress spatial correlations. The development of these features are attributed to local pressures and tensions that develop within small clusters of atoms (e.g. an atom and its nearest neighbors). Atoms with small or large coordination numbers experience compressive and tensile stresses, respectively. These "misfit" clusters are then said to establish long-range elastic fields, which cause the liquid to exhibit some solid-like features. Chen *et al.* do not explain the relatively sharp onset of these features at T_A, though in hindsight one may attribute them to an avoided critical point. They do speculate that a significant structural change may accompany this crossover phenomenon. Incidentally, the authors noted, seemingly only for the sake of estimation, that T_A is roughly twice T_G for liquid Fe. It turns out that this correlation holds true for many metallic liquids, though this wasn't realized until decades later.

1.4.2 The Onset of Cooperative Dynamics at T_A

In 2013, Iwashita, Nicholson, and Egami presented an analysis of MD data of several high-temperature liquid metals to complement Chen *et al.*'s 1988 paper (on which Egami was also an author) and to provide a more detailed picture of the microscopic mechanisms that come into play at T_A that serve to relieve the stresses associated with misfit clusters[53]. Accordingly, they introduced the concept of a local configurational excitation (LCE), in which an atom loses or gains a nearest neighbor, and measured the average lifetime of the configuration of an atom and its nearest neighbors, τ_{SCL}. A heuristic illustration of an LCE process is shown in **Figure 1.5**. This system connectivity lifetime (SCL) was measured by recording the nearest-neighbor* IDs associated with the cluster formed around each atom in the system, at a time step t_o of a

* Here, a nearest neighbor was taken to be any atom that fell within a distance d_{cut} of a given atom. d_{cut} was chosen to be the location of the first minimum of the pair correlation function, though it was not reported if this value was updated with changing temperature.

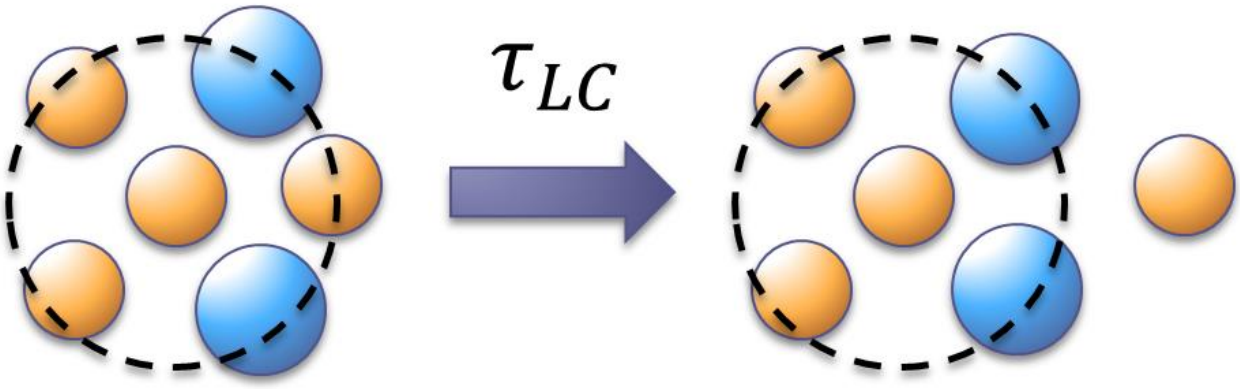

Figure 1.5 A two-dimensional schematic illustration of an LCE. Given an atom (center) and its nearest neighbors (atoms within a distance d_{cut}), τ_{SCL} is a measure of the average time required for the atom to lose or gain a nearest neighbor.

simulation. The average number of nearest neighbors, $N_C(t_o)$, was computed, and the simulation time was advanced until the average number of original neighbors had decreased by 1[*]; the elapsed time corresponds to the local cluster time, τ_{SCL}. That is,

$$N_C(t_o + t_{SCL}) \equiv N_C(t_o) - 1 \tag{1.12}$$

$\tau_{SCL}(T)$ was compared to the temperature-dependent Maxwell relaxation time, $\tau_M(T)$, which measures the shear-stress decorrelation time of a liquid,

$$\tau_M \equiv \frac{\int_0^\infty \langle \sigma_{xy}(t)\sigma_{xy}(0)\rangle dt}{\langle \sigma_{xy}(0)^2\rangle} \tag{1.13}$$

to show, remarkably, that $\tau_{SCL}(T) \approx \tau_M(T)$ for $T > T_A$. This, the authors argue, suggest that the local change in topology of an atomic cluster is the elementary excitation in a high-temperature liquid, which controls the liquid relaxation process (e.g. the viscosity). In this temperature regime, the mean free path of a transverse phonon, ξ_p, is shorter than the distance between

[*] It is noteworthy that an earlier paper by the same authors is cited in reference to the definition of τ_{LC}. Unfortunately, the earlier paper utilizes a different measure of the local cluster lifetime than the one described in the supplemental materials. This has served as a point of confusion in subsequent research efforts.

nearest neighbors, hence all LCEs must be independent above T_A. Near T_A, ξ_p appears to grow sufficiently so that LCE's can become coupled through atomic vibrations. Here, the liquid is thought to become strongly influenced by the features of its energy landscape and by the long-range elastic fields discussed by Chen *et al*.

This work by Iwashita *et al.* explored important new features of the crossover phenomena occurring at T_A and inspired new efforts to closely inspect experimental liquid viscosity data for signatures of these processes. It is prudent to note, however, that the correlation between the temperature, T_1, at which ξ_p surpasses the nearest neighbor distance, and T_A is not particularly strong - especially in the context of the relatively sharp crossover observed at T_A. Furthermore, the discussion of phonons and long-range elastic strain fields is not developed much beyond the assertions made by Chen *et al*. Given these points, it is apparent that details of the mechanisms that become involved at T_A require further investigation, where the observation that $\tau_{SCL}(T) \approx \tau_M(T)$ (for $T > T_A$) provides excellent headway towards this end.

1.4.3 Surprising Empirical Results Regarding T_A, FLDT, & Cooperativity

Soon after the work by Iwashita *et al.* was published, Blodgett, Egami, Nussinov, and Kelton conducted a survey of experimental measurements of containerlessly processed metallic liquids to find several striking results regarding the dynamical crossover at T_A[54]. First and foremost, it was found that all of the metallic liquids exhibited an intimate and unexpected connection between their respective values of T_A and T_G such that: $T_A/T_G = 2.02 \pm 0.015$. Second, it was shown that each liquid viscosity data set can be scaled by a respective constant, η_o, such that they all collapse onto a universal curve whose temperature scale is given by T_A. The functional form of the curve was determined by comparing high and low-temperature Vit106a liquid

viscosity data with a wide variety of popular viscosity fits, including the form predicted by FLDT[*] (equations 1.10 and 1.11) and the VFT form (equation 1.9)[†]. The FLDT form provided the most reliable fit across the broad temperature range. Utilizing the fitting parameters obtained from this procedure, the other liquid data can be collapsed onto a single curve by using only the scaling parameters T_A and η_o. As noted above, the temperature scale can be set, with good accuracy, by using the relationship $T_A \approx 2.02 \times T_G$. Additionally, it is found that the viscosity scaling parameter, on average, is given by the simple but surprising relationship $\eta_o \approx nh$[‡], where n is the liquid particle density and h is Planck's constant. Given these observations, one can argue that the procedure for collapsing the data is essentially fitting-parameter free[§].

The significance of these results is resounding – the fact that the viscosity data of both strong and fragile metallic liquids could be scaled onto a single curve across such a wide temperature is important in and of itself. The success of FLDT in describing this curve and the compelling correlation between T_A and T_G then suggest that the avoided criticality at T_A is of fundamental importance for the ensuing viscous slowdown leading to T_G. Furthermore, the work by Chen *et al.*[52] and Iwashita *et al.*[53] indicate that this crucial dynamical crossover is also linked to the onset of cooperative dynamics that lead to a departure from simple liquid dynamics. These findings set the stage for several important questions: (1) Can the signature of an avoided critical point be observed through the detection of FLDs that grow upon cooling, and do these FLDs develop near T_A? (2) Does the onset of cooperativity amongst LCEs have a clear structural manifestation in the liquid? (3) How does this cooperativity fit into the framework of FLDT? (4) How do the liquid

[*] A fifth fitting parameter is introduced the FLDT form (referred to as KKZNT) in the work by Blodgett *et al.*
[†] The power law form predicted by MCT was not considered because the form cannot be used below T_C, which resides above the low-temperature range of the viscosity data.
[‡] The relationship $\eta_o \approx nh$ is statistically less significant than is $T_A \approx 2.02 \times T_G$ and requires further investigation.
[§] Despite this, the collapsed data shown in this paper does utilize fitted values for T_A and η_o. The collapse is not so dramatic if one scales the data using the relationships $T_A = 2.02 \times T_G$ and $\eta_o = nh$.

features that manifest at T_A relate to the characteristics of the material at T_G? That is, how can one explain the apparent intimate link between T_A and T_G? All four of these questions will be explored through the use of numerical simulations and reported on in the following chapters of this dissertation.

1.4.4 A Computational Approach to Studying T_A

Empirical scattering data and the resulting pair correlation functions do not show obvious signatures of extensive FLDs in glasses[6]. While this certainly does not rule out their existence, it does become clear that empirical results alone may not be sufficient to confirm the mechanisms that come into play near T_A; here, newly developing structural and dynamical signatures are expected to be especially subtle. A classical molecular dynamics (MD) simulation is a powerful theory-agnostic[*] tool that enables one to access the microscopic structural and dynamical details that reproduce the macroscopic properties of a material. One can formulate a reliable semi-empirical potential to describe the forces between the atoms in a material[7]. The philosophy behind this approach, then, is that the appropriate Hamiltonian description of one's ensemble is sufficient to simulate a material and to produce behaviors that closely reflect empirical measurements[11,55]. One ultimately assumes that the underlying microscopic details of the simulated system reflects, to an appreciable degree of accuracy, the microscopic interactions that take place in nature.

[*] Here, the phrase "theory-agnostic" should not be confused with first-principles (or *ab-initio*). Indeed, one adopts a statistical-mechanical description of an ensemble that determines the classical Hamiltonian of the system, which does not contain any electronic degrees of freedom.

There are metallic liquids that are ideal for study in the context of MD simulations due to their relative simplicity, useful properties, and good glass-forming ability (GFA)[*56]. Cu-Zr is a particularly attractive alloy; it is a binary system that exhibits a relatively good glass forming ability across a wide range of compositions[57,58]. For this reason, $Cu_{64}Zr_{36}$[†] is perhaps the most popular metallic liquid to simulate[‡]. There are a couple high-quality semi-empirical potentials that reproduce well the empirical data for $Cu_{64}Zr_{36}$ liquid and glass[11,47]. Using these potentials, it has been shown that a Cu-centered icosahedron is the LPS of the amorphous phase of this system and that its presence dominates the structure of the glass[39,59,60]. Icosahedral clusters are also associated with dynamical heterogeneity in the system, as they possess the slowest-moving particles in the liquid[47,59] and help to inhibit liquid relaxation at low temperatures[61]. Below T_G, extensive icosahedral ordering is responsible for enhancing the mechanical properties of the glass, such as its elastic rigidity[59,62].

In light of the extensive efforts that have been made to arrive at a theory of supercooled liquids, and given the numerous predictions that a rapidly-growing static length scale accompanies the glass transition, it is surprising to find that little effort has been made thus far to connect the excellent phenomenological work that has been done on $Cu_{64}Zr_{36}$ with formal theoretical work. This is, in part, due to the fact that the temperature range over which icosahedral ordering has been studied in detail is limited. Furthermore, much of the analysis considers only a macroscopically-averaged view of the system's icosahedral ordering, whereas microscopic details (e.g. domain sizes, relaxation times, and domain fluctuations) are needed to connect with formal theories. The task of accessing the microscopic details of icosahedral order in sufficiently

[*] The GFA of a liquid is ambiguous and can be indicated by several properties, such as the maximum casting thickness of the glass, the critical cooling rate, and the metastability of the supercooled liquid.
[†] $Cu_{64}Zr_{36}$ is amongst the three best glass forming compositions of this alloy[68].
[‡] This does not include "model" systems such as Lennard Jones systems, which are widely utilized.

large systems, given data sets with sufficiently high time and temperature resolutions, quickly becomes a problem that falls under the umbrella of "big data analysis".

The research presented in the following chapters of this dissertation represents, in part, efforts to develop a framework for working with large data problems in the context of classical MD simulations. Using this framework provides us with access to previously unavailable microscopic details of $Cu_{64}Zr_{36}$. With this information, we find that there are important connections between phenomenological simulation results, formal theoretical predictions, and the recent empirical findings made by Blodgett *et al*[54]. Amongst our results, we show that (1) T_A is indeed associated with the growth of frustrated amorphous order, as suggested by the avoided critical point scenario of FLDT. (2) The development of these FLDs result from the onset of the cooperative dynamics described by Iwashita *et al*.[53]. (3) Tracking the icosahedral ordering as a function of temperature reveals that a rapidly growing length scale, associated with domains of connected icosahedra, arises in the liquid as it is supercooled towards T_G. (4) The timescale associated with rearrangements that occur within these growing domains is linked to longer-ranged cooperativity, and is related to the development of the two-step relaxation process and other standard glassy dynamical features of a supercooled liquid. Items 1, 2, and 4 are reported in a Letter that is presently under review[63]. Item 3 and an analysis of chemical ordering in the icosahedral network are discussed in a 2013 peer-reviewed publication[60].

1.5 Chapter 1 References

1. Mallamace, F. *et al.* On the ergodicity of supercooled molecular glass-forming liquids at the dynamical arrest: the o-terphenyl case. *Sci. Rep.* **4,** 3747 (2014).

2. Vonnegut, B. Variation with temperature of the nucleation rate of supercooled liquid tin and water drops. *J. Colloid Sci.* **3,** 563–569 (1948).

3. Graco. Viscosity. at <http://www.vp-scientific.com/pdfs/www.liquidcontrol.com_eToolbox_viscosity.pdf>

4. Sethna, J. *Entropy, Order Parameters, and Complexity*. (2011).

5. Debenedetti, P. G. & Stillinger, F. H. Supercooled liquids and the glass transition. *Nature* **410,** 259–267 (2001).

6. Cavagna, A. Supercooled liquids for pedestrians. *Phys. Rep.* **476,** 51–124 (2009).

7. Angell, C. A. Glass formation and glass transition in supercooled liquids, with insights from study of related phenomena in crystals. *J. Non. Cryst. Solids* **354,** 4703–4712 (2008).

8. Nadis, S. Ig Nobels hail world's longest-running experiment. *Nature* 938–939 (2005). at <http://www.nature.com/articles/>

9. Zanotto, E. D. Do cathedral glasses flow?—Additional remarks. *Am. J. Phys.* **67,** 260 (1999).

10. Mattern, N. *et al.* Structural behavior of CuxZr100-x metallic glass (x = 35-70). *J. Non. Cryst. Solids* **354,** 1054–1060 (2008).

11. Mendelev, M. I. *et al.* Development of suitable interatomic potentials for simulation of liquid and amorphous Cu–Zr alloys. *Philos. Mag.* **89,** 967–987 (2009).

12. Williams, G. & Watts, D. C. Non-symmetrical dielectric relaxation behaviour arising from a simple empirical decay function. *Trans. Faraday Soc.* **66,** 80 (1970).

13. Castellani, T. & Cavagna, A. Spin-Glass Theory for Pedestrians. **05012,** (2005).

14. Leutheusser, E. Dynamical model of the liquid-glass transition. *Phys. Rev. A* **29,** 2765–2773 (1984).

15. Bengtzelius, U., Gotze, W. & Sjolander, a. Dynamics of supercooled liquids and the glass transition. *J. Phys. C Solid State Phys.* **17,** 5915–5934 (2000).

16. Götze, W. *Liquids, Freezing and the Glass Transition*. (1991).

17. Bouchaud, J.-P., Cugliandolo, L., Kurchan, J. & Mézard, M. Mode-Coupling Approximations, Glass Theory and Disordered Systems. *Science* **208,** 32 (1995).

18. Kirkpatrick, T. R. & Thirumalai, D. Mean-field soft-spin Potts glass model: Statics and dynamics. *Phys. Rev. B* **37,** 5342–5350 (1988).

19. Gross, D. J. & Mezard, M. The simplest spin glass. *Nucl. Phys. B* **240,** 431–452 (1984).

20. Kirkpatrick, T. R. & Wolynes, P. G. Connections between some kinetic and equilibrium theories and the glass transition. *Phys. Rev. A* **35,** 3072–3080 (1987).

21. Kirkpatrick, T. R. & Wolynes, P. G. Stable and metastable states in mean-field Potts and structural glasses. *Phys. Rev. B* **36,** 8552–8564 (1987).

22. Goldstein, M. Viscous Liquids and the Glass Transition: A Potential Energy Barrier Picture. *J. Chem. Phys.* **3728,** (2003).

23. Angell, C. a. Perspectives on the Glass Transition. *J. Phys. Chem. Solids* **49,** 863–871 (1988).

24. Sokolov, a. P. The glass transition: general scenario and crossover temperature. *J. Non. Cryst. Solids* **235-237,** 190–195 (1998).

25. Schrøder, T. B., Sastry, S., Dyre, J. C. & Glotzer, S. C. Crossover to potential energy landscape dominated dynamics in a model glass-forming liquid. *J. Chem. Phys.* **112,** 9834–9840 (2000).

26. Kauzmann, W. The Nature of the Glassy State and the Behavior of Liquids at Low Temperatures. *Chem Rev* **43,** 219–256 (1948).

27. Adam, G. & Gibbs, J. H. On the Temperature Dependence of Cooperative Relaxation Properties in Glass- Forming Liquids. *J. Chem. Phys.* **43,** 139–146 (1965).

28. Gibbs, J. J. H. & DiMarzio, E. a E. Nature of the Glass Transition and the Glassy State. *J. Chem. Phys.* **28,** 373–383 (1958).

29. Garcia-Colin, L. S. & del Castillo, L. F. Theoretical basis for the Vogel-Fulcher-Tamman equation. *Phys. Rev. B* **40,** 7040–7044 (1989).

30. Karmakar, S., Dasgupta, C. & Sastry, S. Growing Length Scales and Their Relation to Timescales in Glass-Forming Liquids. *Annu. Rev. Condens. Matter Phys.* **5,** 255–284 (2014).

31. Charbonneau, P. & Tarjus, G. Decorrelation of the static and dynamic length scales in hard-sphere glass formers. *Phys. Rev. E - Stat. Nonlinear, Soft Matter Phys.* **87,** 1–8 (2013).

32. Berthier, L. & Kob, W. Static point-to-set correlations in glass-forming liquids. *Phys. Rev. E - Stat. Nonlinear, Soft Matter Phys.* **85,** 2–6 (2012).

33. Hocky, G. M., Markland, T. E. & Reichman, D. R. Growing point-to-set length scale correlates with growing relaxation times in model supercooled liquids. *Phys. Rev. Lett.* **108,** 1–5 (2012).

34. Biroli, G., Bouchaud, J.-P., Cavagna, A., Grigera, T. S. & Verrocchio, P. Thermodynamic signature of growing amorphous order in glass-forming liquids. *Nat. Phys.* **4,** 1–15 (2008).

35. Montanari, A. & Semerjian, G. Rigorous inequalities between length and time scales in glassy systems. *J. Stat. Phys.* **125,** 23–54 (2006).

36. Frank, F. C. Supercooling of Liquids. *Proceedings of the Royal Society A: Mathematical, Physical and Engineering Sciences* **215,** 43–46 (1952).

37. Frank, F. C. & Kasper, J. S. Complex alloy structures regarded as sphere packings. II. Analysis and classification of representative structures. *Acta Crystallographica* **12,** 483–499 (1959).

38. Kelton, K. F. *et al.* First x-ray scattering studies on electrostatically levitated metallic liquids: demonstrated influence of local icosahedral order on the nucleation barrier. *Phys. Rev. Lett.* **90,** 195504 (2003).

39. Ding, J., Cheng, Y. Q. & Ma, E. Full icosahedra dominate local order in Cu64Zr34 metallic glass and supercooled liquid. *Acta Mater.* **69,** 343–354 (2014).

40. Malins, A., Eggers, J., Royall, C. P., Williams, S. R. & Tanaka, H. Identification of long-lived clusters and their link to slow dynamics in a model glass former. *J. Chem. Phys.* **138,** 0–9 (2013).

41. Fang, X. W. *et al.* Spatially Resolved Distribution Function and the Medium-Range Order in Metallic Liquid and Glass. *Sci. Rep.* **1,** 19–21 (2011).

42. Kivelson, D., Kivelson, S. a., Zhao, X., Nussinov, Z. & Tarjus, G. A thermodynamic theory of supercooled liquids. *Phys. A Stat. Mech. its Appl.* **219,** 27–38 (1995).

43. Chayes, L., Emery, V. J., Kivelson, S. a., Nussinov, Z. & Tarjus, G. Avoided critical behavior in a uniformly frustrated system. *Phys. A Stat. Mech. its Appl.* **225,** 129–153 (1996).

44. Tarjus, G., Kivelson, S. a., Nussinov, Z. & Viot, P. The frustration-based approach of supercooled liquids and the glass transition: a review and critical assessment. **1143,** 48 (2005).

45. Sausset, F., Tarjus, G. & Viot, P. Tuning the fragility of a glass-forming liquid by curving space. *Phys. Rev. Lett.* **101,** 1–4 (2008).

46. Tarjus, G., Sausset, F. & Viot, P. Statistical Mechanics of liquids and fluids in curved space. 66 (2010). at <http://arxiv.org/abs/1005.2684>

47. Cheng, Y. Q., Sheng, H. W. & Ma, E. Relationship between structure, dynamics, and mechanical properties in metallic glass-forming alloys. *Phys. Rev. B - Condens. Matter Mater. Phys.* **78,** 1–7 (2008).

48. Shintani, H. & Tanaka, H. Frustration on the way to crystallization in glass. *Nature Physics* **2,** 200–206 (2006).

49. Patrick Royall, C., Williams, S. R., Ohtsuka, T. & Tanaka, H. Direct observation of a local structural mechanism for dynamic arrest. *Nat. Mater.* **7,** 556–561 (2008).

50. Pedersen, U. R., Schrøder, T. B., Dyre, J. C. & Harrowell, P. Geometry of slow structural fluctuations in a supercooled binary alloy. *Phys. Rev. Lett.* **104,** 1–4 (2010).

51. Mazoyer, S., Ebert, F., Maret, G. & Keim, P. Correlation between dynamical heterogeneities, structure and potential-energy distribution in a 2D amorphous solid. *Eur. Phys. J. E* **34,** 101 (2011).

52. Chen, S. P., Egami, T. & Vitek, V. Local fluctuations and ordering in liquid and amorphous metals. *Phys. Rev. B* **37,** 2440–2449 (1988).

53. Iwashita, T., Nicholson, D. M. & Egami, T. Elementary excitations and crossover phenomenon in liquids. *Phys. Rev. Lett.* **110,** 1–5 (2013).

54. Blodgett, M., Egami, T., Nussinov, Z. & Kelton, K. F. Unexpected Universality in the Viscosity of Metallic Liquids. 28 (2014). at <http://arxiv.org/abs/1407.7558>

55. Mendelev, M. I. *et al.* Experimental and computer simulation determination of the structural changes occurring through the liquid–glass transition in Cu–Zr alloys. *Philos. Mag.* **90,** 3795–3815 (2010).

56. Cheng, Y. Q. & Ma, E. Atomic-level structure and structure-property relationship in metallic glasses. *Prog. Mater. Sci.* **56,** 379–473 (2011).

57. Wang, W. H., Lewandowski, J. J. & Greer, a. L. Understanding the Glass-forming Ability of Cu50Zr50 Alloys in Terms of a Metastable Eutectic. *J. Mater. Res.* **20,** 2307–2313 (2005).

58. Sha, Z. D. *et al.* Glass forming abilities of binary Cu100-x Zrx (34, 35.5, and 38.2 at. %) metallic glasses: A LAMMPS study. *J. Appl. Phys.* **105,** 1–5 (2009).

59. Lee, M., Lee, C. M., Lee, K. R., Ma, E. & Lee, J. C. Networked interpenetrating connections of icosahedra: Effects on shear transformations in metallic glass. *Acta Mater.* **59,** 159–170 (2011).

60. Soklaski, R., Nussinov, Z., Markow, Z., Kelton, K. F. & Yang, L. Connectivity of icosahedral network and a dramatically growing static length scale in Cu-Zr binary metallic glasses. *Phys. Rev. B - Condens. Matter Mater. Phys.* **87,** (2013).

61. Wu, Z. W., Li, M. Z., Wang, W. H. & Liu, K. X. Correlation between structural relaxation and connectivity of icosahedral clusters in CuZr metallic glass-forming liquids. *Phys. Rev. B - Condens. Matter Mater. Phys.* **88,** (2013).

62. Wakeda, M. & Shibutani, Y. Icosahedral clustering with medium-range order and local elastic properties of amorphous metals. *Acta Mater.* **58,** 3963–3969 (2010).

63. Soklaski, R., Tran, V., Nussinov, Z., Kelton, K. F. & Yang, L. A Locally-Preferred Structure Characterizes All Dynamical Regimes of a Supercooled Liquid. *Arxiv Prepr. arXiv1502.01739*

64. Pauling, L. *The Nature of The Chemical Bond*. (Cornell University Press, 1960).

65. Cavagna, A., Attanasi, A. & Lorenzana, J. Viscoelasticity and metastability limit in supercooled liquids. *Phys. Rev. Lett.* **95,** 1–4 (2005).

66. Gibbs, J. H. Nature of the Glass Transition in Polymers. *J. Chem. Phys.* **25,** 185 (1956).

67. Zhao, J., Simon, S. L. & McKenna, G. B. Using 20-million-year-old amber to test the super-Arrhenius behaviour of glass-forming systems. *Nat. Commun.* **4,** 1783 (2013).

68. Bendert, J. C., Gangopadhyay, a. K., Mauro, N. a. & Kelton, K. F. Volume expansion measurements in metallic liquids and their relation to fragility and glass forming ability: An energy landscape interpretation. *Phys. Rev. Lett.* **109,** 1–5 (2012).

Chapter 2: Dynamical Regimes of Fragile Liquids

2.1 T_A: Avoided Criticality & the Onset of Cooperativity

Sections 1.3.4 and 1.4 introduced the characteristic liquid temperature T_A, which, in short, is thought to be associated with: 1) A transition from Arrhenius to super-Arrhenius growth in liquid viscosity (liquid relaxation time) with decreasing temperature.[1] 2) The development of geometrically-frustrated amorphous order in relation to an avoided critical point (as predicted by frustration-limited domain theory or FLDT)[1–4]. 3) The onset of cooperative dynamics[5] and the development of "solid-like" features in the liquid[6]. 4) And finally, possessing a strong correlation with T_G[7]. This section will be used to demonstrate and analyze the manifestation of these features of T_A in classical molecular dynamics (MD) simulation of liquid $Cu_{64}Zr_{36}$.

2.1.1 Locating T_A

From a conceptual standpoint, determining the value of T_A for a liquid is trivial – one measures a relaxation time in the liquid, τ_R, as a function of temperature and identifies the temperature below which $\tau_R(T)$ begins to exhibit super-Arrhenius growth. The empirical approach to this is to measure the liquid viscosity, which, as is seen in the Green-Kubo relation[8]**,** reflects the liquid's shear-stress relaxation time:

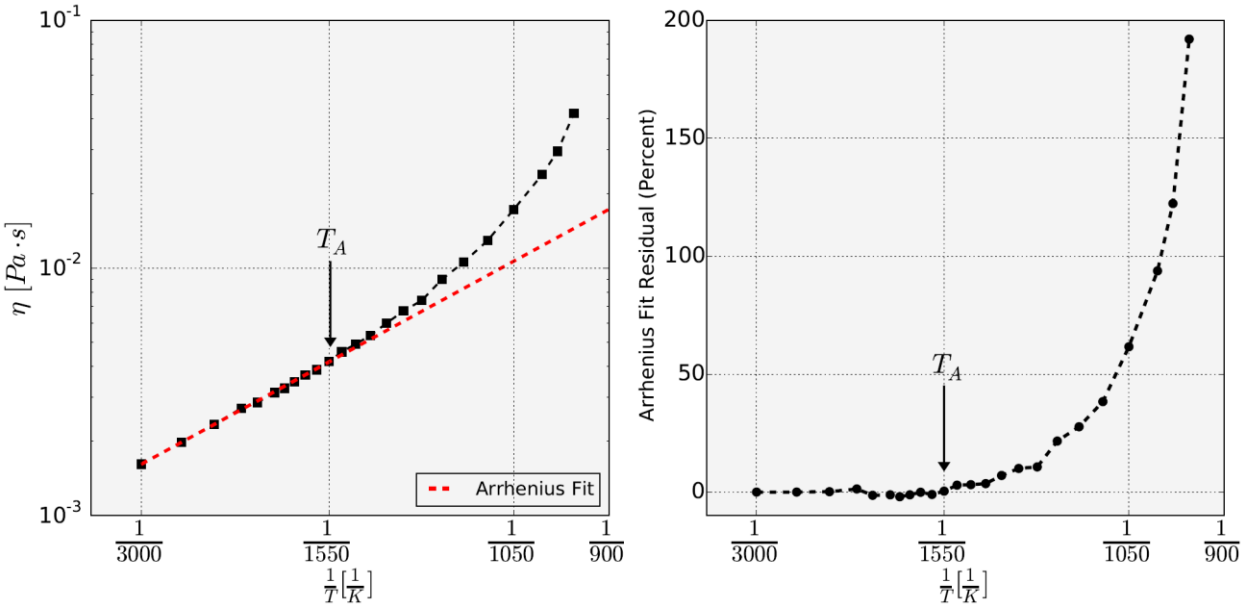

Figure 2.1 (Left) Liquid viscosity data, on a log-scale, versus inverse temperature for $Cu_{64}Zr_{36}$. The red dashed line indicates the high temperature ($T > 1900K$) Arrhenius fit for the data. T_A ($1550K$) is identified as the temperature below which $\eta(T)$ grows faster than the Arrhenius fit. (Right) The percent-residual of the viscosity data from the Arrhenius fit. This emphasizes the relatively clear onset of super-Arrhenius growth in $\eta(T)$.

$$\eta(T) = \frac{V}{k_B T}\int_0^\infty \langle \sigma_{ij}(t)\sigma_{ij}(0)\rangle dt \tag{2.1}$$

Here, $\sigma_{ij}(t)$ is an off-diagonal element of the time-dependent Cauchy shear stress tensor (represented in a cartesian basis)[8], V is the liquid volume, k_B is Boltzmann's constant, and T is the system temperature. The angular brackets formally indicate an ensemble average, but in practice they indicate a long time average over initial conditions. Implicit in this time average is the assumption that the liquid is ergodic and exhibits time-translation invariance; that is, $\langle \sigma_{ij}(t+\tau)\sigma_{ij}(\tau)\rangle \equiv F(t)$. **Figure 2.1** shows the temperature dependence of the liquid viscosity for $Cu_{64}Zr_{36}$, which was measured using the Green Kubo formula (equation 2.1)*. A high-temperature fit ($T > 1900K$) of the data is indicated by a red dashed line and reveals a clear Arrhenius form for $\eta(T)$ until the liquid is cooled to $1550K$. Below $1550\ K$, $\eta(T)$ exhibits

* See the **chapter 4** for further details regarding the calculation of $\eta(T)$.

super-Arrhenius growth - hence T_A is determined to reside at $1550\ K$ for this liquid, which is located well above its liquidus temperature, $1230\ K$[9]. It is noteworthy that this dynamical transition occurs at such a high temperature. Indeed, current numerical studies often tacitly assume that metallic liquids relax only via a simple diffusive process in the vicinity of this temperature, whereas this crossover indicates that multiple liquid relaxation processes can be at play above T_l. More precisely, it is found that the rearrangement of local clusters in the liquid becomes a cooperative process below T_A, and that this contributes to the liquid's accelerated viscous slowdown.

2.1.2 The Onset of Cooperative Structural Rearrangements at T_A

The analysis performed in a paper by Iwashita *et al.*[5] provides a framework for identifying the onset of cooperative structural rearrangements in metallic liquids. Similar to their approach, we measure the Maxwell relaxation time, τ_M (see equation 1.13), of $Cu_{64}Zr_{36}$ to quantify the timescale over which the liquid sustains a solid-like elastic response to a shear stress. Over timescales greater than τ_M, the liquid is able to flow in response to a shear stress, and thus relax. Naturally, a liquid's Maxwell relaxation time is directly related to its viscosity:

$$\tau_M = \frac{k_B T}{V\langle \sigma_{ij}(0)^2 \rangle}\eta \tag{2.2}$$

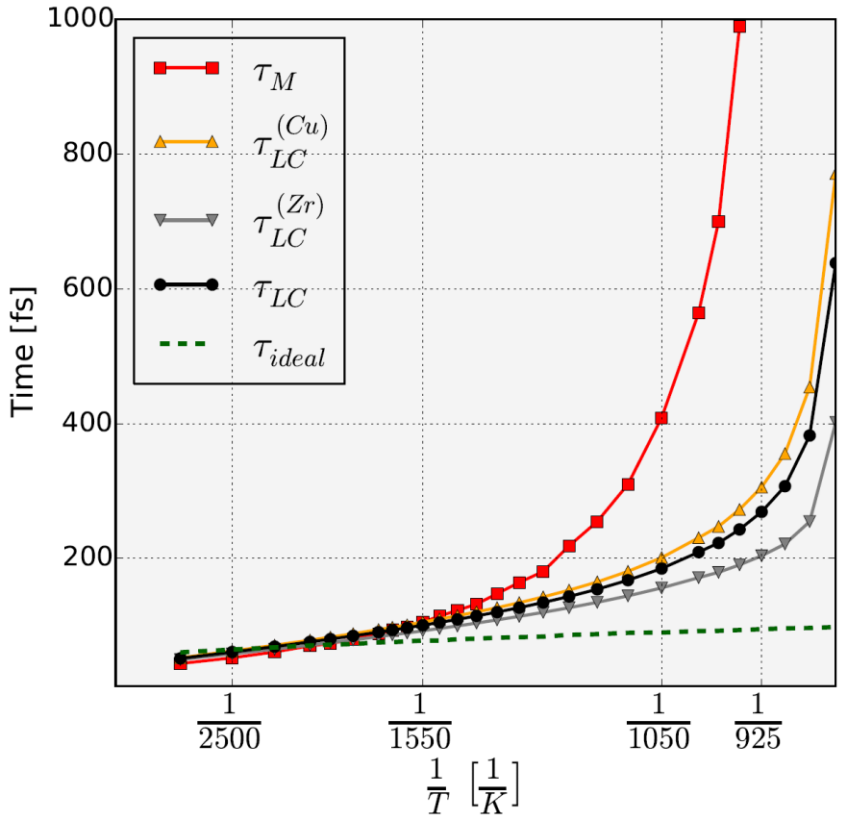

Figure 2.2 A comparison of the temperature-dependent Maxwell relaxation time with the local cluster time of $Cu_{64}Zr_{36}$ (on a log scale). $\tau_{LC}^{(Cu)}$ and $\tau_{LC}^{(Zr)}$ indicate the LCTs for Cu-centered and Zr-centered clusters, respectively. τ_{LC} is the average local cluster time, irrespective of atom-type. τ_{ideal} is an estimate of the local cluster time for non-interacting particles.

In order to understand the process of liquid relaxation in the context of atoms rearranging to accommodate shear stresses, one introduces a timescale known as the local cluster time (LCT), τ_{LC}. We define τ_{LC} to be the average time required for an atom to lose or gain a nearest neighbor (a schematic of this process can be seen in **Figure 1.5**). Here we define the nearest neighbors of a given atom to be the atoms which contribute faces to that atom's Voronoi cell[*†]. Though computationally costly, the radical Voronoi tessellation techniques provide a parameter-free

[*] The simulation of the liquid utilizes periodic boundaries, hence there are no surface effects to consider in the Voronoi analysis.

[†] The Voronoi tessellation scheme involves a set of planes that are defined such that each plane bisects a line that connects two atoms. An atom's Voronoi cell is then given by the set of planes that forms a closed surface containing the atom and enclosing the smallest volume.

method for determining nearest neighbors that can accommodate polydisperse systems appropriately[10–12]. Its advantages over using a hard-cutoff method will be discussed in **chapter 4**.

Figure 2.2 contains the Maxwell relaxation time and local cluster times for $Cu_{64}Zr_{36}$ on a log-scale versus inverse temperature. It is apparent that $\tau_{LC}^{(Cu)} > \tau_{LC}^{(Zr)}$ for all temperatures, and that the Cu-centered clusters become increasingly stable relative to the Zr-centered ones, with decreasing temperature. This is expected to an extent, given that Zr is larger than Cu[*] and thus has a larger coordination number (number of nearest neighbors) on average. This naively indicates that Zr has more opportunities to lose or gain neighbors than does Cu. That this disparity becomes enhanced with decreasing temperature is less trivial; this will be discussed further in the context of chemical ordering in the icosahedron network. Above T_A, the τ_M and τ_{LC} appear to collapse onto a single curve that approaches τ_{ideal} in the limit of large temperature. τ_{ideal} is an estimate of the local cluster time for an ensemble of non-interacting atoms whose spatial distribution is that of the liquid. More specifically, $\tau_{ideal}(T) \equiv \frac{d(T)}{2\sqrt{\langle v^2 \rangle(T)}}$, where $d(T)$ is the distance between the first maximum and the subsequent minimum in the liquid's pair correlation function[†] and $\langle v^2 \rangle(T)$ is the mean-squared velocity of the atoms[‡]. Thus one considers the average time needed for two atoms, moving freely in opposite directions, to leave one another's approximate nearest neighbor shell. The rapid growth of τ_M and τ_{LC} above τ_{ideal} then

[*] It is important, in order to exhibit good glass-forming ability, for a binary alloy to possess an atomic species size mismatch of at least 10%[42]. Indeed, Cu-Zr alloys exhibit a sufficient size mismatch: $R_{Zr}/R_{Cu} \approx 1.26$. This ratio can be obtained by either using Goldshmidt radii or "hard core" radii for Cu and Zr. Here, hard core radii are measured by finding the high-temperature ($T = 3000K$) minimum distance of separation between Cu atoms and Zr atoms, respectively.

[†] The location of first non-zero minimum in the pair correlation function is often used as the hard cutoff value for determining the nearest neighbors of an atom.

[‡] Naturally, $\langle v^2 \rangle$ can be calculated for each of the atomic species simply using the equipartition theorem.

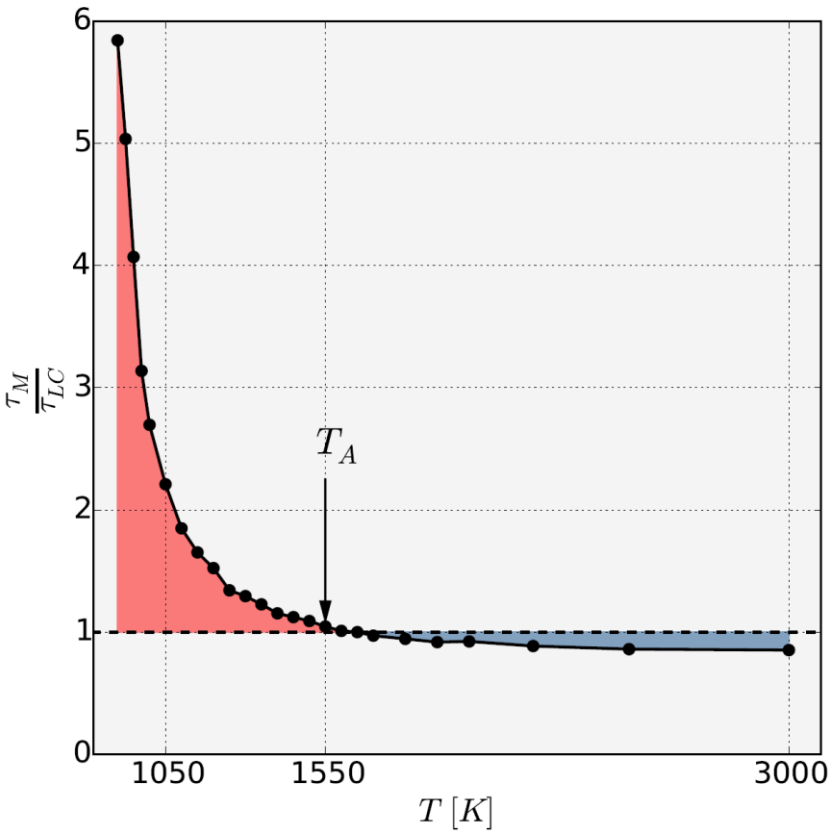

Figure 2.3 The ratio $^{\tau_M}/_{\tau_{LC}}$ versus temperature. An apparent crossover occurs at T_A, such that $\tau_M \approx \tau_{LC}$ for $T \geq T_A$, and $\tau_M > \tau_{LC}$ for $T < T_A$. This signifies a change in the liquid relaxation mechanism upon cooling.

signifies the increasing importance of the liquid's locally-packed structure in restricting particle motions.

Figure 2.3 depicts the temperature dependence of the liquid relaxation time relative to the atomic rearrangement timescale, $^{\tau_M}/_{\tau_{LC}}$. For $T \geq T_A$, one finds that $\tau_M \approx \tau_{LC}$. Upon further cooling, the growth in τ_M begins to accelerate such that $\tau_M > \tau_{LC}$ for $T < T_A$. These observations provide valuable insight towards explaining the characteristic onset of super Arrhenius in $\eta(T)$ below T_A: for high temperatures, a simple change in coordination of individual atomic clusters is sufficient for relaxing the liquid. Hence a single relaxation mechanism - local cluster rearrangements - produces the simple high-temperature exponential growth in $\eta(T)$ upon

cooling. Below T_A, consecutive cluster rearrangements occur within the relaxation timescale. This suggests that, in order to dissipate the liquid's elastic response to a shear stress, multiple cluster rearrangements must ensue in coordination with one another. As argued in FLDT and AGDM, the need to cooperatively rearrange larger regions of the liquid with decreasing temperature amounts to a growing activation energy barrier, which manifests as super Arrhenius growth in $\eta(T)$. Another perspective of this cooperative rearrangement is that, it is not until $\tau_M > \tau_{LC}$ that local atomic clusters have time to rearrange in a solid-like environment in response to more distant shear stresses. It will be shown in a later section that the result of these cooperative rearrangements is the development and growth of geometrically-frustrated amorphous order.

Beyond providing important insight towards the physical mechanisms underlying the dynamical crossover at T_A, the results presented in this section are important from a more practical standpoint as well. Although Iwashita *et al.* first demonstrated the relationship that $\tau_M \approx \tau_{LC}$ for $T > T_A$[5], it was never shown that the temperature at which this relationship broke down coincided with the standard measure of T_A – where $\eta(T)$ crosses over from Arrhenius to super Arrhenius growth. We directly confirm that these temperatures indeed correspond very closely with one another, lending important support that these two phenomena are indeed facets of the same crossover. Furthermore, all earlier measures of τ_{LC} utilized a hard cutoff method for determining nearest neighbors, which was insensitive to polydispersity and perhaps to changing liquid density. The values of τ_{LC} reported here employ a more meaningful definition of nearest neighbors by utilizing radical Voronoi tessellation. It is significant to find that the improved measure of τ_{LC} yields improved statistics that ratify these earlier findings with higher confidence.

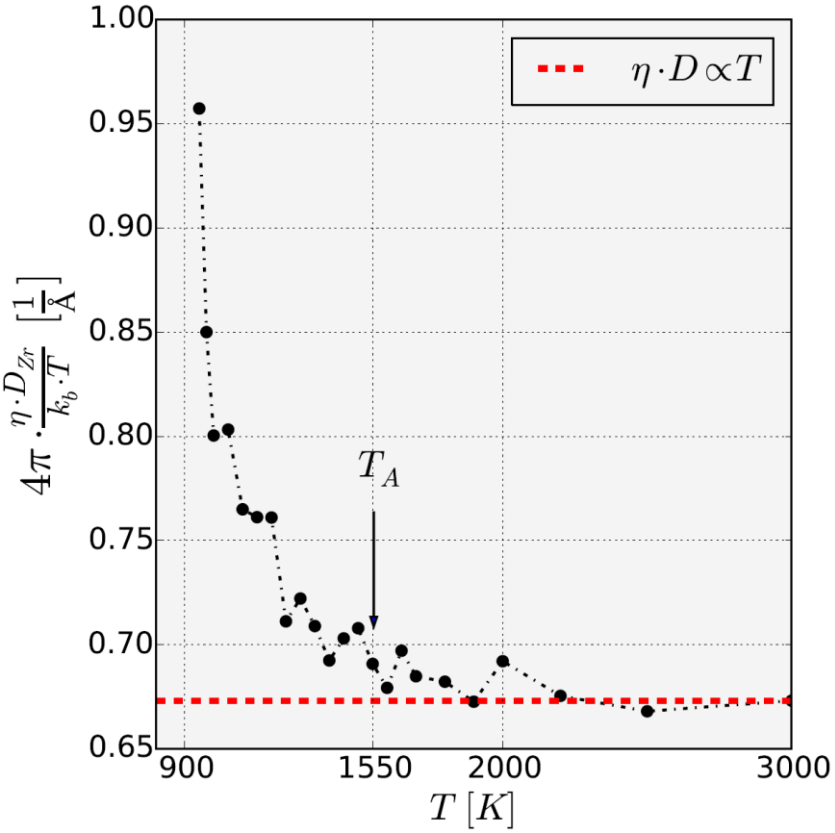

Figure 2.4 The temperature dependence of the Stoke-Einstein ratio for Zr atoms diffusing through the Cu solvent in $Cu_{64}Zr_{36}$. The deviation from the red dashed line near T_A signifies a violation of the Stoke-Einstein relationship.

2.1.3 Violation of the Stokes-Einstein Relationship at T_A

Yet another dynamical landmark is found to reside at T_A – the breakdown of the Stokes-Einstein relationship: $D(T) \propto \frac{T}{\eta(T)R}$[13]. Though derived for a large sphere of radius R diffusing through a solvent with viscosity η at a temperature T, this relationship tends to hold well in high temperature liquids for which D is the self-diffusion coefficient for similarly-sized particles or molecules. Upon supercooling, the relationship is found to break down due to the emergence of dynamical heterogeneity[14–18]; slow-moving regions dictate the timescale of structural relaxations, which is measured by η, whereas fast-moving regions enhance D such that $D \propto \frac{T}{\eta}$ is

no longer valid[*]. This breakdown plays an important role in producing characteristic glassy dynamics in the supercooled liquid. Indeed it is found that the more stark the violation of Stokes-Einstein, the more stretched the non-exponential decay becomes in the liquid's dynamical correlation functions[14].

Figure 2.4 contains simulation data of the Stokes-Einstein ratio, $4\pi \frac{\eta(T) D_{Zr}(T)}{k_B T}$ [†], where D_{Zr} is the coefficient of diffusion for Zr atoms. For high temperatures, the ratio is roughly a constant, 0.67, which is comparable to $1/R_{Zr} \approx 0.65\ 1/\text{Å}$ [‡] in accordance with the first-principles derivation of the relationship. Remarkably, it is found that the ratio deviates sharply from this value once the liquid is cooled below T_A. At first glance, this does not seem too surprising in light of the preceding results – the onset of local cooperative structural rearrangements enhances the structural relaxation time, but the resulting structures are not extensive enough nor are they sufficiently long-lived to inhibit the liquid's diffusivity proportionally[§]. That being said, literature reviews of supercooled liquids suggest that the Stokes-Einstein relationship ought to hold until one reaches a deeply supercooled regime[**19,20]. This prediction appears to be heavily informed by empirical studies of molecular liquids, such as *o*-terphenyl, where the violation occurs near the mode coupling temperature[21,22]. By this standard, one would expect to see the breakdown occur near $900\ K$ in $Cu_{64}Zr_{36}$, rather than at $T_A = 1550\ K$. Although empirical studies of the validity of the Stokes-Einstein relationship in metallic liquids are very limited, their results do support our findings[23–25]. Specifically, they show that the relationship breaks

[*] Specifically, $\eta(T)$ is found to grow far faster than $D(T)$ is able to decrease, so that at temperatures near T_G, $D \gg \frac{T}{\eta}$.

[†] This is the Stokes-Einstein relationship assuming "slip" boundary conditions[43].

[‡] Here, the Goldshmidt radius of Zr is used.

[§] It will be shown that these structures do eventually inhibit diffusion in the liquid, but at a significantly lower temperature.

[**] Namely, one would expect the violation to occur near the mode coupling temperature, or $1.2\ T_G$. Here we observe the breakdown of the Stokes-Einstein relationship near $2\ T_G$.

down far above the mode coupling temperature in metallic liquids, although they make no connection to T_A.

Though simple in form and of fundamental importance, the Stokes-Einstein relationship is difficult to test both experimentally and numerically. Frequently, simulation-based studies utilize measurements of the α-relaxation time (τ_α) in lieu of the liquid viscosity – this is a "short cut" in that one can calculate both D and τ_α using mean square displacement data[*]. It is not clear, however, that τ_α is a suitable approximation of η in this context. Furthermore, the fact that the same microscopic quantity determines both D and τ_α may cause a stronger coupling between these two quantities than is actually found between D and η; hence the Stokes-Einstein relationship may appear to be more robust if one were to utilize τ_α to measure the structural relaxation time. Indeed a simulation-based study of liquid $Cu_{64}Zr_{36}$ utilizing $\tau_\alpha$in lieu of η found that the Stokes-Einstein relationship was valid until the liquid was supercooled to $1050\ K$[26†], which is at odds with our direct check of the relationship.

[*] Furthermore, it is significantly more challenging to obtain converged numerical measures of η than it is τ_α.
[†] This study's results were also affected by their use of an unrealistic semi-empirical potential[28].

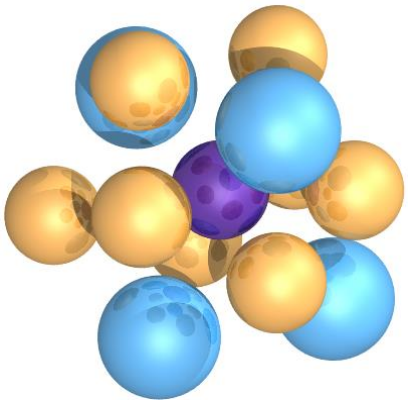

Figure 2.5 An illustration of typical Cu-centered icosahedral cluster of atoms in $Cu_{64}Zr_{36}$. The gold spheres represent Cu atoms while the blue spheres are Zr atoms. The purple sphere marks the center Cu atom. The cluster consists of 13 atoms in total.

It is interesting to note that the Stokes-Einstein relationship also breaks down well above the mode coupling temperature in water[18]. This breakdown accompanies a nearby fragile to strong transition and critical point[*]. It seems that the violation of Stokes-Einstein in $Cu_{64}Zr_{36}$ occurs in a similar context, indicating that this is a signature of an avoided critical point at T_A. Our finding thus stands out as one of the few direct numerical tests of the Stokes-Einstein relationship in realistic metallic liquids, and provides important insight into the cause of the high-temperature violation that is observed in this system and other metallic liquids. Furthermore, it motivates empirical efforts to verify that this breakdown indeed occurs at T_A, whereas earlier studies less precisely concluded that the violation occurs 'well above' the mode coupling temperature.

2.1.4 The Development & Growth of Frustration-Limited Domains

Given that the crossover at T_A is intimately connected to the development of cooperative structural rearrangements amongst locally-packed clusters of atoms and the breakdown of the Stokes-Einstein relationship, how does this crossover manifest in the structure of the liquid, if at all? This outstanding question is indeed a pressing one, yet it is frequently left unanswered in the

[*] This critical point marks a liquid-liquid phase transition in water.

context of most static length scale theories. The use of our unique large data analysis framework allows us to make important headway towards investigating this matter.

As discussed in **1.3.4**, frustration-limited domain theory (FLDT)[1], posits that, in avoiding the critical point at T_A, a liquid should begin to develop domains of amorphous order typified by the locally-preferred structure (LPS). These frustration-limited domains (FLD) are expected to become extensive as the liquid is supercooled and to play essential roles in shaping the system's glassy dynamics. The LPS of $Cu_{64}Zr_{36}$ is a Cu-centered icosahedral cluster of atoms (consisting of 13 atoms in total), which is illustrated in **Figure 2.5**[*]. In the glassy state, icosahedra are found to form highly connected structures by sharing atoms with one another- in the context of FLDT, these are the FLDs of $Cu_{64}Zr_{36}$. To gauge the relative stability of these icosahedral clusters as a function of temperature, we measured the icosahedron lifetime, τ_{icos}, which is the average time it takes for an icosahedral cluster to be disrupted after it is first created. Here, a disruption even includes geometric distortions such that one of the faces on its Voronoi cell is no longer a pentagon. For this reason, it is not obvious that τ_{icos} will exceed τ_{LC} since the latter timescale requires a cluster to lose or gain an atom entirely. A comparison of these timescales is provided in the left panel of **Figure 2.6**. Near $3000\ K$, the two lifetimes are comparable to one another. However, as the liquid is cooled it begins to become more impacted by its energy landscape and the lifetime of its LPS grows steadily beyond the average cluster lifetime. It is important to note that τ_{LC} does not discriminate against any cluster types – included in it are the stable icosahedra themselves. Thus the growth depicted here is truly a lower bound on the growing stability of the LPS relative to other atomic configurations.

[*] See **1.4.4** for discussion and references regarding the background of icosahedral ordering in $Cu_{64}Zr_{36}$.

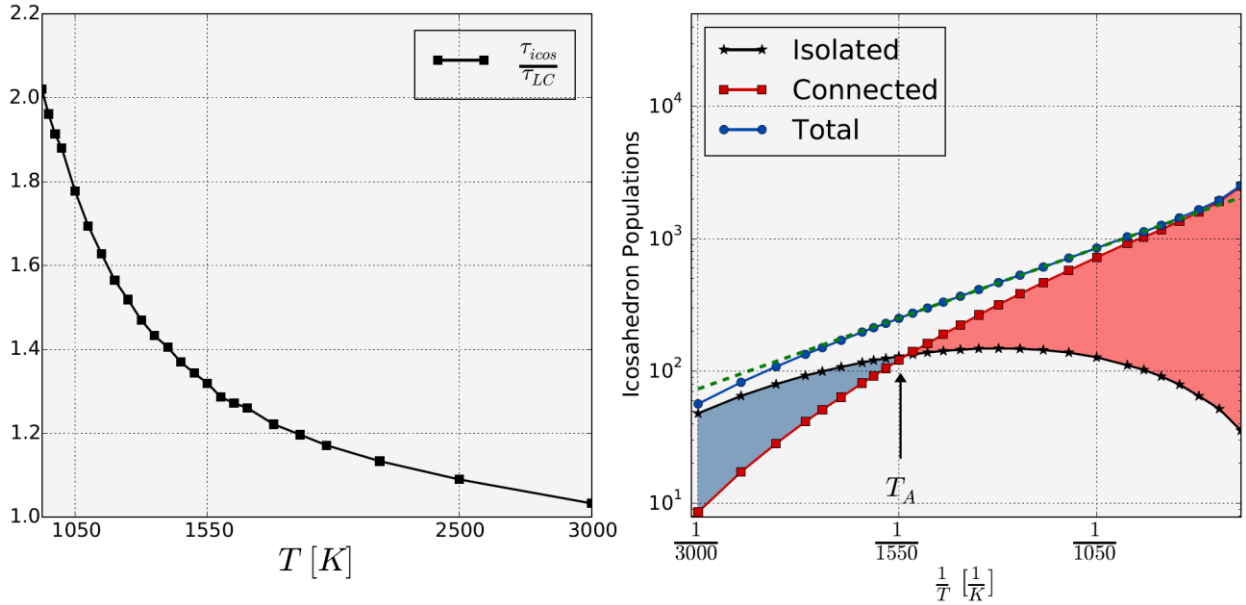

Figure 2.6 (Left) The temperature dependence of the ratio of the icosahedral cluster lifetime to the local cluster time. (Right) The isolated, connected, and total populations of icosahedral clusters, versus inverse temperature, in a 30,000 atom simulation of $Cu_{64}Zr_{36}$ shown on a log scale. At T_A the number of connected icosahedra exceed the isolated ones, and the total population begins to grow exponentially with inverse temperature. A dashed green line shows the exponential fit.

Also shown in **Figure 2.6** (right panel) is the temperature dependence of the populations of isolated and connected icosahedra, as well as the total icosahedron population, in a system size of 30,000 atoms*. For high temperatures, the population of icosahedra is small and is dominated by isolated members. Upon cooling, the number of connected icosahedra increases rapidly, and, remarkably, surpasses the isolated population at T_A. Below T_A, the total number of icosahedra grows exponentially with decreasing temperature, creating extensive FLDs of connected icosahedra. To our knowledge, these findings provide the first account for the structural impact of the onset of cooperativity at T_A. We've shown that as the liquid is cooled it becomes increasingly affected by its energy landscape, and thus the icosahedral clusters become stable relative to other atomic configurations. As the liquid begins to exhibit cooperative structural

* For temperatures above 850 K the populations scale exactly as N, the number of atoms in the liquid. This indicates that system size effects do not hinder the population growth until one is near $T_G \approx 750\ K$.

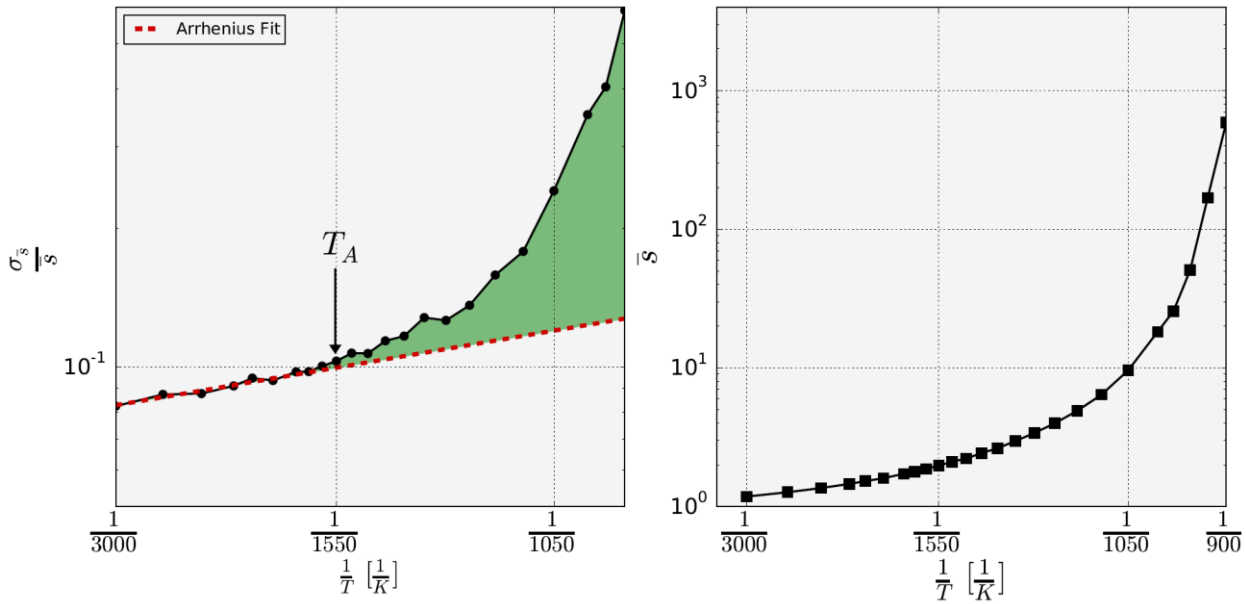

Figure 2.7 (Left) The relative dynamical fluctuations in the icosahedron-domain (FLD) size on a log-scale versus inverse temperature. The high-temperature fluctuations exhibit a weak Arrhenius growth until the system is cooled to T_A. Below this crossover temperature, the FLD fluctuations become increasingly enhanced. (Right) The icosahedron domain size, $\bar{s}$, on a log-scale as a function of inverse temperature. Here, $\bar{s}$ is defined as the average number of icosahedra found in a connected FLD.

relaxation mechanisms at T_A, atoms rearrange amidst the relatively inert icosahedra and form off of them new, connected icosahedra. This also strongly suggests that the cooperative crossover is indeed associated with an avoided critical point: as predicted by FLDT, cooling through T_A results in the development of FLDs. We also find that these FLDs become extensive upon cooling, and begin to exhibit enhanced fluctuations in association with structural rearrangements.

To track the growth and dynamics of FLDs in $Cu_{64}Zr_{36}$, we measured the time and temperature evolution of the distribution of its FLD sizes. Here, the size of a FLD is given by the number of icosahedra participating in a single connected domain. Relevant weighted-averages of the sizes are given by:

$$\bar{s}(t,T) \equiv \frac{\sum_{s_i \in \{s\}_t} s_i^2}{\sum_{s_i \in \{s\}_t} s_i}, \qquad \bar{s}(T) \equiv \frac{\sum_t \sum_{s_i \in \{s\}_t} s_i^2}{\sum_t \sum_{s_i \in \{s\}_t} s_i} \tag{2.3}$$

where $\{s\}_t$ the set of FLD sizes observed at time step t, and the summation index t runs over all recorded time steps at temperature T. The former average represents the average FLD size at time t and the latter is a time-averaged FLD size. Dynamical fluctuations are thus measured using the time-averaged deviation:

$$\sigma_{\bar{s}} \equiv \frac{\sqrt{\sum_t (\bar{s}(t,T) - \bar{s}(T))^2}}{N_t} \tag{2.4}$$

where N_t is the total number of time steps. The left panel of **Figure 2.7** shows the temperature dependence of the relative dynamical fluctuations, $\frac{\sigma_{\bar{s}}}{\bar{s}}$, on a log-scale. For high temperatures, where the liquid dynamics are simple and icosahedral ordering is depressed, the fluctuations exhibit only weak exponential growth with decreasing temperature. Cooling through T_A produces a relatively sharp enhancement in FLD size fluctuations – the onset of cooperative dynamics and emergence of FLD-ordering results in FLDs that attempt to grow beyond their mean size before eventually breaking apart, thus bolstering $\frac{\sigma_{\bar{s}}}{\bar{s}}$. In a sense, these fluctuations represent failed attempts of the system locally sampling deeper regions of its energy landscape, which correspond to further propagating the system's LPS*. Cooling the liquid is found to stabilize these more-extended FLDs and to thus enhance their mean size. The right panel of **Figure 2.7** shows the growth of $\bar{s}(T)$ with decreasing temperature. At T_A, the population of connected icosahedra begin to dominate the total icosahedron population, $\bar{s}(T_A) \approx 2$. This indicates that a typical icosahedral cluster in the liquid is connected to one other icosahedron. This average FLD size proceeds to grow tremendously under cooling – note that this exponentially-shaped curve

* It may seem strange that sampling "deeper" energy wells leads to structures that are bound to break apart. One must keep in mind that creating FLDs comes at an entropic cost, and that the free energy is what must be minimized. This, however, requires its own caveat – the true free energy minimum is the crystal when the liquid is supercooled. We are tacitly assuming that the liquid is constrained in its timescale from arriving at this true minimum.

appears on a log-scale*. This is a remarkable confirmation of essential predictions made by FLDT – amorphous order typified by the liquid's LPS (Cu-centered icosahedra in $Cu_{64}Zr_{36}$) begins to become prominent at T_A and serves a rapidly growing static length scale that accompanies the supercooled liquid's dynamical slowdown†. While it is not currently feasible to empirically observe the development of FLDs near T_A, these simulation results provide perhaps the strongest evidence that one could hope for. Because a real glass forming liquid is being simulated, one can make direct comparisons with experiments to verify findings. Empirically, one does observe the dynamical crossover to super-Arrhenius growth of $\eta(T)$ below T_A[7]. Furthermore, diffraction experiments produce pair correlation functions that agree well with those obtained from simulations of $Cu_{64}Zr_{36}$[27,28]. The agreement between experiment and simulation in these measurements suggest that the underlying microscopic mechanisms are indeed captured by the simulation. It is important to note, also, that liquid simulation results are most reliable for high temperatures (near T_A). Here, liquid relaxation times are sufficiently short so that the limited simulation timescale is still representative of ergodic behavior.

2.1.5 The Correlation Between T_A & T_G

Of the four characteristics of T_A summarized at the beginning of **2.1**, the simplest relationship to confirm is perhaps the most intriguing one – that $T_A \approx 2 \times T_G$. In the context of our work, confirming this correlation for simulated $Cu_{64}Zr_{36}$ does not seem to accomplish much beyond adding this alloy to the long list of metallic liquids for which this relationship has been tested. However, it is valuable to test whether or not the relatively simple semi-empirical potential describing this alloy is accurate enough to reproduce a correlation between such disparate, but

* Indeed, it is found that $\bar{s}(T) \propto e^{Ae^{B/T}}$ for $T_A < T$. This is not a typo.
† The matter of icosahedral ordering serving as a rapidly growing length scale will be discussed in more detail in a later chapter.

important temperatures. Furthermore, the preceding results and discussions in this section provide us with a context in which we can begin to surmise the origin of the surprising connection between T_A and T_G.

First we must discuss some practical limitations that effect all MD simulations. The timescales accessible to classical MD simulations are exceedingly short ($\sim 1 - 100\ ns$). For this reason, it is impossible to directly measure T_G by finding the temperature at which $\eta(T) = 10^{12} Pa \cdot s$. Indeed, this corresponds to simulating a relaxation process that is approximately $10^3\ s$ long, which is far beyond the scope of any simulation*. Rather, one identifies T_G by looking for evidence of the liquid falling out of metastable equilibrium; this can entail looking for structural signatures of the system "freezing" beneath a temperature, or looking for a sudden drop in the supercooled liquid's specific heat. The extracted value of T_G can then be compared with empirical results. One can also locate the temperature at which a fitted form of $\eta(T)$ extrapolates to $10^{12} Pa \cdot s$†. Ultimately, it is important to note that the concept of the glass transition is somewhat ill-defined in the context of MD simulations‡.

* Both A. Cavagna[19] and Y. Cheng *et al.*[27] provide illuminating discussions of the limitations and implications of the "computer laboratory" timescale.

† Given its simplicity and relatively good success, the VFT form is almost invariably utilized for such a task.

‡ The value of T_G is also fundamentally affected by the cooling rate one uses when supercooling a liquid. Fortunately, fragile liquids, such as $Cu_{64}Zr_{36}$, are less sensitive to the cooling rate and T_G likely shifts only by $\sim 10\ K$ across typical rates[19].

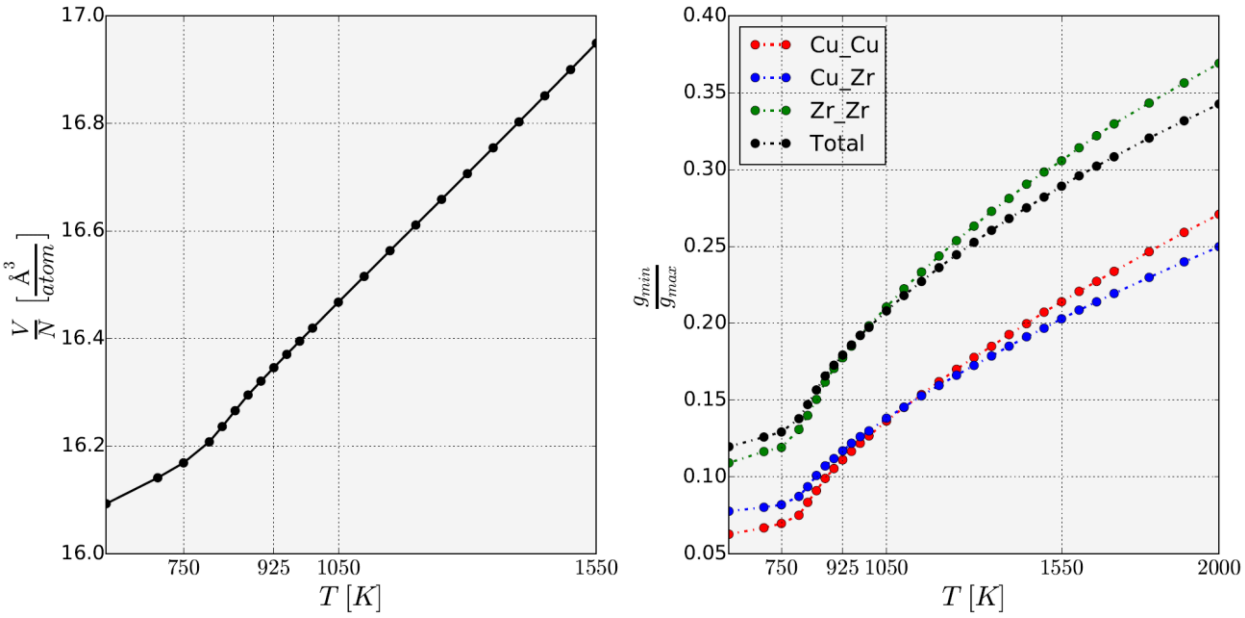

Figure 2.8 (Left) The temperature dependence of the volume per atom in $Cu_{64}Zr_{36}$. A transition between a liquid and crystal-like thermal expansion coefficient occurs near $750\ K$. (Right) The ratio between the height of the first maximum and first nonzero minimum of the partial and total pair correlation functions. The temperature evolution plateaus below approximately $750\ K$.

Upon falling out of equilibrium, the thermal expansion coefficient of the glass changes smoothly in a narrow temperature range from that of the liquid to a value similar to that of a crystal. Thus, we locate the approximate value of T_G in $Cu_{64}Zr_{36}$ by observing the temperature evolution of its volume. The left panel of **Figure 2.8** indicates that a change in thermal expansivity occurs near $750\ K$. An independent study using the same potential finds the same volume behavior; they also find that a sharp change in specific heat occurs at $770\ K$[28]. The right panel of the figure shows the temperature evolution of the ratio of the heights of the first maximum to the first nonzero minimum of the system's partial and total pair correlation functions. As the system falls out of equilibrium, its structure "freezes" and the ratios suddenly become weakly temperature dependent. This occurs between $800\ K$ and $750\ K$ depending on the pair correlation function being considered. Thus, based on these phenomenological considerations, we find that T_G resides near $750\ K$ for this potential, which is in reasonable agreement with the empirically measured glass transition temperature for $Cu_{64}Zr_{36}$, $737\ K$[9]. We therefore find that our simulation results

also satisfy the empirically-observed correlation $T_A \approx 2 \times T_G$ (where $T_A = 1550\ K$ and $T_G = 750\ K$) to reasonable accuracy.

In summary, we have shown that T_A acts as the "barrier" temperature separating the simple behavior of a high temperature liquid from the cooperative, heterogeneous dynamics that drive the increasingly viscous low temperature liquid. Interestingly, this crossover precedes the supercooled regime by several hundred Kelvin, yet cooperative and heterogeneous dynamics are typically thought to be characteristics of a supercooled liquid. In light of these findings and especially of the empirically-rooted relationship $T_A \approx 2 \times T_G$, it seems reasonable to expect that important dynamical and structural features will arise in metallic liquids at temperatures that are considerably higher than current conventions predict. Furthermore, the observed onset of icosahedral ordering at T_A serves not only as important support for FLDT, but also as a preliminary explanation for the apparent link between T_A and T_G. Indeed, the state of $Cu_{64}Zr_{36}$ at T_G is known to be dominated by its icosahedral networks (see **1.4.4** for more details), and the origin of this amorphous phase lies at the apparent avoided critical point at T_A. That being said, there is a major gap between the structure and dynamics developing at T_A and those that are found to precede the glass transition. While T_A exhibits early cooperative and heterogeneous dynamics, the "glassy" dynamics of a deeply supercooled liquid are associated with a pronounced two-step relaxation process and caged particle dynamics. We will now discuss the development of glassy dynamics in supercooled $Cu_{64}Zr_{36}$ in the context of the structures and dynamics that originate at T_A. Furthermore, we will consider how these FLD-based features fit within the context of other theories of supercooled liquids, such as mode coupling theory, and Goldstein activated dynamics.

2.2 Supercooled Regime: Higher Order Cooperativity & the Onset of Glassy Dynamics

Section **1.2** provided an introductory discussion of the characteristic two-step relaxation process that develops, in association with caged particle dynamics, in a supercooled liquid as it nears T_G. Here we look at the development of glassy dynamics in the context of extensive and rapidly-growing FLDs (connected domains of Cu-centered icosahedral clusters) in supercooled $Cu_{64}Zr_{36}$. It is necessary to develop a bridge to link the structural and dynamical features that emerge at the high temperature T_A with the terminal, rigid icosahedron network that shapes the glass below T_G. We will show that a temperature, $T_A > T_D > T_G$, is closely associated with the onset of glassy supercooled liquid dynamics, and that, similar to T_A, this temperature is linked to the emergence of new structural cooperativity. Supercooling through T_D produces tremendous growth in FLDs and rapid unification amongst them. Indeed, on the scale of the simulation ($\sim 3 \times 10^4$ atoms), the average FLD begins to contain a macroscopic number of icosahedra. Hence the FLD size becomes an extensive quantity as does its fluctuations. This leads to some surprising observations, which suggest that T_G may be preceded by a liquid-to-liquid phase transition.

2.2.1 Defining T_D: The Onset of Glassy Dynamics

To identify the temperature range in which supercooled $Cu_{64}Zr_{36}$ exhibits a pronounced two-step relaxation process, we analyze the time-trajectories of the mean squared-displacements (MSDs) of the liquid's particles for different temperatures. **Figure 2.9** contains mean squared-displacement trajectories for liquid temperatures starting at $2000\ K$ and decreasing to $800\ K$ in

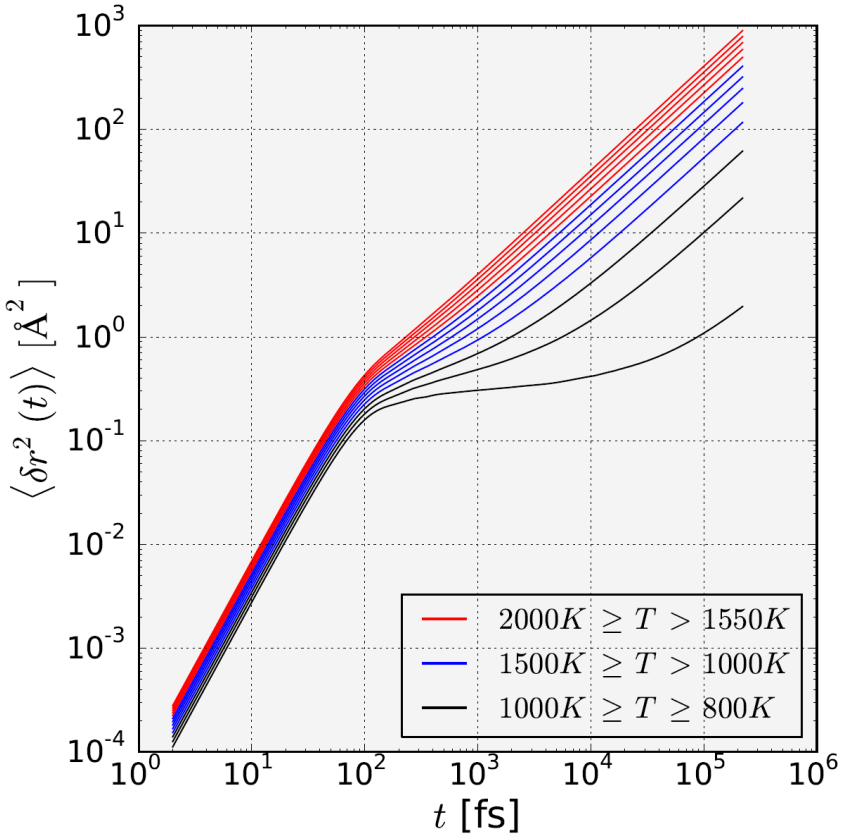

Figure 2.9 The time trajectories of the mean squared-displacements of atoms in $Cu_{64}Zr_{36}$ on a log-log scale. The temperatures included in the plot are separated by 100 K intervals. Dynamical regimes are color coded. A distinct plateau feature develops for temperatures below 1100 K.

intervals of 100 K. The trajectories are color coded to help distinguish between dynamical regimes. The red trajectories reside above T_A. Accordingly, one sees that the dynamics in this regime are simple – the atoms undergo free motion on the timescale of roughly 10^2 fs, and transition to diffusive motion over larger timescales. Here, much of the temperature dependence is a result of the simple kinetic reduction in the average speed of the atoms. Cooling through T_A results in a gradual but important change in the shape of the trajectories. The blue trajectories begin to enter the long-time diffusive motion asymptote ($\langle \delta r^2(t) \rangle \sim 6Dt$) from above (that is, the trajectory is concave up). This signifies the development of physical processes that impede relaxation in the liquid. This, of course, corresponds to the onset of cooperative restructuring and the breakdown of the Stokes-Einstein relationship that was found in relation to cooling through

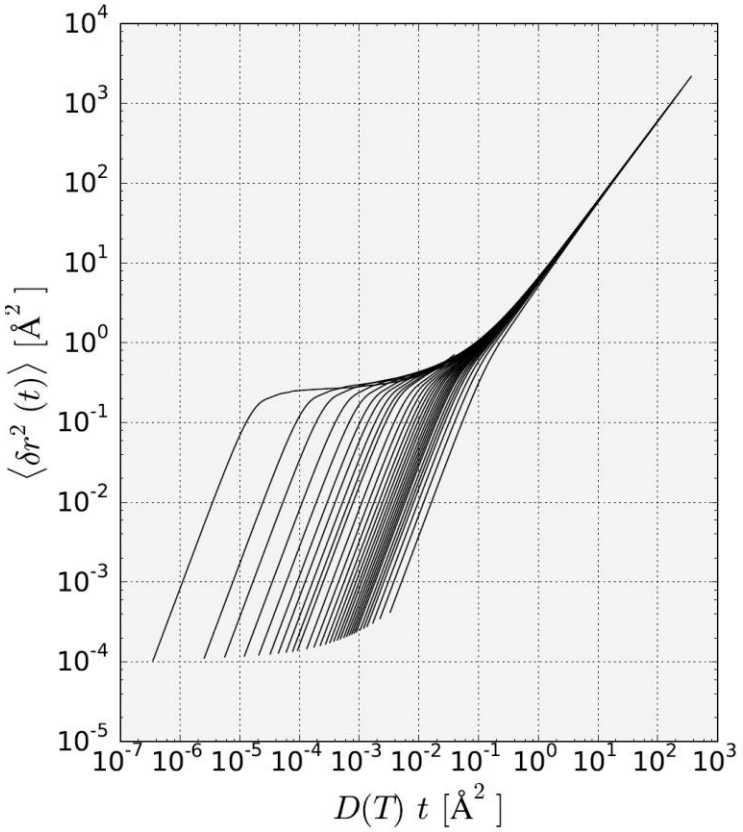

Figure 2.10 MSD time-trajectories plotted on a log-log plot whose timescale is scaled by the temperature-dependent particle diffusivity. This scaling causes low-temperature trajectories to fall to the left of high-temperature ones. The apparent collapse of the trajectories for long times is a manifestation of the time-temperature superposition principle.

the avoided critical point at T_A. The gap separating the free-motion timescale from the diffusive motion one is found to widen rapidly as one supercools below $1100\ K$. This regime corresponds to the black trajectories. Here, one can clearly see the characteristic plateau feature emerge to separate the liquid's β and α-relaxation processes. Within this relatively narrow temperature range, the plateau extends by several orders of magnitude. This mirrors the tremendous viscous slowdown that is occurring simultaneously.

The MSD-trajectories are presented once again, in **Figure 2.10**, but now on a time-axis that is scaled by the particle diffusivity, $D(T) = \lim_{t\to\infty} \frac{\langle \delta r^2(t) \rangle}{6t}$. The eventual collapse of the trajectories onto a universal curve is a manifestation of a phenomenon known as the time-temperature

superposition principle[*29]. This indicates that the strong temperature dependence exhibited in **Figure 2.9** is controlled by a characteristic timescale, which is proportional to $^1/_{D(T)}$, that determines the long-time dynamics of the system. T_A was defined by identifying the temperature below which the liquid relaxation time (reflected by $\eta(T)$) departed from a simple exponential form. Similarly, given this timescale that characterizes long-time supercooled dynamics, we look to $D(T)$ to find an analogous crossover temperature in the supercooled regime of $Cu_{64}Zr_{36}$.

The diffusion coefficients for Cu and Zr atoms, and their composition-weighted average, are plotted on a log scale versus inverse temperature in the left panel of **Figure 2.11**. D_{Cu} and D_{Zr} follow a simple exponentially-decaying curve across a wide temperature window that enters well into the supercooled regime. The right panel of the figure contains a plot of the ratio $\frac{D_{Cu}}{D_{Zr}}$ versus inverse temperature; indeed, this ratio is nearly constant across this temperature range and is determined roughly by the inverse ratio of the atom's effective radii: $\frac{D_{Zr}}{D_{Cu}} \approx \frac{R_{Cu}}{R_{Zr}} = 0.79$[†]. Supercooling through $1050\ K$ produces a stark change in the diffusive dynamics of the system – the diffusion coefficients begin to deviate significantly from the exponential form, and drop much more rapidly with decreasing temperature. In terms of the characteristic timescale discussed above, this corresponds to the onset of super-Arrhenius growth of $\tau_D(T) \sim \frac{1}{D(T)}$. Hence, we label this crossover temperature, $T_D = 1050\ K$, in analogy with T_A.

[*] The curve that is traced out by the lower-temperature trajectories can be fitted using a polynomial. This allows one to define a useful quantity, known as the non-ergodicity parameter, which allows one to quantify the caging plateau.
[†] This ratio is calculated using the "hard-sphere" radii of the atoms, as obtained from the high-temperature partial pair correlation functions. Using Goldschmidt radii yields a similar ratio.

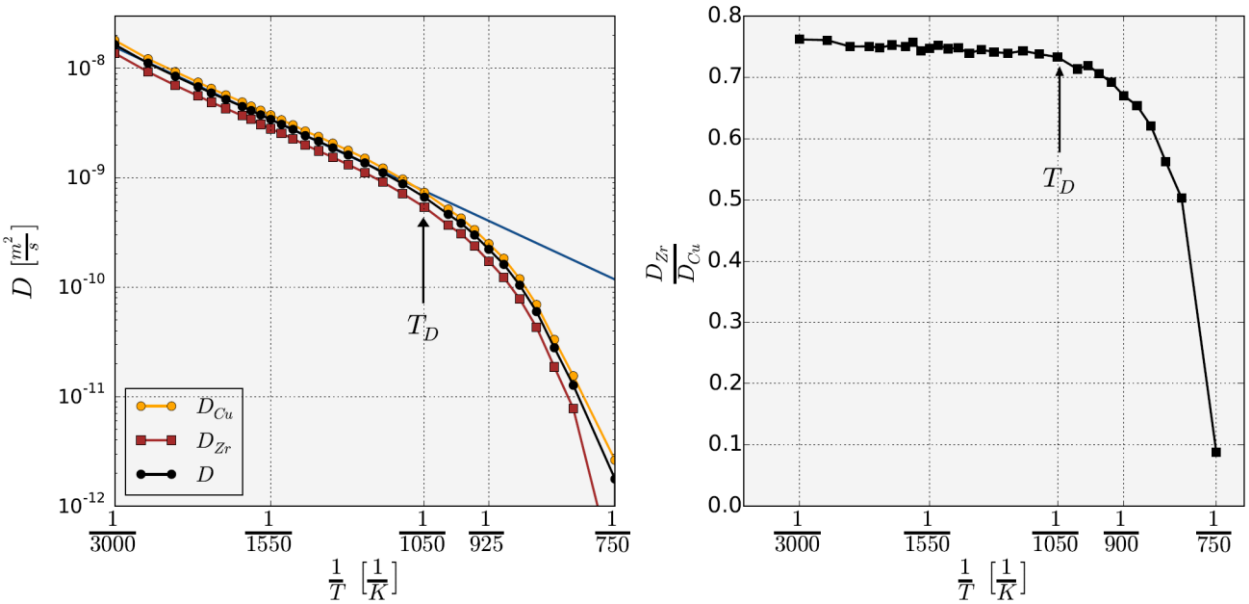

Figure 2.11 (Left) The diffusion coefficients of Cu atoms, Zr atoms, and their composition-weighted average, on a log scale versus inverse temperature. A high-temperature inverse-exponential fit is indicated by a solid blue line. The diffusion coefficients depart from this inverse exponential at $T_D = 1050\ K$. (Right) The ratio of Zr diffusivity to that of Cu versus inverse temperature. Supercooling through T_D results in a sharp decoupling of particle diffusivities.

What is the physical significance of T_D? Reflecting on the MSD trajectories plotted in **Figure 2.9**, the atomic diffusivity is proportional to the y-intercept of the long-time asymptote on the log-log scale. Thus, the dramatically-extending plateau feature that develops in the trajectories corresponds to the rapid drop in $D(T)$ that begins at T_A. *We therefore conclude that T_D marks the onset of the pronounced caged particle dynamics that typify the two-step relaxation process associated with supercooled liquids dynamics.* As seen in the right panel of **Figure 2.11**, T_D also corresponds to the temperature below which the Cu and Zr diffusivities sharply decouple from one another. Both of these observations indicate that a structural feature is emerging at T_D that strongly affects the supercooled liquid's dynamics. This becomes clear when one considers that Cu and Zr cease to diffuse via the same physical mechanism at T_D. Here, the system's energy landscape begins to disproportionately impede the activation of the larger Zr atoms, whereas the Cu atoms likely participate in collective high mobility regions of the liquid[30]. This enhanced,

biased energy landscape effect, and the resulting structure that it produces, is then likely to be responsible for the caged particle dynamics that greatly depress the diffusivities of both species. Recently, an empirical study of a Zr-based metallic liquid also found that the diffusivities of the liquid's components decouple at a temperature residing above the mode coupling temperature, lending support for our findings regarding T_D[31].

Beyond its broader implications of structure-affected dynamics, the decoupling of D_{Cu} and D_{Zr} at T_D, in conjunction with earlier measurements of τ_{LC}, provides us with more detailed information about the specific structure that develops at T_D. When Basuki *et al.* detected high-temperature decoupling of diffusivities in a Zr-based metallic liquid, they found, as we did, that D_{Zr} is depressed relative to the diffusivities of the other components of the liquid[31]. They explain this dynamical asymmetry in the context of T. Egami's local configurational excitations (LCE), arguing that there must be a larger activation barrier associated with changing the nearest neighbor coordination shell of Zr than there is for Cu, and that this encapsulates the depressed behavior of Zr. Interestingly, we find that this is not the case[*]. As shown in **Figure 2.2**, $\tau_{LC}^{(Zr)} < \tau_{LC}^{(Cu)}$ for all temperatures, indicating that it is systematically easier to change the coordination of Zr than it is Cu. This is counterintuitive in light of the fact that $D_{Zr} > D_{Cu}$ and that both inequalities become stronger with decreasing temperature. Ultimately these contrasting relationships reflect a difference in the structural roles played by Cu and Zr. Although Zr is slow to diffuse at low temperatures, its nearest neighbor structure is less robust than is Cu's. From the perspective of Cu-centered icosahedra being the LPS of $Cu_{64}Zr_{36}$, Cu atoms uniquely reside at

[*] Confusion may have resulted from the fact that Egami *et al*.[5] used a single hard cutoff value to determine the coordination shell of its atoms. This means that Zr's coordination shell radius is likely underestimated, while Cu's is overestimated. In this situation, Zr's coordination shell only consists of its most intimate neighbors, while are less likely to change than are more distant neighbors. Cu suffers from the opposite scenario. Hence $\tau_{LC}^{(Zr)}$ may be artificially inflated (but unintentionally so, surely) by the use of this single cutoff distance.

the center of these packed structures. While Zr atoms serve as stable vertex atoms in this cluster, their neighboring atoms that lay outside of the cluster may move freely relative to the icosahedron, thus changing the coordination of the Zr atom and depressing $\tau_{LC}^{(Zr)}$. This hints at the crucial role played by Zr in connecting adjacent icosahedra to form an FLD; this matter will be discussed in detail in a later chapter.

It is prudent to note that T_D is close to the temperature where convention would suggest that the Stokes-Einstein relationship ought to break down and dynamical heterogeneities emerge (keeping in mind that these landmarks occur at T_A instead, in $Cu_{64}Zr_{36}$). Indeed, the decoupling of component diffusivities certainly indicate that dynamical heterogeneities become exceedingly pronounced at T_D, which may suggest why an empirical search for heterogeneities would first detect signatures here. That is, heterogeneities are expected to be small in extent and short-lived at T_A – probes used in experiments to detect these heterogeneities may inadvertently average over them and thus conclude that the liquid is still homogeneous. It was noted earlier that some studies utilize the α-relaxation time, τ_α, in lieu of $\eta(T)$ to test the Stokes-Einstein relationship, and that τ_α is calculated using long-time particle displacements, as is $D(T)$. In light of the results presented in **Figure 2.11**, perhaps these studies detect the breakdown of the inverse exponential decay of $D(T)$ at T_D, that manifests simultaneously in $D(T)$ and τ_α, rather than the actual viscous decoupling of $\eta(T)$ and $D(T)$, which we found occurs at T_A. It would thus be fruitful to do a direct comparison of $\frac{\eta(T)D(T)}{T}$ versus $\frac{\tau_\alpha D(T)}{T}$ to verify this conjecture.

2.2.2 Higher Order Cooperativity & FLDs

Given the apparent emergence of a structural signature at T_D that causes both a rapid decrease in atomic diffusivities and a decoupling of D_{Cu} and D_{Zr} in the supercooled liquid, we turn our

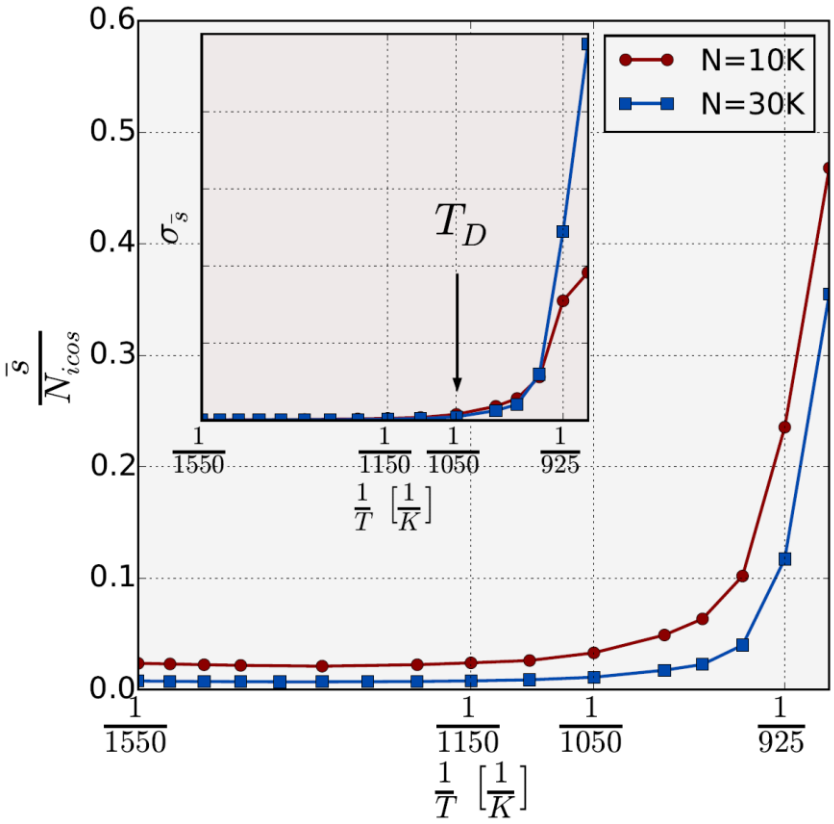

Figure 2.12 (Main) The fraction of icosahedra contained in a single, average FLD as a function of inverse temperature for simulations of 10^4 atoms and 3×10^4 atoms. Cooling through T_D (1050 K), a macroscopic fraction of icosahedra are incorporated into the FLD (on the scale of the simulation). (Inset) The dynamical fluctuations in domain size as a versus inverse temperature for both system sizes. Enhanced fluctuations arise upon cooling through T_D.

attention to the FLDs that emerged at T_A to consider what roles they play in this supercooled regime. At T_D, the average FLD size, $\bar{s}$, is 10 (see **Figure 2.7**), which boasts a fivefold increase from the size measured at T_A. The main panel of **Figure 2.12** shows, versus inverse temperature, the fraction of the liquid's icosahedra that are contained in an average FLD. This includes data for simulation system sizes of 10^4 atoms and 3×10^4 atoms, respectively. Above T_D, a typical FLD contains a negligible fraction of icosahedra. Upon supercooling through T_D, this fraction beings to grow appreciably and, on the scale of these simulations, an average FLD begins to represent a macroscopic portion of the icosahedron population. Analogous behavior is exhibited by the dynamical fluctuations of the FLDs, as measured by $\sigma_{\bar{s}}$ (equation 2.4), which is shown in

the inset of **Figure 2.12**. Here, the fluctuations indicate attempts made by FLDs to grow beyond $\bar{s}$ before collapsing. As the FLDs begin to incorporate a large fraction of the liquid's icosahedra, the fluctuations are found to become dramatically enhanced. Both of these features support our interpretation that the supercooled dynamics developing at T_D are indeed heavily influenced by the energy landscape, and that a major structural signature, i.e. extensive connected domains of icosahedra, is emerging in association with this. The decoupling of D_{Cu} and D_{Zr}, then, is caused by a compositional dependence of the dynamics created by this structure. A crucial finding is that *the Cu-centered icosahedra and the connected domains that they form are Zr-rich compared to the system composition* (this result will be presented formally in a later chapter). Hence, solid-like regions formed by FLDs preferentially incorporate Zr atoms, while liquid-like regions are Cu rich[*].

[*] If one leaves a piece $Cu_{64}Zr_{36}$ of metallic glass in storage for long enough, the sample's surface will eventually take on a distinct Cu color. Though anecdotal, this does suggest that the more mobile, liquid like regions in the material are indeed Cu-rich.

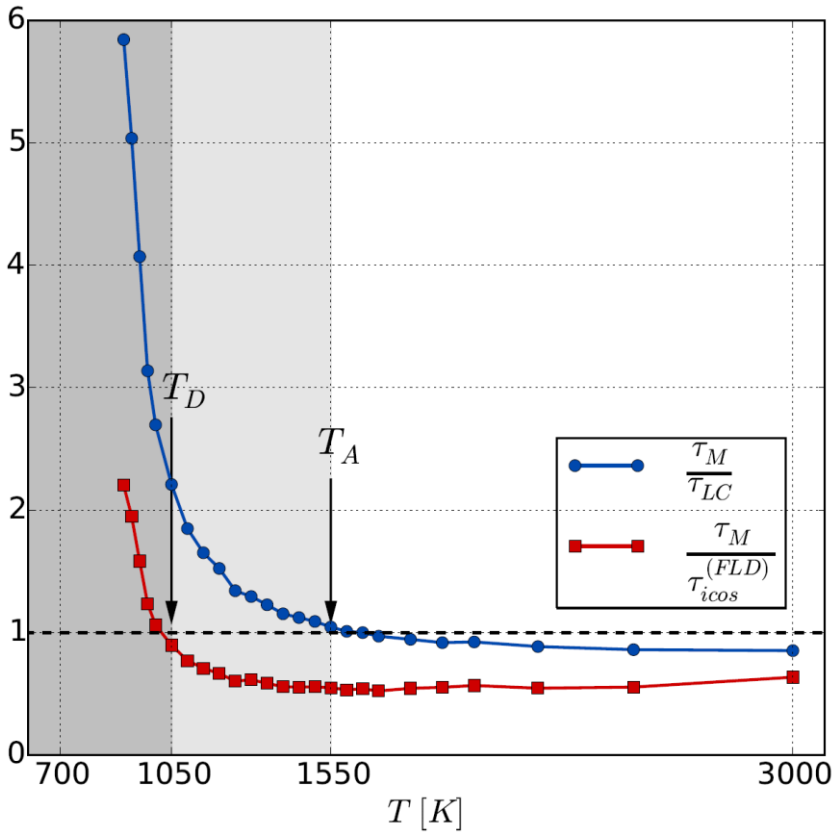

Figure 2.13 The ratio of the Maxwell relaxation time, τ_M, relative to τ_{icos}^{FLD} and τ_{LC}, respectively, versus temperature. The two characteristic temperatures correspond to crossings of these ratios through 1, signifying the onset of cooperative dynamics on different scales.

It proves to be fruitful to also analyze the extensive FLD ordering at T_D in the context of structural rearrangement timescales. Similar to our discussion of the onset of cooperative structural rearrangements at T_A, we introduce the timescale τ_{icos}^{FLD}, which measures the average lifetime of an icosahedron that participates in an FLD via an interpenetrating connection[*]. Similar to τ_{icos}, this measure is sensitive to geometric distortions of the icosahedron in addition to the loss or gain of vertex atoms. The motivation for defining this timescale is that interpenetrating icosahedra are found to serve as the most stable and highly-connected nodes in the FLD[32], hence their lifetimes reflect the structural lifetimes inherent to FLDs. **Figure 2.13**

[*] The centers of interpenetrating icosahedra are Voronoi neighbors of one another, which is a major reason why many simulation studies focus on this type of connection (i.e. it is trivial to detect). This connection involves the two icosahedra sharing 7 atoms in total: 5 vertex atoms and their respective center atoms.

displays a comparison of τ_{icos}^{FLD} to the Maxwell relaxation time τ_M (see equation 2.2) via the ratio τ_M/τ_{icos}^{FLD}. Here it is found that $\tau_M < \tau_{icos}^{FLD}$ for $T_D < T_D$, indicating that the FLDs are relatively inert on the timescale during which the liquid responds elastically to shear stresses. Remarkably, once the liquid is supercooled through $T_{D,}$ one finds that $\tau_M \geq \tau_{icos}^{FLD}$ and thus the FLDs can begin to restructure within the timescale of the liquid relaxation process*. This suggests that FLDs can begin to cooperatively rearrange in response to shear stresses in the liquid and restructure in an elastic environment. This, then, is reflected in the enhanced dynamical fluctuations that were demonstrated in **Figure 2.12** – the cooperative rearrangements manifest as attempts made by the liquid to locally sample deep regions of the energy landscape and briefly form exceedingly extensive FLDs.

It is striking to find that the characteristic temperatures T_A and T_D serve as both structural and dynamical landmarks in their respective dynamical regimes. In the case of T_A, we find that the liquid relaxation time, measured via $\eta(T)$, begins to grow faster than exponentially undercooling and that this marked the early onset of cooperative atomic rearrangements that produced the initial FLDs. At T_D, the timescale measured by $1/D(T)$ begins to grow faster than exponentially, and large-scale cooperative motions within FLDs produce extensive growth of icosahedral ordering in the supercooled liquid, with connected domains of icosahedra beginning to incorporate macroscopic fractions of icosahedra. This emerging structural feature produces caged particle dynamics and causes a separation in dynamics based on atomic species. These considerations demonstrate a newfound unification between the features of the liquid at a relatively high temperature with more characteristic features associated with glassy dynamics.

* To be clear, what really matters is that the behavior of τ_M/τ_{icos}^{FLD} changes dramatically near T_D – that $\tau_M \approx \tau_{icos}^{FLD}$ at T_D holds no special significance. Rather, it is important that $\tau_M \gg \tau_{icos}^{FLD}$ for $T < T_D$.

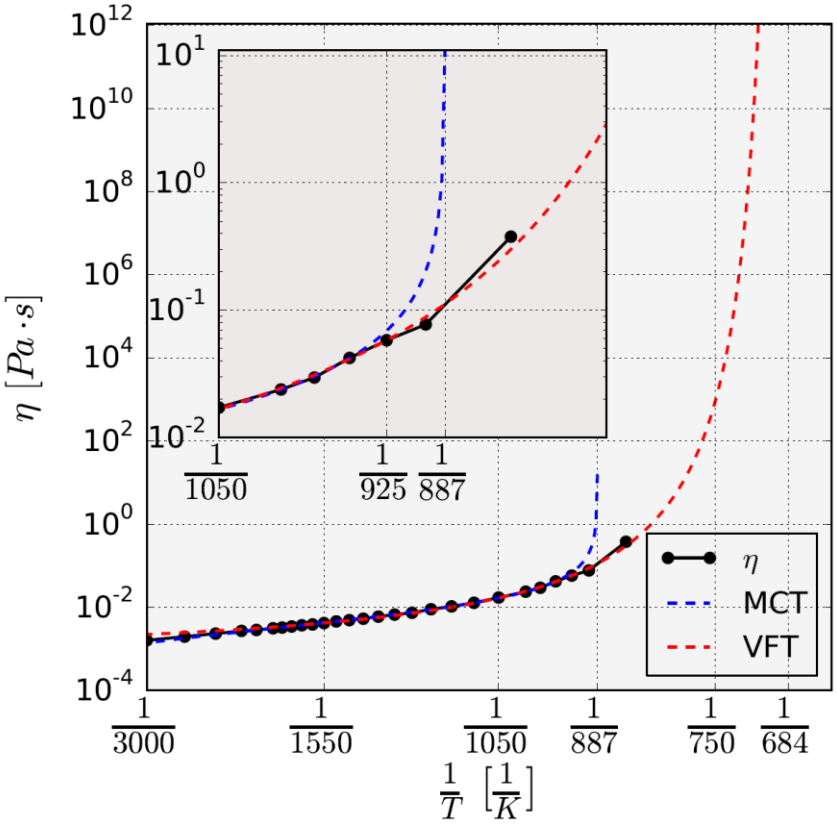

Figure 2.14 Simulation-measured values of $\eta(T)$ for $Cu_{64}Zr_{36}$ and the MCT-fitted and VFT-fitted functions. The mode-coupling temperature, T_c, is located at 887 K. The Kauzmann temperature, T_K, is located at 684 K. (Inset) A magnified view of the departure of the MCT fit from the data.

Furthermore, this connection begins to bring into focus the correlation $T_A \approx 2 \times T_G$ – the glassy dynamics that precede the glass transition indeed originate at the avoided critical point at T_A*.

2.2.3 Mode Coupling, Activated Dynamics, & Criticality

Although we have arrived at a relatively cogent picture of the structure and dynamics of liquid $Cu_{64}Zr_{36}$ both above and within the supercooled regime, we still must consider how the features of this picture fit into the context of some other prevalent theories of supercooled liquids†.

Namely, we are interested in identifying the mode coupling temperature T_c, which coincided

* Of course it is still not apparent why T_A is so nicely summarized as being specifically twice T_G. The insight to explain why this is, is almost certainly inaccessible to our simulation-based study that focuses on broader phenomena.

† Refer to **1.3** for an overview of these theories.

with a dynamical crossover to thermally activated dynamics, and the Kauzmann temperature, T_K, where the VFT fit of $\eta(T)$ predicts a diverging viscosity. **Figure 2.14** shows the viscosity data as a function of inverse temperature along with fitted curves associated with MCT and ADGM. The MCT fitted curve is of the form:

$$\eta(T) = \frac{m}{(T - T_c)^{\gamma}} \tag{2.5}$$

where $m = 2.26\ Pa \cdot s \cdot K^{\gamma}, \gamma = 0.966$, and the mode coupling temperature is $T_c = 887\ K$. This power law form fits well the viscosity data from $3000\ K$ down to approximately $925\ K$, where the curve begins to sharply deviate from the data. This can be seen clearly in the inset of the figure, which is a magnified view of the plot in the vicinity of T_c. As discussed in Chapter 1, MCT predicts that the energy landscape of the system undergoes a topological transition at T_C such that local energy minima no longer have saddle point directions through which the system can leave the minimum. T_c is found to be roughly $1.2 \times T_G$ ($T_G \approx 750\ K$), which is approximately what one expects for fragile supercooled liquids[20]. Here, the supercooled liquid's dynamics are expected to become dominated by activated hopping. The VFT form for the fitted curve is:

$$\eta(T) = \eta_o e^{\left(\frac{A}{T - T_k}\right)} \tag{2.6}$$

where $\eta_o = 1.53 \times 10^{-3} Pa \cdot s$, $A = 876\ K$, and the Kauzmann temperature is $T_K = 684\ K$. At T_K, the supercooled liquid's equilibrium configurational entropy extrapolates to zero, indicating

the presence of a true thermodynamic phase transition to a glass*. The VFT curve fits well the viscosity data in the super-Arrhenius regime, overestimating the viscosity for $T > T_A$.

To begin our analysis of $Cu_{64}Zr_{36}$'s structure and dynamics in the context of these theories we first note that T_c and T_K are both located at sensible values. Indeed, we expect T_D to exceed T_c as the former temperature marks the initial development of a two-step relaxation feature in the liquid's dynamical correlation function, whereas T_c corresponds to a terminal temperature at which the developed plateaus in the correlation functions would diverge if activated hopping were not available to restore ergodicity. Hence T_D naturally and necessarily precedes T_c in the supercooling process. Additionally, the VFT-fit predicts that the extrapolated divergence in $\eta(T)$ occurs beneath the glass transition: $T_G > T_k$†. This, of course, must be the case given a reasonable measurement of T_G and a reliable VFT fit since $\eta(T)$ is known to be strictly finite for $T < T_G + \Delta T$. Further discussion of the significance of T_k in the context of $Cu_{64}Zr_{46}$ can be found in Chapter 3.

We now consider the behavior of the growing FLDs in the vicinity of T_c to see if any distinguishing features arise in the system as activated dynamics begin to drive the system's ergodic evolution. **Figure 2.15** contains the relative FLD fluctuations across the entire temperature range that we considered, for two system sizes. The high-temperature behavior of this curve, e.g. the deviation from a slowly-growing Arrhenius fit at T_A, was previously discussed in the context of **Figure 2.7.** Beyond this departure, we find several remarkable features. First, the relative fluctuations obey the typical scaling of $1/\sqrt{N}$ that one finds in equilibrium[33],

* As mentioned in Chapter 1, resent experimental evidence suggests that extrapolating $\eta(T)$ below T_G using the VFT form overestimates the low-T empirical measurements of the viscosity. This suggests that the Kauzmann temperature may indeed be a mere figment of a naïve extrapolation.

† It is notable that the glass transition predicted from the VFT fit, e.g. $\eta_{VFT}(T_G) = 10^{12} Pa \cdot s$, is $T_G \approx 710\ K$. Given the extent of the extrapolation made by the fit, this is in reasonable agreement with the adopted value $750\ K$.

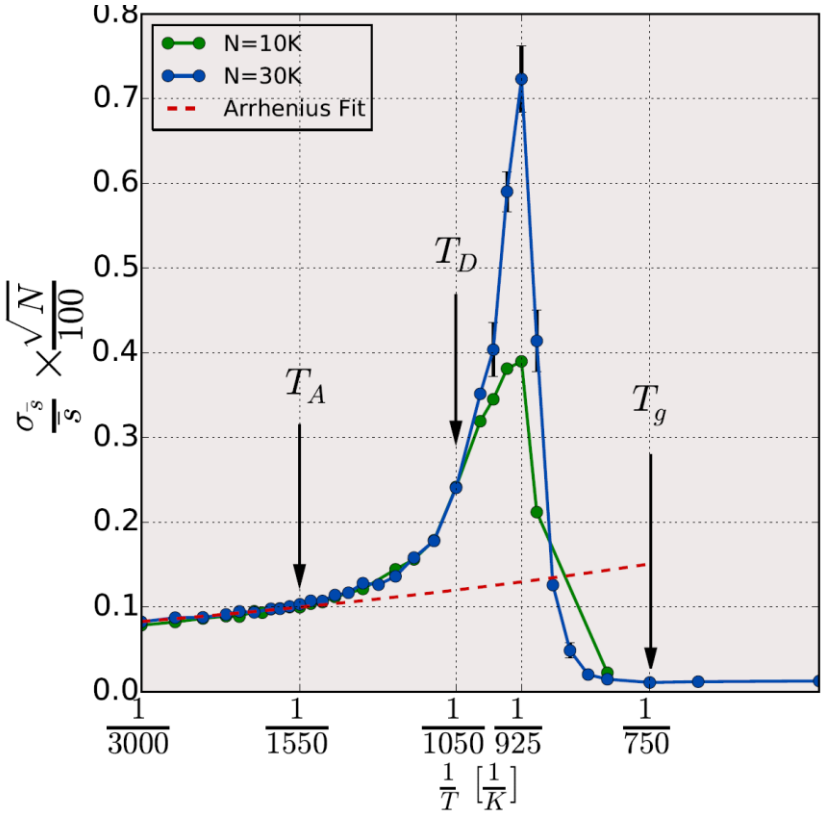

Figure 2.15 The relative FLD-size fluctuations versus inverse temperature, plotted for two systems sizes. At T_A, the relative fluctuations deviate from the slowly-growing Arrhenius form. Below T_D, the standard $1/\sqrt{N}$ scaling breaks down as the fluctuations begin to grow independently of system size. A distinct peak feature at $925\ K$ precedes the mode couple temperature, $T_c \approx 890K$.

however this scaling breaks down upon cooling below T_D. The curve's height at $925\ K$ appears to grow as $\sqrt{N}$ on our scaled fluctuation axis. Here, *the relative fluctuations in the average icosahedron-domain size grow independently of system size*. This means that finite fluctuations would develop even in the limit of infinite system size. Second, below $925\ K$, where the MCT power law fit begins to significantly deviate from $\eta(T)$, the fluctuations rapidly diminish and approach zero before the system reaches T_G, producing a distinct peak feature preceding T_c.

Before discussing our interpretation of these prominent feature in **Figure 2.15** , we must first take care to consider the validity of our simulation in the supercooled regime, where we know the simulation timescale will eventually fail to capture ergodic behavior in the system. In the

context of our present considerations, is the peak feature in **Figure 2.15** merely a signature of our simulation falling out of equilibrium due to the rapid growth of the liquid relaxation time (τ_M) in this vicinity? Indeed, when this does happen, one would expect that measured dynamical fluctuations would become small. At $900\ K$, where the fluctuations are already found to sharply decrease, we permit multiple independent simulations to equilibrate for $\Delta\tau_{equil} \approx \tau_M \times 10^4$. The fluctuations are then measured across the timespan $\Delta\tau_{meas} \approx \tau_M \times 10^2$. While these considerations do not rigorously guarantee that the observed dynamics at $900\ K$ reflect truly ergodic behavior, they do strongly suggest that the peak feature is not simply a manifestation of supercooled liquid falling out of equilibrium. That being said, by $825\ K$ we undoubtedly are no longer accurately describing equilibrium phenomena in the system.

Carrying on with our analysis, it is at first glance quite surprising to find that the relative fluctuations begin to scale with system size below T_D. One may wonder how the FLDs can begin to "know" how large the system is if the FLDs do not yet span the system. This is reminiscent of critical phenomena in percolating systems; here, small changes in the FLD configurations - the breaking and forming of individual icosahedral clusters – result in enormous (e.g. extensive) changes in the connectivity of FLDs through the system. The right side of the peak, then, indicates that the icosahedron density has crossed a critical value such that the average size of the icosahedron network becomes robust in the face of the addition and removal of icosahedra. By $870\ K$, half of the atoms in the liquid participate in forming icosahedra at any given time. As noted above, this stabilization occurs very near T_c, where activated hopping is believed to become the main mechanism for liquid relaxation. To be clear, it is not correct to think that the icosahedron network persists as a rigid solid amidst a liquid background at T_c; in spite of the shrinking fluctuations, the FLDs do break apart and reform constantly as the supercooled liquid

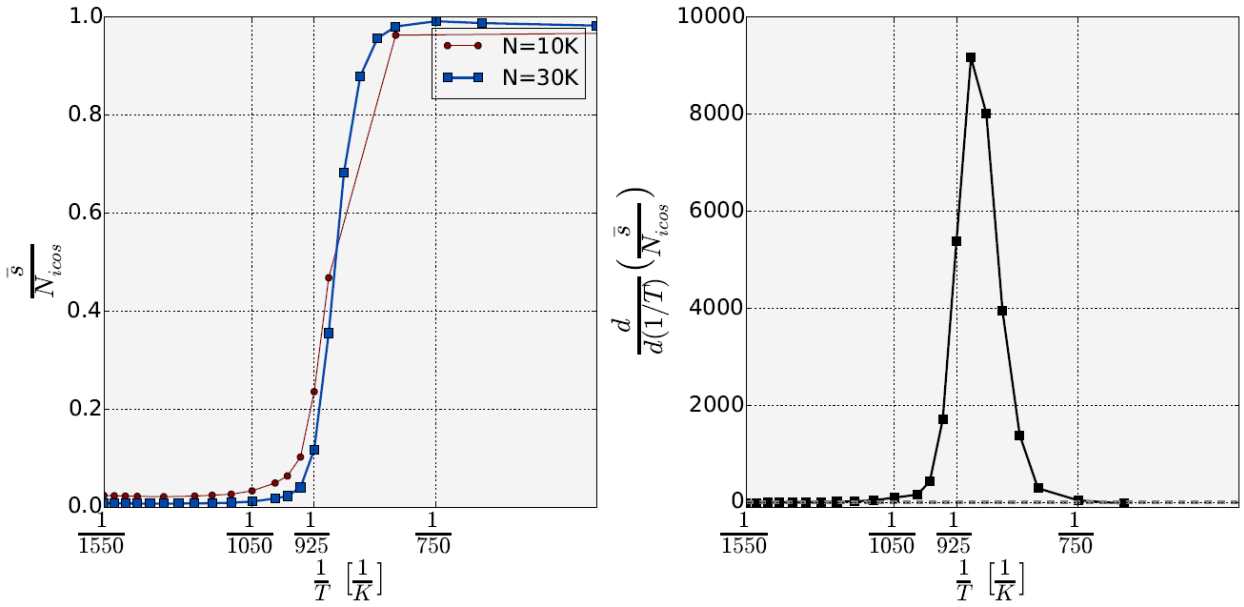

Figure 2.16 (Left) The fractional occupation of the icosahedron population of an average FLD. Cooling below T_D leads to a rapid percolation of the FLD. (Right) The FLD-occupation susceptibility demonstrates the sharp transition between the disorder-dominated and icosahedron-dominated phases of the system.

evolves. By 825 K, 95% of the (out-of-equilibrium) liquid's icosahedra are contained in a single FLD – the icosahedron network percolates the 30,000 atom simulation volume.

The features of this critical-like behavior suggest the possibility of a liquid-liquid phase transition residing in the supercooled regime of $Cu_{64}Zr_{36}$. Indeed, the literature on liquid-liquid transitions (LLTs), which has been championed and pioneered most notably by H. Tanaka[34–37], shares many common topics with the discussion provided in this dissertation. Central to both this topic and the present work are cooperative interactions amongst locally-preferred structures yielding bond-ordered medium ranged order in the liquid[*]. Here, we propose that the peak in **Figure 2.15** separates a higher-temperature liquid phase, in which the system is dominated by disordered structure, and a low-temperature liquid phase, in which the system is dominated by

[*] It may interest the reader to know that the majority of the analysis presented in this work was conducted with almost no (conscious) influence from the literature on LLTs. It wasn't until after the majority of this research was completed that I began to read these papers carefully. It was quite surprising to find that the literature so closely matched the narrative that I had developed to explain the behavior of $Cu_{64}Zr_{36}$. This certainly lends strong support to the theory developed by H. Tanaka, whose predictions naturally and rather explicitly manifest themselves in this system.

extensive domains of the locally-preferred structure (e.g. Cu-centered icosahedra). The nature of this second liquid phase, which lies entirely within the supercooled region of the phase diagram (at zero pressure), may then be instrumental in precipitating the tremendous viscous slowdown that ensues as the system is cooled towards T_G. This transition is conveyed well by **Figure 2.16**, which shows the rapid growth of the fractional occupation of the icosahedron population in an average FLD. Prior to the transition ($T > T_D$), the probability of observing an icosahedron participating in in a "macroscopically-sized" FLD is zero. After cooling through the liquid-liquid transition ($T \approx 900\ K$), this probability is one. Note that in the limit of large N, the relative fluctuations depicted on an unscaled version of **Figure 2.15** will go to zero for $T > T_D$ and that this curve will closely match with the peaked FLD-occupation susceptibility plotted in the right panel of **Figure 2.16**[*].

While this picture of a LLT is compelling in light of many of the features of liquid $Cu_{64}Zr_{34}$ that we have found, and although the glass is known to be dominated by icosahedral ordering[38], there are important outstanding questions that we cannot yet answer. First, does the peak feature in **Figure 2.15** truly reflect critical behavior? It is possible that subtle system size effects are at play and that the apparent size-independent scaling of the FLD fluctuations actually breaks down once one increases the system size sufficiently. Second, are there other measurements that can be made to rigorously show that this is indeed an actual phase transition? Can these signatures be detected empirically? Third, what would **Figure 2.15** and **Figure 2.16** look like if we were able to ensure that we were genuinely capturing equilibrium dynamics down to, say, T_k?

[*] In the limit of large N, the peak in **Figure 2.15** will be centered at a higher temperature and will be narrower than the peak in the susceptibility. As we will discuss, this discrepancy may be an artifact of the unrealistically-fast quench rate used in our simulation and the fact that the liquid falls out of equilibrium at as it approaches T_G.

With regards to the last question, some basic progress can be made by considering some existing studies of Cu-Zr glass. What would the relative fluctuation curve look like if we could simulate the quench rates used in experiments, and if we could dilate the timescale of our simulation sufficiently to observe ergodic behavior near T_G? Simulation-based studies suggest that we would observe further enhanced icosahedral ordering near T_G than what we observe in our limited simulations[38–41]. Maozhi Li *et al.* and Zhang $et\ al.$ find that utilizing slower cooling rate to reach T_G augments the observed number of icosahedra and the medium-range order associated with the FLDs in the system. This is corroborated by E. Ma *et al.*, who further demonstrate that aging $Cu_{64}Zr_{36}$ at $800\ K$ for $300\ ns$ results in an impressive increase in the number of icosahedra in the system. This is accompanied by an increase in the number of connections shared between icosahedra and an order of magnitude enhancement of τ_{LC} in the system. These findings provide important evidence to support what our intuition already leads us to believe: as the system is quenched less rapidly and is given more time to relax, it is able to better explore the low-energy configurations of its energy landscape. This produces atomic configurations that more thoroughly manifest the LPS of the system – Cu-centered icosahedral clusters. Given these considerations, one cannot claim, if we were to remain in equilibrium throughout the supercooled regime, that the relative fluctuations in the FLD size would simply continue to grow with decreasing temperature[*]. That is, the peak feature in **Figure 2.15** is bound to emerge simply considering the rapidly growing density of the icosahedron population in the (metastable) equilibrium supercooled liquid. These observations also suggest that the low-temperature side of percolation transition shown in **Figure 2.16** would be even sharper were the liquid held in equilibrium – a completely-connected FLD may form above $825\ K$, and a clear LLT temperature

[*] This is a relatively common (and prudent) argument that is made when readers first see the rather surprising peak feature in **Figure 2.15** .

would lie in the narrow temperature range separating $\frac{\bar{s}}{N_{icos}} = 0$ and $\frac{\bar{s}}{N_{icos}} = 1$. This would thus produce a narrower susceptibility peak that is shifted towards higher temperature, leading to a closer agreement between the susceptibility curve and the relative fluctuations plotted in **Figure 2.15** (when the limit of large N is taken).

2.3 Summary & Outlook

In summary, we analyzed across a broad temperature range the dynamics of a classical MD simulation of $Cu_{64}Zr_{36}$ in the context of its locally-preferred structure (LPS) – Cu-centered icosahedral clusters of atoms. In doing so, we identified two characteristic temperatures, $T_A = 1550\ K$ ($T_A > T_l$, the liquidus temperature) and $T_D = 1050\ K$ ($T_D > T_c$, the mode coupling temperature). These temperatures mark the crossover from Arrhenius to super-Arrhenius behavior, with decreasing temperature, of liquid timescales controlled by $\eta(T)$ and $1/D(T)$, respectively.

Cooling through T_A results in the violation of the Stokes-Einstein relationship* and yields the onset of liquid dynamics that are controlled by cooperative structural rearrangements amongst neighboring clusters of atoms. This manifests structurally as the development of small, connected domains of icosahedral clusters. This is a rather remarkable confirmation of the predictions of frustration-limited domain theory (FLDT), and lends credence to the interpretation that T_A is in fact an avoided critical point whose presence is instrumental in shaping the ensuing viscous slowdown of the liquid as it is cooled.

* Given that $\eta(T)$ departs from its exponential form at a higher temperature than $1/D(T)$ ($T_A > T_D$), it is obvious that the Stokes-Einstein relationship must be violated at T_A. That being said, it is far from obvious as to why these quantities depart from their exponential forms, why they do so at different temperatures, and where these temperatures are located. The reader may wonder why I am taking the time to point out this relatively simple observation. It turns out that such a point may not be so salient to, say, a referee who is evaluating the paper containing these findings.

Supercooling through T_D marks the early development of the two-step liquid relaxation processes that characterize the liquid's (metastable) equilibrium dynamics near T_G. Additionally, the self-diffusivities of the liquid's species, $D_{Cu}(T)$ and $D_{Zr}(T)$, become decoupled below this temperature. This strongly suggests that liquid begins to become strongly influenced by its energy landscape at T_D and that a structural feature manifests that impedes the diffusive motion of Zr atoms disproportionately. This structural feature, we argue, is the Zr-rich and extensive frustration-limited domains (FLDs) of connected icosahedra, which have grown rapidly with supercooling. Measurements of the lifetimes of icosahedral clusters in the system suggest that these FLDs begin to restructure cooperatively near T_D – this manifests via enhanced fluctuations of the average FLD size, $\bar{s}$. These fluctuations suddenly drop near T_c (mode coupling), producing a striking peak in the $\sigma_{\bar{s}}/\bar{s}$ curve. Remarkably, we find that $\sigma_{\bar{s}}/\bar{s}$ appears to remain finite in the limit of large system size below T_D. To understand this possible critical behavior, we define an order parameter given by the fractional occupation of the icosahedron population in an average FLD, $\Omega \equiv \bar{s}/N_{icos}$. A rapid transition from $\Omega = 0$ to $\Omega = 1$ is found, and a sharply peaked susceptibility resembles the behavior exhibited by $\sigma_{\bar{s}}/\bar{s}$. This suggests that a liquid-liquid transition (LLT) may occur between a disordered phase and a FLD-dominated phase in supercooled $Cu_{64}Zr_{36}$, preceding the glass transition. Keeping in mind that this icosahedral order originates at T_A, above which the system behaves like a simple liquid, this analysis summarizes and unifies major features of all the dynamical regimes of $Cu_{64}Zr_{36}$.

Perhaps the most immediate and pressing issue that stands to be resolved, in the context of the above summary, is the further verification of the N-independent scaling of $\sigma_{\bar{s}}/\bar{s}$ below T_D. It is feasible to perform the appropriate simulation and analysis on a system of $N = 10^5$ atoms to test

the scaling beyond 3×10^4 atoms, but this is likely near the practical limit*. As is, the scaling found from 10^4 atoms to 3×10^4 is encouraging, but is certainly not definitive. Additionally, more rigorous checks of the ergodicity of the liquid beneath $\sim 900\ K$ are warranted. It would be valuable to utilize slower quench rates and longer equilibration times to confirm that the transition from $\Omega = 0$ to $\Omega = 1$ occurs in a narrower temperature range (if this is indeed what happens). Of course, one could utilize worse quench rates and equilibration times to attempt to "broaden" the LLT towards the same end.

Perhaps this is too obvious to state explicitly, but one must look for empirical evidence of the LLT to the icosahedron-dominated phase in $Cu_{64}Zr_{36}$ before it will be taken seriously by the glass community at large. Originally, our investigation of the dynamics of $Cu_{64}Zr_{36}$ focused exclusively on features near T_A. This was ideal as the liquid relaxation times are sufficiently short here such that ergodic behavior is easily captured by MD simulations. However, our findings at T_A inevitably led us to lower and lower temperatures as we hoped to connect the icosahedral ordering that emerged at this temperature with the percolating icosahedral network that is known to characterize the glass. It is both fortunate and very unfortunate that signature of then possible LLT occurs where it does: it begins at a high enough temperature where we can refer to our results with confidence, but extends to low enough temperatures where it is essentially impossible to guarantee the absolute reliability of our findings. In light of the above considerations, of what we would expect were we to remain in equilibrium, it is the author's (biased) opinion that our interpretation of the low-temperature results are neither cavalier nor are

* The simulation itself is not the limiting performance factor – the use of GPUs allows us to increase N without paying too high a price. Rather, the amount of data that must be recorded in order to conduct the appropriate analysis (e.g. particle positions and, from these, the Voronoi signatures) can easily reach the order of terabytes for 10^4 atoms (when considering all the timesteps and temperatures that must be recorded), and this scales like N.

they unfounded. That being said, the universe does not care about my opinion[*]. We therefore hope that these findings will motivate and serve as a roadmap for future experiments to look for signatures of this LLT.

In the following chapter we will focus on features of icosahedral ordering that manifest on a scale that is accessible by experiment. This entails looking at the temperature-evolution of the spatial pair-correlation functions of $Cu_{64}Zr_{36}$ as well as the chemical ordering that is created by the icosahedron-network.

2.4 Chapter 2 References

1. Tarjus, G., Kivelson, S. a., Nussinov, Z. & Viot, P. The frustration-based approach of supercooled liquids and the glass transition: a review and critical assessment. **1143,** 48 (2005).

2. Kivelson, D., Kivelson, S. a., Zhao, X., Nussinov, Z. & Tarjus, G. A thermodynamic theory of supercooled liquids. *Phys. A Stat. Mech. its Appl.* **219,** 27–38 (1995).

3. Chayes, L., Emery, V. J., Kivelson, S. a., Nussinov, Z. & Tarjus, G. Avoided critical behavior in a uniformly frustrated system. *Phys. A Stat. Mech. its Appl.* **225,** 129–153 (1996).

4. Nussinov, Z. Avoided Phase Transitions and Glassy Dynamics In Geometrically Frustrated Systems and Non-Abelian Theories. *Phys. Rev. B* **69,** 014208 (2002).

5. Iwashita, T., Nicholson, D. M. & Egami, T. Elementary excitations and crossover phenomenon in liquids. *Phys. Rev. Lett.* **110,** 1–5 (2013).

6. Chen, S. P., Egami, T. & Vitek, V. Local fluctuations and ordering in liquid and amorphous metals. *Phys. Rev. B* **37,** 2440–2449 (1988).

7. Blodgett, M., Egami, T., Nussinov, Z. & Kelton, K. F. Unexpected Universality in the Viscosity of Metallic Liquids. 28 (2014). at <http://arxiv.org/abs/1407.7558>

8. Tadmor, E. & Miller, R. *Modelling Materials: Continuum, Atomistic, and Multiscale Techniques*. (Cambridge University Press, 2011).

[*] I told this to my students in Physics 118 repeatedly.

9. Mattern, N. *et al.* Structural behavior of CuxZr100-x metallic glass (x = 35-70). *J. Non. Cryst. Solids* **354,** 1054–1060 (2008).

10. Park, J. & Shibutani, Y. Common errors of applying the Voronoi tessellation technique to metallic glasses. *Intermetallics* **23,** 91–95 (2012).

11. Park, J. & Shibutani, Y. Effects of Atomic Size for Voronoi Tessellation Technique on Binary and Ternary Systems of Metallic Glasses. *Mater. Trans.* **47,** 2904–2909 (2006).

12. Park, J. & Shibutani, Y. Weighted Voronoi tessellation technique for internal structure of metallic glasses. *Intermetallics* **15,** 187–192 (2007).

13. Einstein, a. Über Die Von Der Molekularkinetischen Theorie Der Warme Geforderte Bewegung Von in Ruhenden Flussigkeiten Suspenderten Teilchen. *Ann. Phys.* **17,** 549–60–560 (1905).

14. Cicerone, M. T. & Ediger, M. D. Enhanced translation of probe molecules in supercooled o-terphenyl: Signature of spatially heterogeneous dynamics? *J. Chem. Phys.* **104,** 7210–7218 (1996).

15. Berthier, L. Dynamic heterogeneity in amorphous materials. *Physics (College. Park. Md).* **4,** 7 (2011).

16. Sillescu, H. Heterogeneity at the glass transition: a review. *J. Non. Cryst. Solids* **243,** 81–108 (1999).

17. Ediger, M. D. SPATIALLY HETEROGENEOUS DYNAMICS IN SUPERCOOLED LIQUIDS. *Annu. Rev. Phys. Chem.* **51,** 99–128 (2000).

18. Chen, S.-H. *et al.* The violation of the Stokes-Einstein relation in supercooled water. *Proc. Natl. Acad. Sci. U. S. A.* **103,** 12974–12978 (2006).

19. Cavagna, A. Supercooled liquids for pedestrians. *Phys. Rep.* **476,** 51–124 (2009).

20. Debenedetti, P. G. & Stillinger, F. H. Supercooled liquids and the glass transition. *Nature* **410,** 259–267 (2001).

21. Mapes, M. K., Swallen, S. F. & Ediger, M. D. Self-diffusion of supercooled o-terphenyl near the glass transition temperature. *J. Phys. Chem. B* **110,** 507–511 (2006).

22. Swallen, S., Bonvallet, P., McMahon, R. & Ediger, M. Self-Diffusion of tris-Naphthylbenzene near the Glass Transition Temperature. *Phys. Rev. Lett.* **90,** 1–4 (2003).

23. Brillo, J., Pommrich, a. I. & Meyer, a. Relation between self-diffusion and viscosity in dense liquids: New experimental results from electrostatic levitation. *Phys. Rev. Lett.* **107,** 1–4 (2011).

24. Brillo, J., Chathoth, S. M., Koza, M. M. & Meyer, a. Liquid Al80Cu20: Atomic diffusion and viscosity. *Appl. Phys. Lett.* **93,** 1–4 (2008).

25. Meyer, a., Petry, W., Koza, M. & Macht, M. P. Fast diffusion in ZrTiCuNiBe melts. *Appl. Phys. Lett.* **83,** 3894–3896 (2003).

26. Lad, K. N., Jakse, N. & Pasturel, A. Signatures of fragile-to-strong transition in a binary metallic glass-forming liquid. *J. Chem. Phys.* **136,** (2012).

27. Cheng, Y. Q., Sheng, H. W. & Ma, E. Relationship between structure, dynamics, and mechanical properties in metallic glass-forming alloys. *Phys. Rev. B - Condens. Matter Mater. Phys.* **78,** 1–7 (2008).

28. Mendelev, M. I. *et al.* Development of suitable interatomic potentials for simulation of liquid and amorphous Cu–Zr alloys. *Philos. Mag.* **89,** 967–987 (2009).

29. Olsen, N. B., Christensen, T. & Dyre, J. C. Time-temperature superposition in viscous liquids. *Phys. Rev. Lett.* **86,** 1271–1274 (2001).

30. Heesemann, a., Zöllmer, V., Rätzke, K. & Faupel, F. Evidence of Highly Collective Co Diffusion in the Whole Stability Range of Co-Zr Glasses. *Phys. Rev. Lett.* **84,** 1467–1470 (2000).

31. Basuki, S. W. *et al.* Decoupling of Component Diffusion in a Glass-Forming Zr46.75Ti8.25Cu7.5Ni10Be27.5 Melt Far above the Liquidus Temperature. *Phys. Rev. Lett.* **113,** 1–5 (2014).

32. Soklaski, R., Nussinov, Z., Markow, Z., Kelton, K. F. & Yang, L. Connectivity of icosahedral network and a dramatically growing static length scale in Cu-Zr binary metallic glasses. *Phys. Rev. B - Condens. Matter Mater. Phys.* **87,** (2013).

33. Sethna, J. *Entropy, Order Parameters, and Complexity*. (2011).

34. Kurita, R. & Tanaka, H. Critical-like phenomena associated with liquid-liquid transition in a molecular liquid. *Science* **306,** 845–848 (2004).

35. Tanaka, H. General view of a liquid-liquid phase transition. *Phys. Rev. E. Stat. Phys. Plasmas. Fluids. Relat. Interdiscip. Topics* **62,** 6968–76 (2000).

36. Murata, K. & Tanaka, H. Liquid–liquid transition without macroscopic phase separation in a water–glycerol mixture. *Nat. Mater.* **11,** 436–443 (2012).

37. Tanaka, H., Kawasaki, T., Shintani, H. & Watanabe, K. Critical-like behaviour of glass-forming liquids. *Nat. Mater.* **9,** 324–331 (2010).

38. Ding, J., Cheng, Y. Q. & Ma, E. Full icosahedra dominate local order in Cu64Zr34 metallic glass and supercooled liquid. *Acta Mater.* **69,** 343–354 (2014).

39. Li, M., Wang, C., Hao, S., Kramer, M. & Ho, K. Structural heterogeneity and medium-range order in ZrxCu100−x metallic glasses. *Phys. Rev. B* **80,** 1–7 (2009).

40. Zhang, Y. *et al.* Cooling rates dependence of medium-range order development in Cu64.5Zr35.5 metallic glass. *Phys. Rev. B* **91,** 1–8 (2015).

41. Zhang, F. *et al.* Effects of sub-Tg annealing on Cu64.5Zr35.5 glasses: A molecular dynamics study. *Appl. Phys. Lett.* **104,** 061905 (2014).

42. Miracle, D. B., Sanders, W. S. & Senkov, O. N. The influence of efficient atomic packing on the constitution of metallic glasses. *Philos. Mag.* **83,** 2409–2428 (2003).

43. Inoue, A. *et al. Bulk Metallic Glasses*. (Springer, 2008).

Chapter 3: Static Signatures of Dynamical Regimes

In Chapter 2, we leveraged our ability to analyze microscopic, time-dependent features of simulated $Cu_{64}Zr_{36}$ to gain new insights into the structural and dynamical phenomena that characterize its different dynamical regimes. Here we discuss static (long-time-averaged) measurements of the system that are accessible to empirical studies. We hope to connect temperature-dependent features in this data with the characteristic temperatures T_A $(1550\ K)$, T_D $(1050\ K)$ and the ensuing rapid development of icosahedral order in supercooled $Cu_{64}Zr_{36}$, which were discussed in Chapter 2. In this way, we create a road map for future experiments to check our results.

We remind the reader that T_G was found to reside near $750\ K$, given the semi-empirical potential and quench rate that we utilize in our simulation. It must be emphasized that although we will present data ranging from $3000\ K$ down to $600\ K$, the low temperature data is not necessarily representative of equilibrium data. Below approximately $900\ K$ the time averages conducted are not guaranteed to be sufficiently long to allow the system ergodically explore phase space[*]. In this temperature range, multiple independent simulations are analyzed for a given temperature to help correct for this. That being said, the topic of ergodicity will not be belabored in the forllowing sections, so it is important for the reader to keep these considerations in mind when viewing low-temperature data and to know that this matter is not a mere technicality.

[*] Despite this, it is not until $750\ K$ that we see the system clearly "freeze" on our simulation timescale, which is how we identify T_G.

3.1 Static Structure Factors & Pair Correlation Functions

X-ray and neutron diffraction experiments provide measurements that yield atom-pair spatial correlation statistics in materials. The coherent-scattering intensity distribution can be used to calculate the static structure factor, $S(q)$, where $q = 4\pi \sin(\theta)/\lambda$, which can be Fourier transformed to produce the real-space pair correlation function, $g(r)$. Chemical species-specific structural information can be obtained by tuning the x-ray energies through the species' respective absorption edges – a technique called anomalous X-ray scattering[1]. Isotope substitution can be used with neutron scattering to also produce species-specific information in the distribution function. The species-specific spatial distribution of pairs of atoms is given by the partial pair correlation function (PPCF)[2]:

$$g_{\alpha\beta}(r) = \frac{N}{4\pi r^2 \rho N_\alpha N_\beta} \sum_{i=1}^{N_\alpha} \sum_{j=1}^{N_\beta} \delta(r - |\vec{r}_i - \vec{r}_j|) \tag{3.1}$$

where N is the total number of atoms in the system, α and β index the atomic species being considered, i and j index the atoms of the appropriate species, and ρ is the number density. Thus given an atom of type α, $g_{\alpha\beta}(r)$ reflects the probability of finding an atom of type β a distance r away. The PPCF is normalized such that $g_{\alpha\beta}(r) = 1$ for a random distribution of atoms. The (species-independent) total pair correlation function (TPCF) is thus given by the weighted sum of PPCFs:

$$g(r) = \sum_{\alpha,\beta} \sum_{i=1}^{N_\alpha} \sum_{j=1}^{N_\beta} \frac{N_\alpha N_\beta}{N^2} g_{\alpha\beta}(r) \tag{3.2}$$

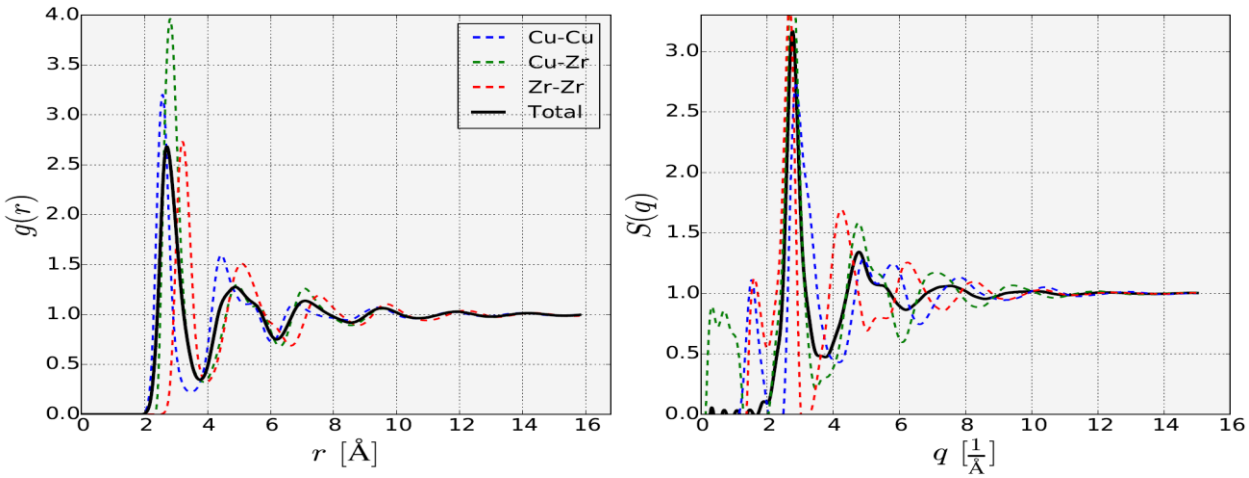

Figure 3.1 (Left) The total pair correlation function, $g(r)$, of $Cu_{64}Zr_{36}$ at 750 K and the partial pair correlation functions that comprise it. $g(r) \to 1$ for large r, indicating that pairs of atoms become structurally uncorrelated at large distances in the glass – unlike what one would find in a crystalline structure. (Right) The total and partial structure factors for the same system. These directly reflect the coherent scattering intensities obtained from X-ray or neutron diffraction experiments, where $q = 4\pi \sin(\theta)/\lambda$. $g(r)$ and $S(q)$ are related via Fourier transform.

The partial structure factors (PSFs) are related to the PPCFs through the equation:

$$S_{\alpha\beta}(q) = 1 + \frac{4\pi\rho}{q}\int_0^\infty r\left[g_{\alpha\beta}(r) - 1\right]\sin(qr)dr \tag{3.3}$$

and the species-independent total structure factor (TSF) is given by:

$$S(q) = \sum_{\alpha,\beta}\frac{c_\alpha c_\beta f_\alpha f_\beta}{(\sum_\alpha c_\alpha f_\alpha)^2}S_{\alpha\beta}(q) \tag{3.4}$$

where c_α is the molar fraction of the species, and f_α is the atomic scattering factor. Here, we use the atomic number of a species for its scattering factor. **Figure 3.1** contains the TPCF (Left) and the TSF (Right), and the partial functions that comprise them, for $Cu_{64}Zr_{36}$ at 750 K. The sequence of peaks and troughs in $g(r)$ corresponds to distances where atoms are correlated and anti-correlated with one another. Thus a shell-like structure appears to form, on average, around an atom. In total, short ($r < \sim 7$Å) and medium (~ 7Å $< r < \sim 15$Å) range order (SRO and MRO) manifests in the system, but no long range order (LRO) is detected by the pair correlation

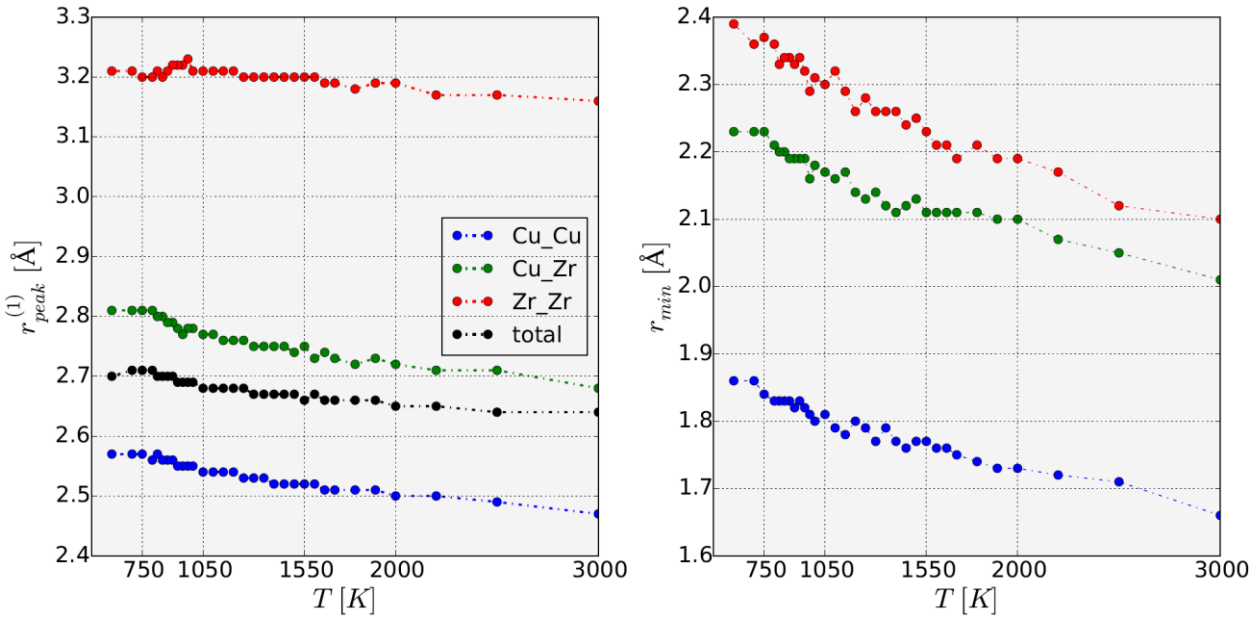

Figure 3.2 (Left) The first-peak position of the PPCFs and TPCF versus temperature. The peak is found to retract with increasing temperature for each PPCF, demonstrating that the anomalous thermal contraction exhibited by $g(r)$ is not the result of a shift in PPCF peak heights. (Right) The minimum distance recorded between pairs of atoms is also found to decrease with increasing temperature ($r_{min}^{(total)} = r_{min}^{(Cu-Cu)}$).

function*. Notice that the PPCFs can have rich features, such as the distinct split-peak in the second shell of $g_{CuCu}(r)$, that are subtle or even hidden in $g(r)$. In general, important structural information can be lost by averaging over the PPCFs – when species-sensitive measurements cannot be conducted, simulations are often utilized to produce PPCFs to augment the interpretation of the empirically-determined $g(r)$†.

3.1.1 Anomalous Thermal Contraction of the First Coordination Shell

A recent analysis of empirical $g(r)$ data by Gangopadhyay *et al.*[3] found a striking anomaly common to a wide variety of metallic liquids – nearly ubiquitously, the first peak position of a

* It is possible that some symmetries in the atomic structure can only be detected by higher-order correlation functions that are sensitive to bond orientation order[19].

† A major caveat here is that the simulation yields a $g(r)$ that actually matches closely with the empirical result. We produced $g(r)$ data that agreed well with experimental data for Cu-rich compositions of Cu-Zr[20]. The semi-empirical potential that we utilize was formulated specifically for $Cu_{64}Zr_{36}$ – deviations from this composition lead to larger discrepancies in the SRO features of $g(r)$ that are found by experiment.

liquid's $g(r)$ was found to contract with increasing temperature, despite the fact that each liquid possessed a positive temperature coefficient of volume expansion $\left(\frac{1}{V}dV/dT\right)$.

The subsequent peaks are then found to expand sufficiently to account for the overall expansion of the liquid with increasing temperature. To understand this phenomenon, one must first consider the behavior of the individual PPCFs – it is possible that the first peak in each PPCF expands with increasing temperature and that a shift in the relative peak heights manifests as a contraction in the first shell of $g(r)$. If this is indeed what occurs, then there is no anomaly. Rather, there would be a consistent trend in the SRO favoring packing around an alloy's smallest species. As concluded in the study, this is not the case; the first peaks of all the PPCFs do contract with increasing temperature. This trend is shown in **Figure 3.2**, in which the left panel contains the first-peak position for the PPCFs[*]. The right panel contains a plot of the minimum recorded pair distance versus temperature and shows a similar contraction, though this is less notable[†].

These findings indicate that all of these metallic liquids are undergoing a microscopic structural change that resembles the ordering that we have observed in $Cu_{64}Zr_{36}$. The interpretation here is that at low temperatures the supercooled liquids have developed significant SRO according to the system's locally-preferred structure (LPS). In the context of $Cu_{64}Zr_{36}$, this is Cu-centered icosahedral clusters of atoms. These clusters then connect to form connected domains (a frustration-limited domain (FLD) in our system). As the liquid is heated, the MRO domains become less stable and the LPSs become disjoint from one another – this corresponds to the

[*] The 1st peak position is taken to be the value at which the correlation function is a maximum.
[†] The thermal contraction of r_{min} is to be expected to a degree – increasing the temperature symmetrically broadens the peaks of the PPCFs. Considered from another perspective, at a high temperature atoms collide with higher kinetic energies and thus can be found at closer distances than at low temperatures.

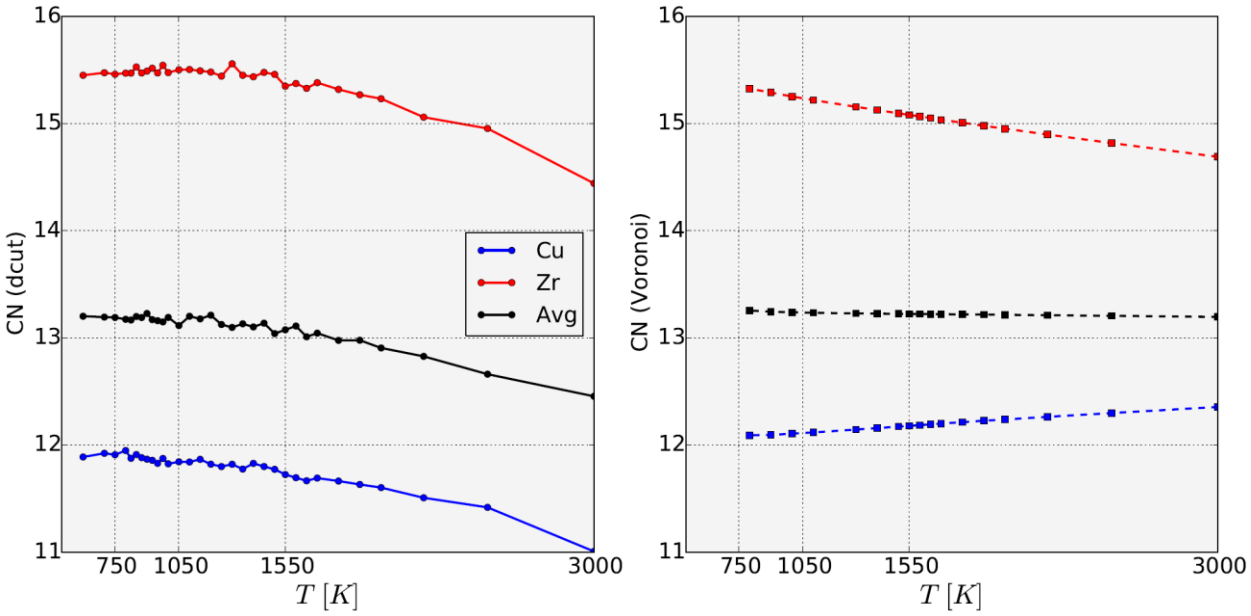

Figure 3.3 (Left) The average coordination number (CN) of Cu, Zr, and their atom, versus temperature. Both species are found to lose nearest neighbors with increasing temperature. The CN is calculated by integrating the appropriate PPCFs to their first minimums. (Right) The average CN of the species as determined by the number of Voronoi neighbors that they share. Here, the CN of Cu atoms decreases with decreasing temperature.

observed expansion in the 2nd and 3rd peaks of $g(r)$. On the other hand, the LPSs become unstable as well; this causes a typical atom to have fewer nearest neighbors packed in its vicinity, or in other words, the coordination number (CN) of the atom is reduced. Thus at higher temperatures, only tightly-bound clusters of atoms are able to persist. These stronger bonds have shorter bond distances, hence the atoms have fewer nearest neighbors and the nearest neighbor shell contracts.

We provide support for this interpretation by analyzing the temperature dependence of the CNs of Cu, Zr, and their average, in $Cu_{64}Zr_{36}$. The data presented in the left panel of **Figure 3.3** confirms that the average CN for each species indeed decreases with increasing temperature. From $750\ K$ to $3000\ K$, both species are found to lose roughly one nearest neighbor as the liquid's low-temperature SRO becomes disrupted. Furthermore, the rate of loss of nearest neighbors appears to accelerate when the liquid is heated above $1550\ K$, or T_A. Here it was found

that cooperative rearrangements amongst atomic clusters cease to manifest in the liquid relaxation process, and the Stokes-Einstein relationship begins to hold. Thus this transition supports our findings that SRO begins to stabilize in the system below T_A. However, this acceleration does not appear in the peak contraction trends shown in **Figure 3.2**, except for in the Zr-Zr curve. This may indicate that tracking the peak maximum does not capture all of the details of the first shell contraction, or that the CN is not the only factor determining the contraction.

Up to this point, the CNs being considered were calculated by integrating $r^2 g_{\alpha\beta}(r)$ from 0 Å to $r_{min}^{\alpha\beta}$ *, and taking the appropriate linear combinations for the different species†. Thus CNs calculated in this way, which we'll now call CN_{dcut}, depend on these hard-cutoff distances and are insensitive to cluster geometries beyond the radial distribution of the neighbor atoms from the center atom. Another method for determining the structural coordination of an atom and its neighbors is by performing a weighted Voronoi tessellation of the liquid structure[4,5]. In this instance, one considers an atom's Voronoi neighbors to comprise its nearest neighbor shell. An atom's CN can then be determined by counting the number of faces of its Voronoi cell – this will be distinguished as CN_{Voro}. CN_{Voro} thus reflects the packing geometry of neighbor atoms about a center atom and is parameter independent. That being said, the Voronoi tessellation process is entirely impartial to the physics that we are concerned with - there is no guarantee that a distant Voronoi neighbor and an atom are interacting in a meaningful way such that the atoms are "coordinated". The average $CN_{Voro}^{(\alpha)}$, where α labels the species of the central atom, are plotted in

* $r_{min}^{\alpha\beta}$ is the position of the first nonzero minimum of $g_{\alpha\beta}(r)$.

† For example, $CN^{(Cu)} = \frac{4\pi\rho}{N}\left(\int_0^{r_{min}^{Cu-Cu}} N_{Cu}^2 r^2 g_{CuCu}(r)dr + \int_0^{r_{min}^{Cu-Zr}} N_{Cu}N_{Zr} r^2 g_{CuZr}(r)dr\right)$

the right panel of **Figure 3.3**, and show striking differences to $CN_{dcut}^{(\alpha)}$. $CN_{Voro}^{(Cu)}$ and $CN_{Voro}^{(Zr)}$ are found to vary nearly linearly with temperature such that $CN_{Voro}^{(Avg)}$ of an average atom is approximately a constant for all temperatures. That is, while Zr is found to lose Voronoi neighbors as the liquid is heated, Cu gains Voronoi neighbors. Ultimately, for a given species, the CNs calculated using the two methods approach one another with decreasing temperature. The opposite trends of $CN_{cut}^{(Cu)}$ and $CN_{Voro}^{(Cu)}$ suggest that at high temperatures the clusters around Cu tend to be irregularly packed. Consider that, at $3000\ K$, an average Cu atom only has 11 neighbors within its cutoff distances, but has 13 Voronoi neighbors. This indicates that the 11 neighbors are packed such that there are "gaps" in the cluster; Voronoi cells cannot have gaps, so distant atoms will fill the gaps left by the 11 intimate neighbors and contribute as Voronoi neighbors. As the temperature is reduced and the liquid becomes increasingly impacted by its energy landscape the Cu-centered clusters become more regularly packed (for instance, regular icosahedra form) and the discrepancy between the two methods diminish. The Zr atoms exhibit a different trend – as a Zr atom gains more packing neighbors, its number of Voronoi neighbors increase accordingly. This indicates that it is easier to create a regularly packed structure about the larger Zr atom using the smaller Cu solvent atoms. It is not clear why the different $CN_{Voro}^{(\alpha)}$ possess such featureless trends as the temperature is adjusted, in contrast to the behavior of $CN_{dcut}^{(\alpha)}$. The fact that $CN_{Voro}^{(Avg)}$ is nearly constant across the entire temperature range suggests that these may be phenomena rooted in the fundamental tessellation process.

Ultimately, our analysis supports the findings of Gangopadhyay *et al.*[3] - that the anomalous thermal contraction of the first coordination shell in metallic liquids reflects the local loss of nearest neighbor atoms with increasing temperature. In the context of our earlier analysis, it

appears that SRO – the formation of relatively stable, increasingly coordinated local clusters of atoms (e.g. Cu-centered icosahedra) – begins to set in as the liquid is cooled to T_A. By utilizing weighted Voronoi tessellation methods, we also find that this ordering is associated with the development of more regularly-packed geometries for Cu-centered clusters

3.1.2 Structural Signatures of Fragility

Throughout Chapter 1 and 2, we discussed liquids whose viscosities ($\eta(T)$) exhibit super-Arrhenius growth as the liquids are supercooled towards T_G – this accelerated viscous slowing is deemed "fragile" behavior by the glass community. On the other hand, so-called "strong" liquids exhibit Arrhenius growth in $\eta(T)$ throughout the supercooled regime, indicating that a single relaxation mechanism persists across this temperature range to produce a robust exponential behavior. The canonical fragile and strong glasses are *o*-terphenyl and SiO_2, respectively[6], and many liquids are found to exhibit behaviors that lie between fragile and strong. The fragility of a liquid can thus be quantified by how steeply $\eta(T)$ approaches the calorimetric glass transition value of $10^{12} Pa \cdot s$. Hence the kinetic fragility index of a liquid is defined as[6]

$$m \equiv \left(\frac{d\,(\log \eta)}{d(T_G/T)}\right)_{T=T_G} \tag{3.5}$$

As discussed in Chapter 1, the VFT-form, $\eta(T) = \eta_o(T)\exp(A/(T - T_K))$, can provide an excellent fit for supercooled-liquid viscosity data. In its derivation, the fragility, as determined by A/T_k, is related to the excess entropy of the configuration of the liquid compared to the material's crystal structure. Mauro *et al.*[7] argued that this link between a liquid's fragility and its thermodynamic properties ought to have a structural signature. Specifically, it was posited that the fragility of a liquid should manifest through the rate of structural change that is exhibited

during supercooling – similar to the growth of $\eta(T)$ in a fragile liquid, the structure should be found to change rapidly near T_G. This was motivated by the observation that, when extrapolating high temperature empirical data of $S(q)$ down to T_G, fragile liquids exhibited a larger mismatch between the extrapolated curve with the actual data at T_G than did strong liquids. In the absence of intermediate data in the supercooled region, it was argued that changes in the features of $S(q)$ in fragile liquids must accelerate in this narrow temperature range in order to match the data at T_G. A structural fragility index, γ, was introduced to quantify the magnitude of the aforementioned mismatch from the extrapolated curve. **Figure 3.4** contains plots of the temperature-dependent data of the heights of the first and second peak of $S(q)$ for $Cu_{64}Zr_{36}$. γ is indicated in the left panel of the figure, illustrating the extrapolation process described above.

A survey of empirical data conducted by Mauro *et al.* revealed a clear correlation between γ and the kinetic signatures of fragility (namely, A/T_k) for a variety of liquids, indicating that a liquid's fragility is indeed reflected by the evolution of its structure. This is at odds with the widely-held, but vaguely-justified belief that the structural aspects of the glass transition are unimportant[8]. On the other hand, these empirical findings match closely with what we observe in $Cu_{64}Zr_{36}$ – the initial onset of the super-Arrhenius growth of $\eta(T)$ at T_A and its tremendous growth near T_G coincide with the early development and subsequent rapid proliferation of icosahedral ordering in the liquid. This study strongly suggests that similar structural ordering behavior should be expected to arise in other fragile liquids.

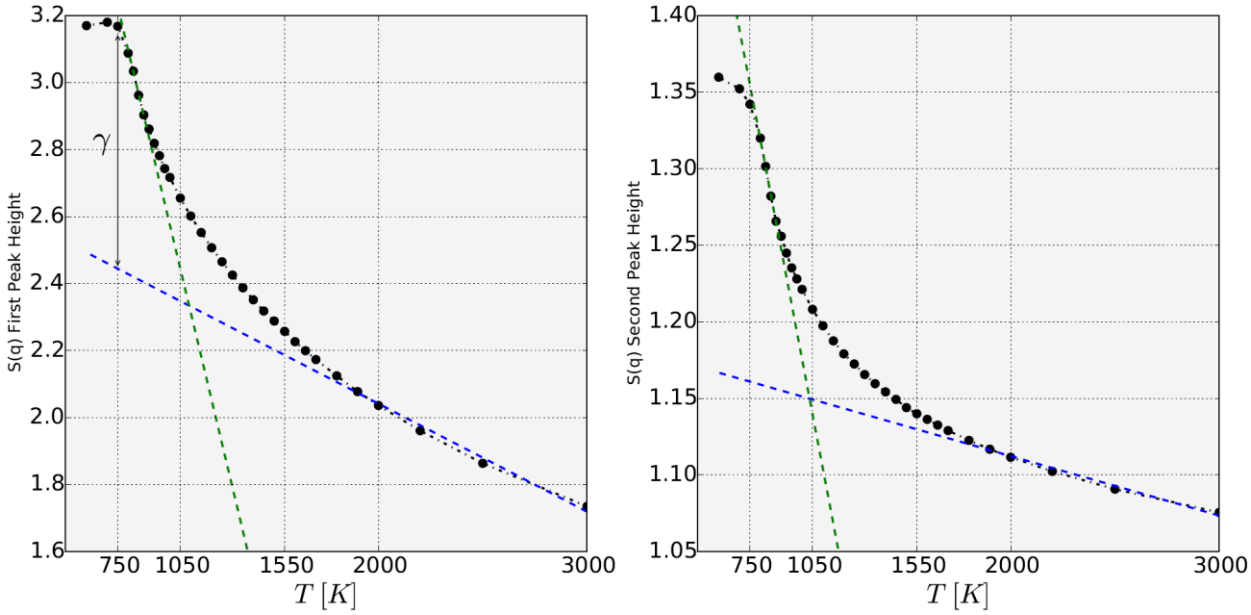

Figure 3.4 The temperature-dependent evolution of features of $S(q)$ for $Cu_{64}Zr_{36}$. (Left) The evolution of the first-peak height of $S(q)$. (Right) The evolution of the second-peak height of $S(q)$. Both features exhibit accelerated growth upon cooling through, approximately, T_A, leading to a "mismatch" between the low-T and high-T extrapolated behaviors (dashed lines). This mismatch is proposed to be a structural signature of the liquid's fragility, which is indicated in the left panel by γ.

The $S(q)$ peak height data displayed in **Figure 3.4** exhibits the accelerated change in the liquid structure that was predicted by the empirical study. Furthermore, we find that the high-T and low-T asymptotes* appear to consistently cross near T_D, the temperature below which connected domains of icosahedra are found to grow rapidly and eventually percolate the system. Though this only superficially connects the structural signature of fragility with the observed icosahedral ordering in the system, we have found in a preliminary survey of experimental data that $T_D \approx 1.4 \times T_G$ appears as a crossover temperature in the same way for several other fragile liquids.

* We remind the reader that, due to limitations of the timescale accessible by the simulation, the low-T data determining this asymptote is no longer formally representative of the ergodic supercooled liquid.

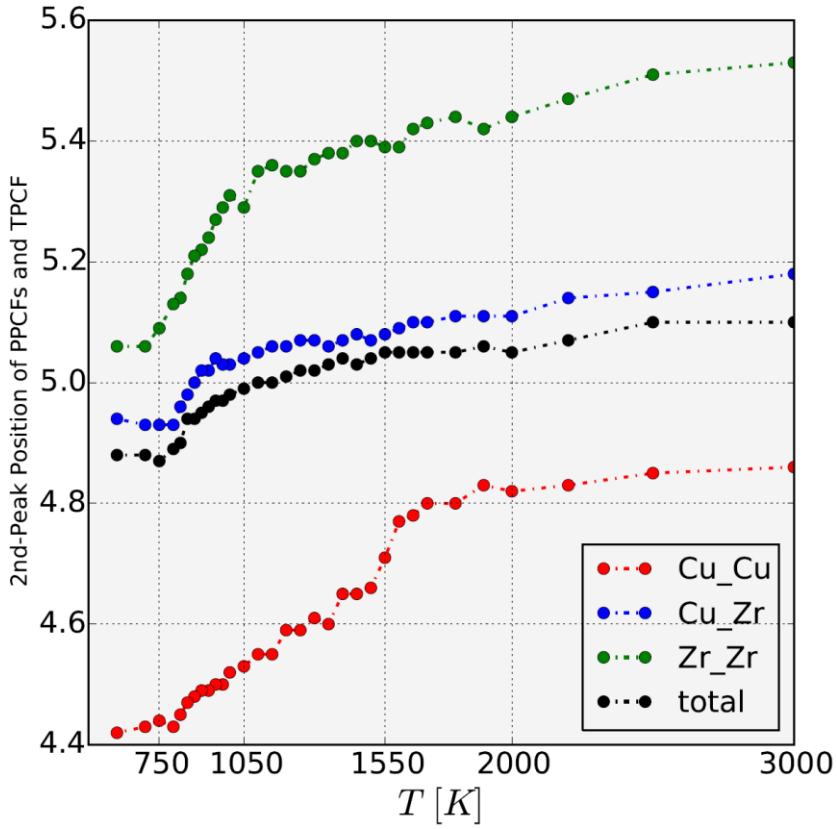

Figure 3.5 The temperature evolution of the 2nd-peak position of the PPCFs and TPCF of $Cu_{64}Zr_{36}$. Abrupt changes in the peak trajectories occur for $g_{CuCu}(r)$ at T_A and for $g_{ZrZr}(r)$ at T_D.

Taking advantage of our access to species-specific correlations, we now consider the temperature evolution of features of the PPCFs of $Cu_{64}Zr_{36}$. To focus on longer-ranged ordering than the previously considered locally-packed clusters, we track the positions of the second-peaks of the PPCFs with changing temperature, as shown in **Figure 3.5**. Quite remarkably, we find that the peak trajectories of $g_{CuCu}(r)$ and $g_{ZrZr}(r)$ change abruptly at T_A and T_D, respectively. Below these respective temperatures the second peaks are found to contract rapidly with decreasing temperature. More specifically, a broad second peak of the liquid contracts slowly under cooling

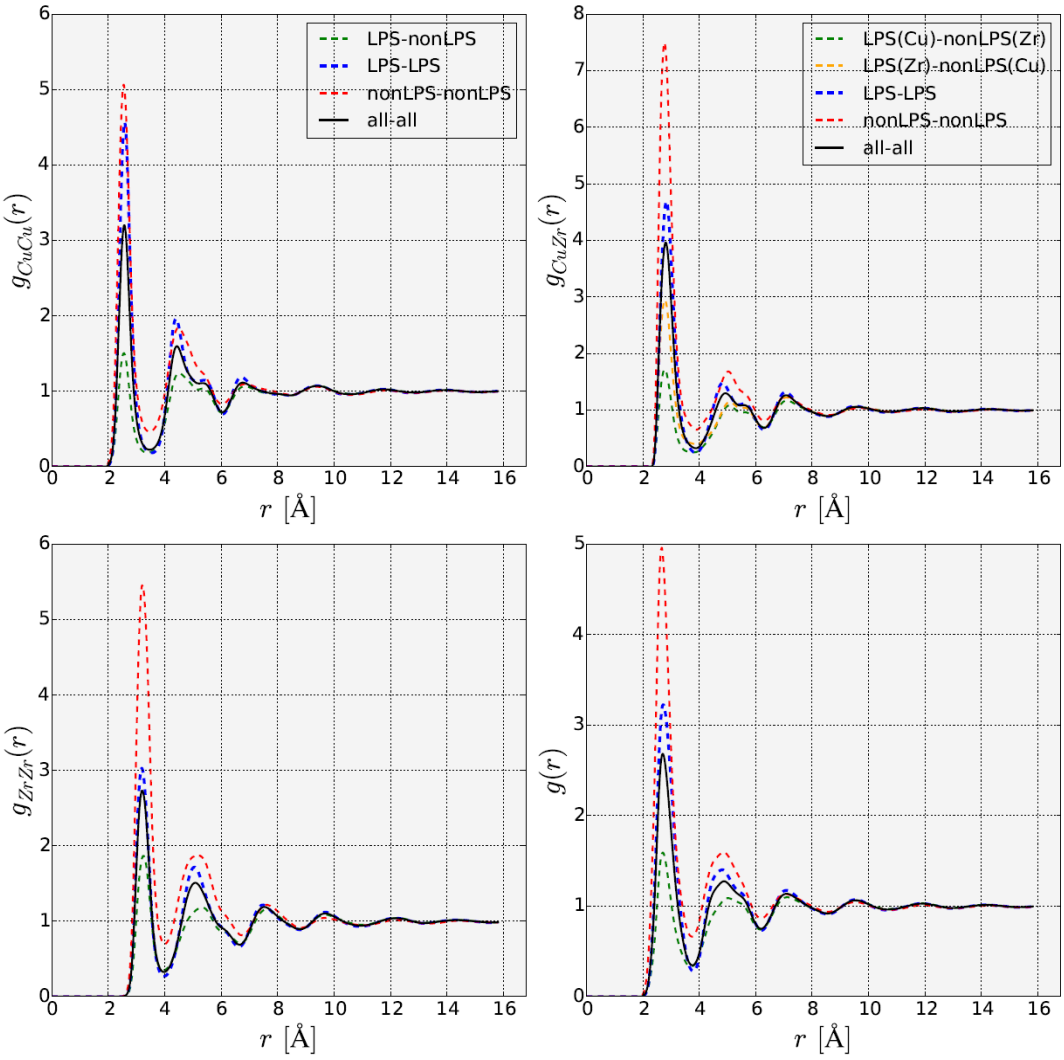

Figure 3.6 Decomposition of the PPCFs and TPCFs into contributions from LPS atoms (those that participate in Cu-centered regular icosahedra) and nonLPS atoms (those that do not). The data here is for $Cu_{64}Zr_{36}$ at 750 K.

until a sharper peak emerges from within the broad one at the characteristic temperature. As the system is cooled further, this MRO feature becomes more sharply defined and the associated structure becomes more densely packed. This interpretation is informed by our analysis of the PPCFs, which we have decomposed into contributions from atoms that participate in icosahedra and those that do not. This decom position is shown for the PPCFs of $Cu_{64}Zr_{36}$ at 750 K in **Figure 3.6**. Here we denote atoms participating in icosahedra as LPS (standing for locally-preferred structure) and those that do not as nonLPS. In the top-left panel, it can be seen that the

contribution of the correlations between pairs of LPS atoms is indeed responsible for the sharp second peak followed by the distinct shoulder in $g_{CuCu}(r)$. Similar features can be found in the second-peaks of the other PPCFs, though the contribution from LPS atoms is less dramatic.

The enhanced first and second peaks of the nonLPS-nonLPS PPCFs may appear to be counter intuitive at first glance – one would expect the LPS-LPS PPCF to dominate the system at T_G. This is indeed the case, however the normalization factor in Equation 3.1 depends on $1/N_{nonLPS}^2$, which increases with decreasing temperature, and thus magnifies $g^{nonLPS}(r)$. To correct for this, we renormalize $g^{LPS}(r) - 1$ and $g^{nonLPS}(r) - 1$ (the total pair correlation functions for LPS atoms and nonLPS atoms, respectively) so that the correlation counts are measured relative to the total number of atoms in the liquid, rather than the number of LPS (or nonLPS) atoms, which changes with temperature[*]. These functions are plotted for a wide range of temperatures in **Figure 3.7**. The left panel of the figure demonstrates the rapid development of extensive domains of connected icosahedra in the system. At high temperatures, icosahedra form almost exclusively as isolated clusters of atoms, yielding only SRO signatures in $g^{LPS}(r)$. Upon supercooling, MRO features begin to develop and by $800\ K$ correlations arise beyond 12 Å amongst the icosahedra[†]. As discussed in Chapter 2, this is very likely an underestimate of the degree and extent of icosahedral ordering that occurs under realistic laboratory conditions[9,10]. The trend exhibited by $g^{nonLPS}(r)$ with decreasing temperature is nearly reversed from the behavior of $g^{LPS}(r)$ – as the liquid is supercooled, fewer atoms participate in nonLPS configurations and the range of the ordering diminishes. Indeed, the extent of the MRO features of the correlation function eventually recede such that by $800\ K$ they extend only weakly to

[*] These TPCFs are then rigidly shifted up by 1 so that a random distribution again yields a correlation of 1.
[†] Fang *et al.* provide evidence that the MRO being formed by the icosahedra is specifically a Bergman-type supercluster[21].

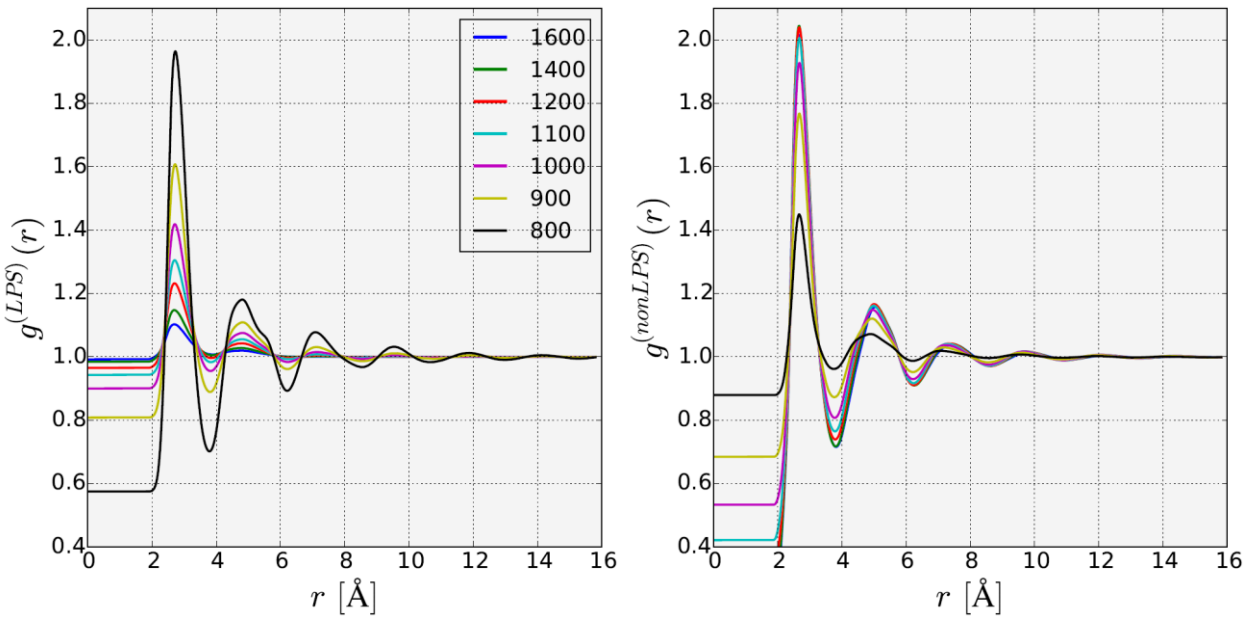

Figure 3.7 (Left) The total pair correlation function between atoms that participate in Cu-centered regular icosahedra. The TPCF is plotted for multiple temperatures, showing the development of icosahedral MRO in $Cu_{64}Zr_{36}$. (Right) The TPCF for atoms that do not contribute to the icosahedral ordering. By contrast, isolated liquid-like regions of nonLPS develop with decreasing temperature.

~8 Å. These findings support the interpretations that $Cu_{64}Zr_{36}$ glass consists of an extensive icosahedron network amidst interspersed liquid-like regions of non-icosahedron configurations of atoms[11,12].

In the following section we will show that the distinction between LPS and nonLPS (icoshedron-involved and not) atoms has a chemical aspect in addition to a structural one. That is, chemical ordering is involved in the formation of icosahedra and the connections formed amongst allows the icosahedron network to "tune" its local compositions.

3.2 Chemical Ordering & Icosahedron Populations

Structural models developed by Miracle *et al.*[13,14] and a comprehensive study of metallic glassed conducted by Sheng *et al.*[15] strongly suggest that the different types of short-ranged order (SRO) and medium-ranged order (MRO) exhibited by metallic glasses are determined largely by

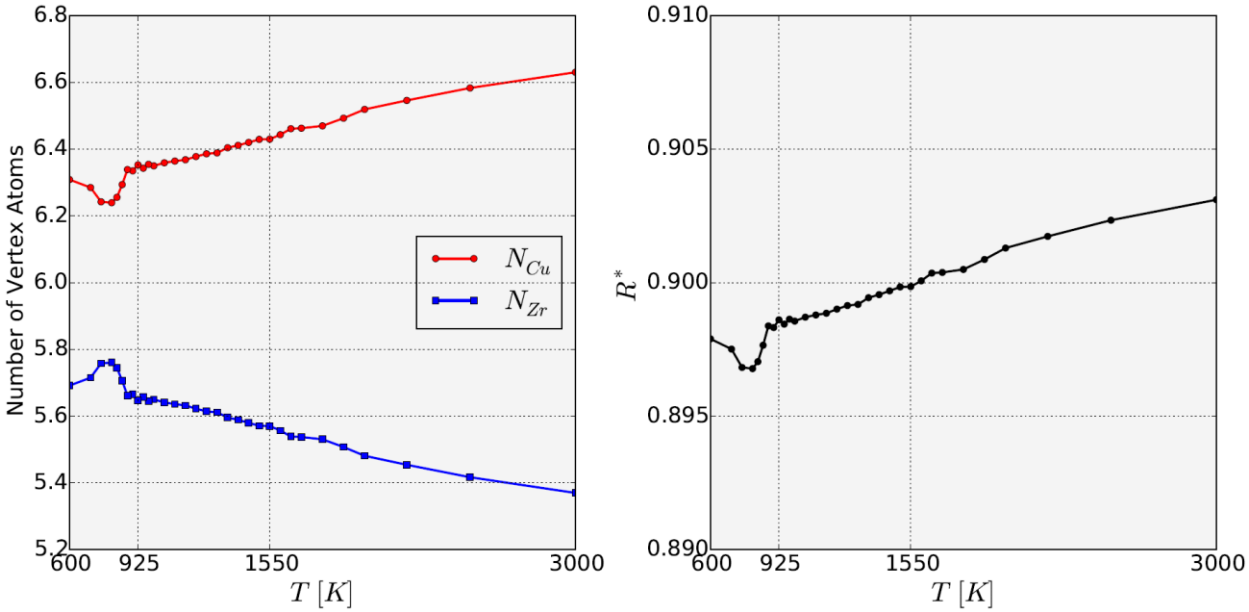

Figure 3.8 (Left) The number of Cu and Zr atoms, respectively, comprising the twelve-atom shell of an average icosahedron in $Cu_{64}Zr_{36}$. The shell composition is found to incorporate Zr atoms with increasing frequency at low temperatures. (Right) The critical ratio R^*, is found to reside near 0.902, which is the ideal value for regular icosahedral ordering.

efficient packing schemes*. The locally-preferred structure (LPS) of a glass, then, is determined largely by the relative radii and concentrations of its species. The so-called critical ratio, R^*, is defined to be the ratio of the radius of a solute atom to the radius of the "average" solvent particle surrounding it: $R^* \equiv \frac{R_{solute}}{R_{solvent}}$. This value is found to strongly dictate the type of local packing that is preferred in a glass. For $R^* \approx 0.902$, regular icosahedral type packing is preferred. According to these initial considerations it seems to be impossible for $Cu_{64}Zr_{36}$ to develop icosahedral ordering: the Zr solute atoms are larger than the Cu solvent atoms, thus $R^* > 1$. This alloy is found to deviate from the model, yet it still adheres to the ascribed critical ratio for icosahedral. Cu behaves as the central solute atom with a combination of Cu and Zr atoms serving as the twelve vertex atoms. In **Figure 3.8** we plot the average number of Cu and Zr atoms that are found in the shell of a regular icosahedron, with varying temperature. Zr

* It is important to note that the packing of hard spheres does not adequately capture all of the essential features of a glass' structure. The atoms in a glass have an appreciable "softness" due to the harmonic quality of their potentials[22]. In fact, it has been found that hard sphere systems grow crystal-like order near the glass transition, rather than icosahedral order[23].

become incorporated into the average icosahedron shell with increasing frequency as the liquid is cooled and icosahedral ordering becomes prolific – this chemical ordering will prove to be of significant importance. The right panel of the figure shows that corresponding values of R^*, as calculated by $R^* = \frac{12R_{Cu}}{N_{Cu}R_{Cu}+N_{Zr}R_{Zr}}$ where $R_{Cu} = 0.855$ Å and $R_{Zr} = 1.06$ Å*. We find that the average icosahedron composition indeed reflects the efficient packing scheme prescribed by $R^* \approx .902$. To achieve this packing ratio, an icosahedron takes on a composition ranging from $Cu_{58.7}Zr_{41.3}$ at $3000\ K$ to $Cu_{56.7}Zr_{43.3}$ at $900\ K$. How can the icosahedra achieve a composition that is Zr-rich in comparison to the global composition of the alloy, when over 60% of the material's atoms are found to participate in icosahedra? The answer is: by forming Zr-rich connections.

Before continuing, we note that a sharp feature appears below $900\ K$ in the curves in **Figure 3.8**; this sudden growth in the representation of Zr atoms in the icosahedron shell coincides with the rapid percolation of the icosahedron domain. However, this may be an artifact of the system being insufficiently relaxed at these low temperatures. It is not clear that this is the case, however, as the deflection is found to reverse directions below T_G, where the system is surely insufficiently relaxed.

* These are effectively "hard sphere" radii – they are half the minimum pair-distances recorded in $g_{CuCu}(r)$ and $g_{ZrZr}(r)$ at $2500\ K$.

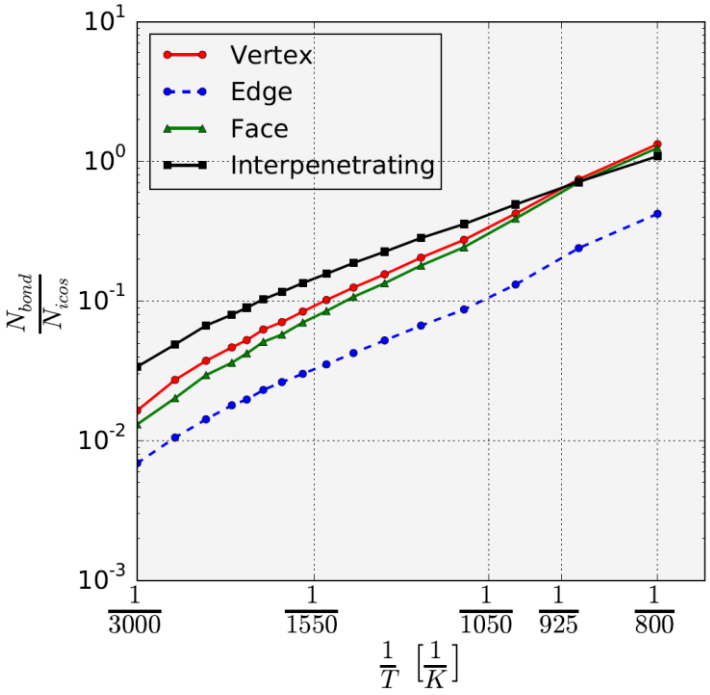

Figure 3.9 The number of vertex-sharing, edge, face, and interpenetrating connections present per icosahedron, plotted on a log scale versus inverse temperature.

Figure 3.9 shows on a log scale versus inverse temperature the growing number of vertex, edge, face-sharing, and interpenetrating connections that form per icosahedron with decreasing temperature. The frequency of each connection type grows exponentially as the liquid is cooled below T_A, and this exponential growth accelerates for the non-interpenetrating connections for temperatures below T_D. An analysis of the chemical compositions of these connections show that the non-interpenetrating connections are all significantly Zr-rich in comparison with the icosahedron shell composition[16]. Near T_G, over 75% of the vertex-shared atoms, 80% of the edge-shared atoms, and 50% of the face-shared atoms are Zr atoms, whereas the shell composition is ~43% Zr. The composition of the interpenetrating connections, which require two icosahedra to share 7 atoms – 5 shell atoms are shared, and the Cu center of one icosahedron serves as a shell atom of the other (and vice versa) – matches nearly perfectly the icosahedron-

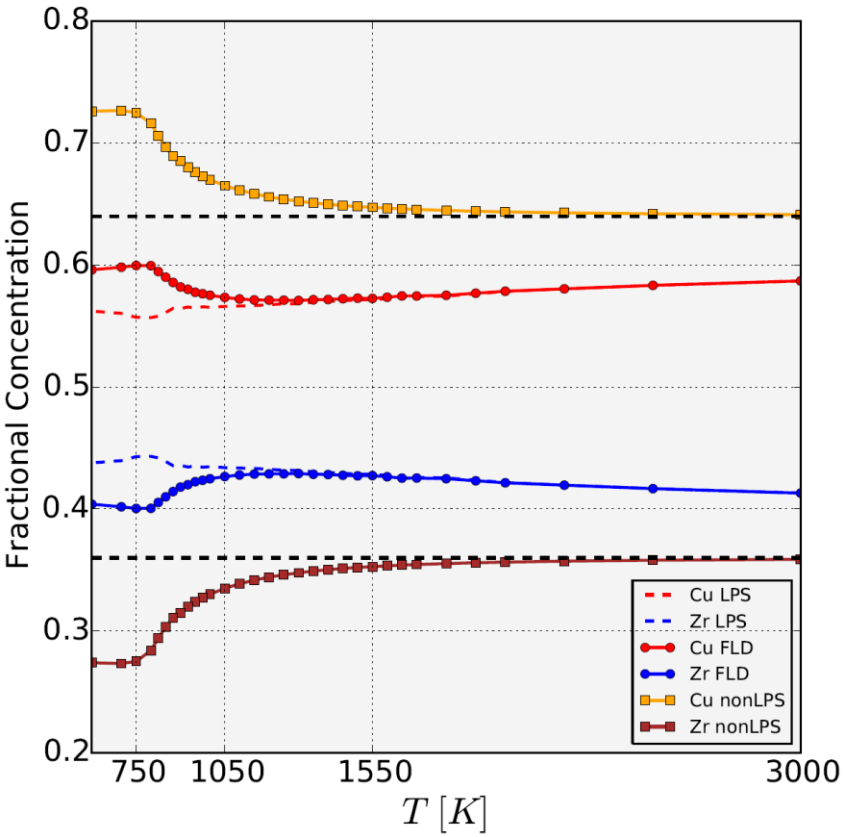

Figure 3.10 The concentration of: Cu atoms in an average icosahedron (red dashed-line), Cu atoms in the icosahedron domain (red circles), Cu atoms in non-icosahedron structures (yellow squares), Zr atoms in an average icosahedron (blue dashed-line), Zr atoms in the icosahedron domain (blue circles), Zr atoms in non-icosahedron structures (brown squares).

shell composition. An interpenetrating connection involves the coordination of too many atoms for the icosahedra to preferentially share Zr atoms over Cu atoms in the shell.

Though straight forward, this analysis of the chemical ordering that is mediated by the connections between icosahedra greatly informs our understanding of the utility of forming a highly-connected icosahedron network; furthermore, this is the first known account of this chemical ordering in Cu-Zr alloys. It is widely assumed by the current literature on Cu-Zr glasses and other icosahedron-forming systems that only the interpenetrating connections between icosahedra played an important role in the icosahedron network. While it is true that it is these connections that are chiefly responsible for making the network strong and elastic in the

glass[17,18], this bias is also partially a matter of mere convenience[*]. Here we see that non-interpenetrating connections play an essential role in facilitating icosahedral ordering – they mediate the sharing of Zr atoms amongst icosahedra such that the icosahedra can exist in a locally Zr-rich environment while the composition of the overall icosahedron domain is, necessarily, closer to the alloy composition. Stated differently, icosahedron domains are not only limited by geometric frustration, they are also limited by the alloy's composition. Non-interpenetrating connections between icosahedra allow the local composition of the system to be "tuned" to accommodate icosahedral ordering.

This chemical ordering begins to manifest on a macroscopic level as the liquid is supercooled. **Figure 3.10** shows the concentration of Cu and Zr atoms, respectively, in an average icosahedron (LPS), in the population of all icosahedra (FLD), and in the population of atoms not involved in icosahedra (nonLPS). Below T_A, the composition of nonLPS population begins to become Cu-rich relative to the native alloy composition in order to accommodate the growing population of icosahedra. Below T_D, the compositions of the LPS and FLD deviate from one another – as the FLD becomes extensive with system size, Zr-rich connections form so that the local composition of the LPS is preserved, but the composition of the FLD approaches that of the alloy. Indeed, by T_G the LPS composition is roughly $Cu_{57}Zr_{43}$, whereas the FLD composition is $Cu_{60}Zr_{40}$, and the nonLPS regions of the glass are dramatically Cu-rich with a composition of $Cu_{73}Zr_{27}$. We thus conclude that supercooling $Cu_{64}Zr_{36}$ leads to pronounced chemical ordering

[*] It is trivial to identify interpenetrating connections in the icosahedron network. Two icosahedra whose centers are Voronoi neighbors must be interpenetrating. Thus one can construct the interpenetrating network immediately from the results of the Voronoi analysis. Unfortunately, this convenience appears to bias much of the analysis towards this end. One of my first major projects as a graduate student was to write some Python code that would allow me to thoroughly analyze all connection types in the icosahedron network.

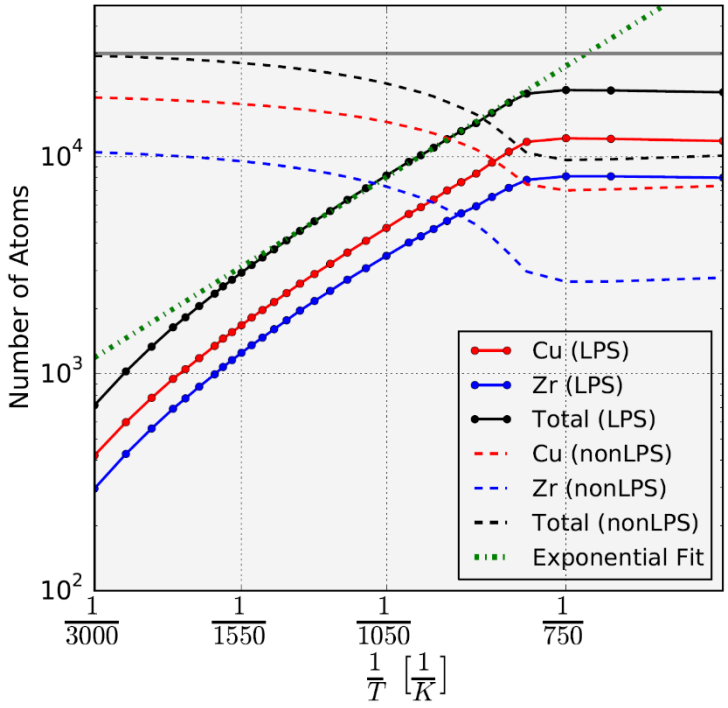

Figure 3.11 The number of atoms participating in icosahedra and non-icosahedra in a 3×10^4 atom simulation, on a log scale versus inverse temperature.

in the material such that *the glass consists of a Zr-rich backbone of connected icosahedra amidst Cu-rich liquidlike defect regions*.

Lastly, we discuss the temperature-dependent evolution of the Cu, Zr, and total populations of the LPS and nonLPS structures in a simulation containing 3×10^4 atoms (**Figure 3.11**). The rapid exponential growth of the number of atoms involved in the LPS is quite striking – extrapolating this growth to low temperatures, where our simulation falls out of equilibrium, suggests that every atom in the system would participate in an icosahedron by $720\ K$, were we able to continue to observe ergodic behavior here. This temperature resides significantly above the Kauzmann temperature ($T_k \approx 684\ K$), where the VFT-extrapolation of $\eta(T)$ predicts that the liquid viscosity diverges. We argue that both frustration and system-composition constraints are bound to limit the growth of icosahedral ordering such that the extrapolated behavior to $720\ K$

eventually breaks down. This barrier to icosahedral ordering may then cause $\eta(T)$ to fall beneath its VFT-extrapolated trajectory such that the divergence at T_k is never realized. Of course, this is merely a conjecture at this stage, and is one that cannot be investigated using our current methodologies. That being said, it is natural to compare the extrapolated behaviors of these quantities: the supposed divergence at T_k is intimately related to structural ordering in the system as the excess entropy of the liquid vanishes here. Yet, we find that the liquid structure becomes terminally-occupied by icosahedra above T_k. Perhaps our VFT fit of $\eta(T)$ did not include enough low-temperature data to provide a reliable extrapolation, and T_k indeed resides near $720\ K$. These considerations are highly speculative, but are worth being made.

3.3 Summary & Outlook

In this chapter, we analyzed static-signatures of the developing icosahedral ordering that ultimately dominates $Cu_{64}Zr_{36}$ glass and connected them with recent empirical studies of metallic liquids. Our simulation reproduces the anomalous thermal contraction of the first coordination shell and supports the structural interpretation that explains this phenomenon[3]. We then analyzed the temperature evolution of the liquid static structure factor and pair correlation functions, supporting empirical findings that liquid fragility can be quantifiably-linked to measurable structural features[7].

A discussion of packing efficiency revealed that an icosahedron requires a composition that is Zr-rich relative to the alloy composition. Ultimately we find that non-interpenetrating connections between icosahedra allow icosahedra to preferentially share Zr atoms amongst one another and thus "tune" their local composition. This leads to dramatic chemical ordering in the

supercooled liquid, resulting in a highly-connected, Zr-rich rigid icosahedron network amidst Cu-rich liquid like defects in the glass.

In retrospect, it is surprising that the chemical ordering that occurs in conjunction with the formation of the icosahedron network has been largely overlooked by most numerical studies of Cu-Zr. Indeed, the compositional requirements for forming specific local structures is well known[14,15]. Yet, our analysis appears to be unique - at least in the context of Cu-Zr alloys. The combined simplicity and magnitude of these findings makes this stand out, in my opinion, as one of the most resounding results presented in this dissertation. We must ultimately look for techniques that would allow empirical studies to detect this chemical ordering[*]. As a last remark, it is interesting to consider that $Cu_{64}Zr_{36}$ is a better glass former than is $Cu_{57}Zr_{43}$ even though the latter composition is nearly ideal for the formation of an individual icosahedron. This is likely due to the fact that having a more Cu-rich composition requires that icosahedra share Zr atoms, resulting in a more highly-connected and thus densely packed icosahedron network, which affects the macroscopic structure and overall dynamics of the material in a way that is amenable to glass formation.

3.4 Chapter 3 References

1. Egami, T. & Billinge, S. *Underneath the Bragg peaks: Structural analysis of complex materials*. (Elseview, 2003).

2. Cheng, Y. Q. & Ma, E. Atomic-level structure and structure-property relationship in metallic glasses. *Prog. Mater. Sci.* **56,** 379–473 (2011).

[*] I was very excited when I first heard an anecdotal account from a colleague who noticed that samples of Cu-Zr glasses, when left in storage for long times, eventually develop a distinct Cu-coloring on its surface. I interpreted this as the gradual migration of the Cu-rich liquid like defects to the surface of the sample. Obviously, this is very biased thinking on my end.

3. Gangopadhyay, a. K. *et al.* Anomalous thermal contraction of the first coordination shell in metallic alloy liquids. *J. Chem. Phys.* **140,** (2014).

4. Okabe, A., Boots, B., Sugihara, K., SN, C. & Kendall, D. G. *Spatial Tessellations - Concepts and Applications od Voronoi Diagrams*. *Geographical Information Systems* (Wiley, 2000). doi:10.1002/9780470317013

5. Park, J. & Shibutani, Y. Common errors of applying the Voronoi tessellation technique to metallic glasses. *Intermetallics* **23,** 91–95 (2012).

6. Angell, C. a. Formation of glasses from liquids and biopolymers. *Science* **267,** 1924–1935 (1995).

7. Mauro, N. a., Blodgett, M., Johnson, M. L., Vogt, a. J. & Kelton, K. F. A structural signature of liquid fragility. *Nat. Commun.* **5,** 1–7 (2014).

8. Cavagna, A. Supercooled liquids for pedestrians. *Phys. Rep.* **476,** 51–124 (2009).

9. Zhang, Y. *et al.* Cooling rates dependence of medium-range order development in Cu64.5Zr35.5 metallic glass. *Phys. Rev. B* **91,** 1–8 (2015).

10. Zhang, F. *et al.* Effects of sub-Tg annealing on Cu64.5Zr35.5 glasses: A molecular dynamics study. *Appl. Phys. Lett.* **104,** 061905 (2014).

11. Zhang, Y. *et al.* Impact of deformation on the atomic structures and dynamics of a Cu-Zr metallic glass: A molecular dynamics study. *Phys. Rev. B* **90,** 1–9 (2014).

12. Ding, J., Patinet, S., Falk, M. L., Cheng, Y. & Ma, E. Soft spots and their structural signature in a metallic glass. *Proc. Natl. Acad. Sci.* **111,** 14052–14056 (2014).

13. Miracle, D. B., Sanders, W. S. & Senkov, O. N. The influence of efficient atomic packing on the constitution of metallic glasses. *Philos. Mag.* **83,** 2409–2428 (2003).

14. Miracle, D. B. A structural model for metallic glasses. *Nat. Mater.* **3,** 697–702 (2004).

15. Sheng, H. W., Luo, W. K., Alamgir, F. M., Bai, J. M. & Ma, E. Atomic packing and short-to-medium-range order in metallic glasses. *Nature* **439,** 419–425 (2006).

16. Soklaski, R., Nussinov, Z., Markow, Z., Kelton, K. F. & Yang, L. Connectivity of icosahedral network and a dramatically growing static length scale in Cu-Zr binary metallic glasses. *Phys. Rev. B - Condens. Matter Mater. Phys.* **87,** (2013).

17. Lee, M., Lee, C. M., Lee, K. R., Ma, E. & Lee, J. C. Networked interpenetrating connections of icosahedra: Effects on shear transformations in metallic glass. *Acta Mater.* **59,** 159–170 (2011).

18. Ding, J., Cheng, Y. Q. & Ma, E. Full icosahedra dominate local order in Cu64Zr34 metallic glass and supercooled liquid. *Acta Mater.* **69,** 343–354 (2014).

19. Steinhardt, P. J., Nelson, D. R. & Ronchetti, M. Icosahedral bond orientational order in supercooled liquids. *Phys. Rev. Lett.* **47,** (1981).

20. Blodgett, M. E. & Kelton, K. F. Estimated partial pair correlation functions in Cu–Zr liquids. *J. Non. Cryst. Solids* **412,** 66–71 (2015).

21. Fang, X. W. *et al.* Spatially Resolved Distribution Function and the Medium-Range Order in Metallic Liquid and Glass. *Sci. Rep.* **1,** 19–21 (2011).

22. Inoue, A. *et al. Bulk Metallic Glasses*. (Springer, 2008).

23. Leocmach, M. & Tanaka, H. Roles of icosahedral and crystal-like order in the hard spheres glass transition. *Nat. Commun.* **3,** 974 (2012).

Chapter 4: Methods

4.1 LAMMPS Simulation

The numerical simulations conducted in the context of this dissertation are classical molecular dynamics (MD) simulations that utilizes the LAMMPS (Large-scale Atomic/Molecular Parallel Simulator) software distributed by Sandia National Laboratories[1]. The results that we present come from two sets of simulations of $Cu_{64}Zr_{36}$: 1) a set of 10^4-atom simulations[2], 2) a set of 3×10^4-atom simulations[3]. Both simulations utilize a semi-empirical potential developed by Mendelev *et al.*[4], which describes many-body interactions using the Finnis and Sinclair (FS)[5] generalization of the embedded atom method (EAM)[6,7]. The potential was developed with an emphasis on reproducing both the liquid and glass properties of Cu-Zr alloys. It was shown to provide a very good description of the structures and some properties of $Cu_{64.5}Zr_{35.5}$. The native units used by these simulations are the "*metal*" units (see LAMMPS manual).

The 10^4-atom simulations evolved the atoms in the liquid according to a canonical (NVT) ensemble, where the volume is set so that the average pressure is zero. A heat bath degree of freedom is introduced into the equations of motion to control the temperature of the system via Nose-Hoover thermostat algorithm[8]. The equations of motions are updated using a step size of $5\ fs^*$, and a quench rate of $10^{12}\ K/s$ was used. Additional details can be found in our Physical Review B publication[2]. The simulation results were used to report the chemical composition of the icosahedron connections, as discussed in **3.2**.

[*] A very important practical note: upon restarting a LAMMPS simulation, one must explicitly set the simulation timestep size once again otherwise the default step size will be used. This is not clearly stated in the LAMMPS manual and is an easy mistake to make that would have catastrophic consequences.

The 3×10^4-atom simulations utilized non-Hamiltonian equations of motion describing positions and velocities that sample an isothermal-isobaric (constant N, $\langle P \rangle$, and $\langle T \rangle$) ensemble[9] with $\langle P \rangle = 0\ bars$. The LAMMPS thermostat parameter T_{damp} was set to $0.5\ ps$ and the barostat parameter P_{damp} was set to $5.0\ bars$. The equations of motion were integrated using the verlet run style. Cubic periodic boundaries are utilized. Each simulation was initialized with a random atomic configuration that evolves at $T = 3300\ K$ for $0.5\ ns$ to achieve equilibrium. The liquid was then quenched at a rate of $10^{11}\ \frac{K}{s}$ down to its target temperature and subsequently relaxed for $20\ ns$ before collecting structural and dynamical data. The integration time step during the quenching and relaxation period was $5\ fs$. The integration step was then decreased to $2\ fs$ and data was collected in snapshots at each time step. For a given target temperature, atomic-level data, such as the positions and velocities, were recorded for $0.2\ ns$ and Voronoi analysis was performed for each time step (see **4.3**); the system's Cauchy stress tensor was recorded for $8\ ns$. To help ensure that the observed structural signatures represent the average, uncorrelated behavior of the system, additional independent simulations were conducted for each target temperature below $T = 1000\ K$ as well as for $1050\ K$, as $2200\ K$, and $2500\ K$. To check for system size effects, independent simulations of $N = 10{,}000$ were also conducted for each temperature.

All aspects of the LAMMPS simulations, data collection, and analysis were conducted by Ryan Soklaski using the TACC computing clusters Lonestar and Stampede. The 3×10^4-atom simulations were performed using Stampede's GPU nodes.

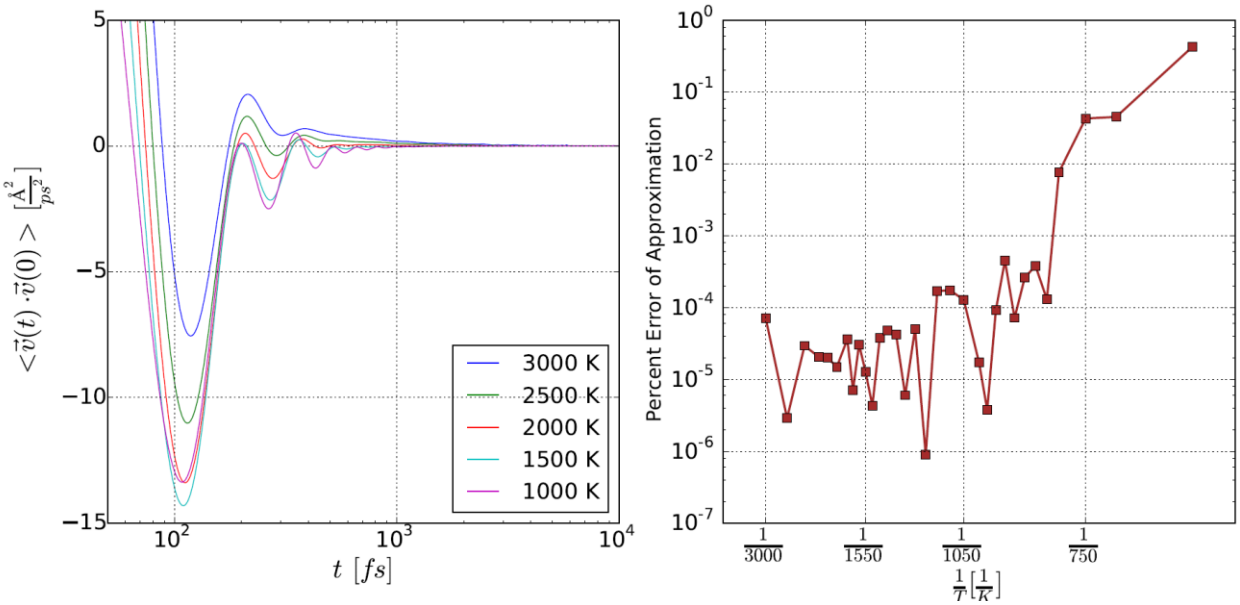

Figure 4.1 (Left) Velocity autocorrelation functions for multiple temperatures plotted versus log time. (Right) The percent error of approximation associated with using the trapezoidal sum method in lieu of an integral.

4.2 Calculating Particle Diffusivities

The self-diffusion coefficients are calculated using the Green-Kubo formula for the velocity autocorrelation function:

$$D \equiv \lim_{t\to\infty} \frac{1}{N}\sum_{i=1}^{N} \frac{\langle|\vec{r}_i(t)-\vec{r}_i(0)|^2\rangle}{6t} = \lim_{t\to\infty} \frac{1}{3N}\sum_{i=1}^{N}\int_0^t \langle\vec{v}_i(t)\cdot\vec{v}_i(0)\rangle dt \tag{4.1}$$

where the right equality holds rigorously only in the limit of infinite time and when time-translation invariance holds, e.g. $\langle\vec{v}_i(t'')\cdot\vec{v}_i(t')\rangle = Z(t''-t')$. In practice, both of these conditions are met satisfactorily – we find good agreement between our calculated values of D, and those that are calculated independently using the mean squared-displacement long-time asymptotes[4]. The angle brackets formally represent an ensemble average. Here, we replace this with an average over the initial conditions corresponding to 9×10^4 consecutive time steps. The time integral is computed using the trapezoidal discrete sum approximation, summing over 10^4 timesteps. As seen in the right panel of **Figure 4.1**, the error of approximation associated with

using the trapezoidal sum is less than 0.001% for temperatures above $800\ K$, and never exceeds 1%. Note in the left panel of **Figure 4.1** that the high temperature velocity autocorrelation functions exhibit non-exponential, slowly decaying long-time tails that are common in fluids and are associated with the development of vortices[10]. One must be careful to check that the integral has converged sufficiently when these long tails are present. The value of the particle mean-squared displacement is calculated using the equation:

$$\langle|\vec{r}_i(t) - \vec{r}_i(0)|^2\rangle = 2\int_0^t (t-s)\langle\vec{v}_i(t)\cdot\vec{v}_i(0)\rangle ds \tag{4.2}$$

which, again, requires time-translation invariance to hold rigorously. We utilize the same ensemble average and time integral approximations here as described above.

The merit of utilizing velocity autocorrelations in lieu of recording the atom mean squared-displacement trajectories is that, for the latter measurement, one must track every instance that an atom passes through a periodic boundary and correct the trajectory to account for this "warp". While this is not difficult, it is an extra step of analysis that can be avoided if one records the atom velocities.

The velocity correlations were computed using a Python program, effic_diff_N30K.py, written by Vy Tran and Ryan Soklaski. The diffusion coefficients and mean squared-displacement trajectories were calculated and analyzed in an iPython notebook, New_Diffusion.ipynb, written and maintained by Ryan Soklaski. All relevant derivations, background research, and other related work was performed by Ryan Soklaski.

4.3 Calculating Viscosity

The liquid viscosity was calculated using the Green-Kubo formula:

$$\eta = \frac{V}{k_B T} \int_o^\infty \langle \sigma_{ij}(t) \sigma_{ij}(0) \rangle dt \tag{4.3}$$

where V is the system volume, T is the temperature, k_B is the Boltzmann constant, and $\sigma_{ij}(t)$ is an off-diagonal element of the time-dependent Cauchy stress tensor. The stress tensor can be calculated from summing atomic-quantities:

$$\sigma_{ij} = \frac{1}{V} \sum_\alpha \left(m^\alpha \vec{v}_i^\alpha \vec{v}_j^\alpha + \sum_{\beta > \alpha} \vec{F}_i^{\alpha\beta} \left(\vec{r}^\alpha - \vec{r}^\beta \right)_j \right) \tag{4.4}$$

where m, $\vec{v}$, and $\vec{r}$ are the mass, velocity, and position of a particle. α and β are summation indices that run over each atom. i, j are cartesian component indices. $\vec{F}^{\alpha\beta}$ is the force exerted on particle α due to particle β, with periodic boundaries used. This tensor excludes the many body force term that is included in the FS-EAM style potential. σ_{ij} is formally symmetric when using the EAM-FS potential. This tensor is recorded from LAMMPS during simulations. The angular brackets in equation 4.3 are replaced with an average over initial conditions taken over 10^6 consecutive timesteps. Simpson's rule was used to approximate the integral. The error associated with this approximation was negligible.

It is difficult to obtain converged values of η – integrating the autocorrelation function of the macroscopic quantity σ_{ij} produces significantly more noise than does, for example, the microscopic velocity autocorrelation function, which can be averaged over all of the atoms. This is why it is necessary to average over so many initial conditions and to use a relatively large

system size (3×10^4 atoms). Additionally, we utilize a trick derived by Daivis and Evans[11] (see the appendix of the cited work) that allows the stress tensor to be re-summed to utilize all of its elements (rather than excluding its diagonal elements), and thus improve the statistics of the Green-Kubo integral. The revised form of the Green-Kubo relation is:

$$\eta = \frac{V}{10k_BT}\int_o^\infty \sum_{i,j}\langle P_{ij}(t)P_{ij}(0)\rangle\, dt \tag{4.5}$$

where $ij = xx, yy, zz, xy, yx, xz, zx, yz, zy$ (all entries of the 9-element tensor) and

$$P_{ij} = \frac{\sigma_{ij} + \sigma_{ji}}{2} - \frac{\delta_{i,j}}{3}\sum_k \sigma_{kk} \tag{4.6}$$

These relationships hold only in isotropic fluids and cannot be used near T_G. We confirmed that equations 4.3 and 4.4 yield the same value of η, and found that the latter provides a better-converged result. The Maxwell relaxation time is computed directly from η:

$$\tau_M = \frac{k_BT}{V}\frac{\eta}{\langle\sigma_{ij}(0)^2\rangle} \tag{4.7}$$

The stress tensor autocorrelation integrals were performed by Vy Tran and Ryan Soklaski in a Mathematica notebook maintained by Vy Tran. Further analysis, including matters regarding the Stokes-Einstein relationship, analytical fits, and data plots were conducted in the iPython notebooks, New_Diffusion.ipynb and Plotting_Data.ipynb, that were written and maintained by Ryan Soklaski.

4.4 Voronoi Analysis

Voronoi analysis was performed utilizing the Voro++ software library written by Chris Rycroft. The high performance of this software was essential for the large volume of data that was processed. The Voronoi analysis was performed using weighted bisectors (with radii **BLAH**) and with periodic boundaries. The Voro++ code was modified by Ryan Soklaski so that the command-line utility can read from std-in and write to std-out.

Voro++ does not natively support small face removal. Vy Tran wrote a program to remove small faces from Voronoi cells. A small face was removed from a Voronoi cell if that face comprised less than 0.5% of the cell's surface area. This cutoff area was determined by finding the cutoff fraction which "stabilized" the average coordination number of the system: $\frac{d(CN)}{d(cut)} = 0$ & $\frac{d^2(CN)}{d(cut)^2} > 0$. A problem with removing faces using this method is that neighbor pairs are no longer guaranteed to by symmetric. That is, a face joining atom A and atom B may be a small face for A, but not for B. In this instance, the face is removed from A and not from B and thus A will be a neighbor of B but B will not be a neighbor of A. It was determined that this issue had no effect on our analysis, but it could easily manifest in other types of analysis. To avoid this issue, one can specify an absolute cutoff area rather than a relative fraction.

The Voronoi analysis and small face removal was performed using the TACC facilities via a Python program, lammps_rewrite_serial.py, written by Vy Tran[*]. All relevant data collection and analysis was performed by Ryan Soklaski.

[*] Voro++ is called as a subprocess by Python in this program.

4.5 Pair Correlation & Static Structure Analysis

Pair correlations were calculated for all recorded position timesteps. A binning algorithm was written so that pairs separated beyond d_{cut} ($\approx$ 16 Å) were not considered. This is essential for improving performance efficiency as it reduces the complexity from the naïve N^2 scaling. Periodic boundaries are accounted for using the minimum image method:

$$d_i^{\alpha\beta} = \min\left\{\left|r_i^{\alpha} - r_i^{\beta}\right|, \left|r_i^{\alpha} - r_i^{\beta}\right| - L_i\right\} \tag{4.8}$$

where α and β index atom IDs, $i \in \{x, y, z\}$, "min" takes the minimum value of its arguments, L_i is the simulation box length, and $d_i^{\alpha\beta}$ is the distance between atoms α and β along direction i. This restricts d_{cut} such that $d_{cut} < \frac{1}{2} \times \min\{L_x, L_y, L_z\}$.

Pair correlations were measured between pairs of atoms that were distinguished by species type (e.g. Cu vs Zr), and structure type (e.g. participates in an icosahedron vs does not).

The binning algorithm was developed by Vy Tran and Ryan Soklaski. A Python program (bin_ppc.py, written by Ryan Soklaski) was used to measure the partial pair correlation functions for all of the relevant distinctions of atoms, using the TACC facilities. The subsequent calculation of the total pair correlation functions, partial and total static structure factors, and all of the relevant analysis was conducted in an iPython notebook ppc_plot.ipynb that was written and maintained by Ryan Soklaski.

4.6 Icosahedron Network Analysis & Cluster Lifetimes

The average local cluster time, τ_{LC}, was measured by recording the time required for an atom to lose or gain a Voronoi neighbor. The average lifetime is then given by the weighted-average:

$$\tau_{LC} = \frac{\sum_i t_i^2}{\sum_i t_i} \tag{4.9}$$

where i runs over all lifetimes recorded for all atoms during a simulation. The icosahedron lifetimes, τ_{icos}, are calculated using the same methods, but here we detect all instances where an atom's Voronoi signature becomes or departs from $\langle 0,0,12,0,\dots,0\rangle$*. Thus t_i is the lifetime of a single regular icosahedron (with a Cu center).

Two icosahedra are connected if they share one or more atoms. The icosahedron network is then described by utilizing the basic properties of a graph. The icosahedra at a given timestep constitute the nodes of the graph, and connections between icosahedra are mapped to edges between the corresponding nodes. A frustrated-limited domain (FLD) is formally classified in this analysis as connected subgraph. The distribution of connection types, FLD sizes, icosahedron composition, FLD composition, number of atoms involved in the icosahedron network, and icosahedron IDs are recorded for every timestep for which the atomic position data was stored.

The above measurements were made using a Python program, voro.py, that was written by Ryan Soklaski. This program also measured the lifetime of local connectivity (or "Egami time") (see Supplemental Materials of our preprint[3]). This analysis was performed using the TACC facilities.

All analyses of the icosahedron population and composition data was performed in an iPython notebook, Icos_Network.ipynb, that was written and maintained by Ryan Soklaski. All analyses of the local cluster times, icosahedron lifetimes, and FLD properties (sizes, fluctuations, etc.)

* The signature of a Voronoi cell is $\langle n_3, n_4, \dots, n_j, .. \rangle$, where n_j denotes the number of faces possessing j edges.

were performed in an iPython notebook, Plotting_Data.ipynb, that was written and maintained by Ryan Soklaski.

4.7 Chapter 4 References

1. LAMMPS Software Package. at <http://lammps.sandia.gov/>

2. Soklaski, R., Nussinov, Z., Markow, Z., Kelton, K. F. & Yang, L. Connectivity of icosahedral network and a dramatically growing static length scale in Cu-Zr binary metallic glasses. *Phys. Rev. B - Condens. Matter Mater. Phys.* **87,** (2013).

3. Soklaski, R., Tran, V., Nussinov, Z., Kelton, K. F. & Yang, L. A Locally-Preferred Structure Characterizes All Dynamical Regimes of a Supercooled Liquid. *Arxiv Prepr. arXiv1502.01739*

4. Mendelev, M. I. *et al.* Development of suitable interatomic potentials for simulation of liquid and amorphous Cu–Zr alloys. *Philos. Mag.* **89,** 967–987 (2009).

5. FINNEY, J. RANDOM PACKINGS AND STRUCTURE OF SIMPLE LIQUIDS .1. GEOMETRY OF RANDOM CLOSE PACKING. (1970). doi:10.1098/rspa.1970.0189

6. Daw, M. S. & Baskes, M. I. Semiempirical, quantum mechanical calculation of hydrogen embrittlement in metals. *Phys. Rev. Lett.* **50,** 1285–1288 (1983).

7. Daw, M. S. & Baskes, M. I. Embedded-atom method: Derivation and application to impurities, surfaces, and other defects in metals. *Phys. Rev. B* **29,** 6443–6453 (1984).

8. Hünenberger, P. H. Thermostat algorithms for molecular dynamics simulations. *Adv. Polym. Sci.* **173,** 105–147 (2005).

9. Shinoda, W., Shiga, M. & Mikami, M. Rapid estimation of elastic constants by molecular dynamics simulation under constant stress. *Phys. Rev. B - Condens. Matter Mater. Phys.* **69,** 16–18 (2004).

10. Schaink, H. M. & Hoheisel, C. Molecular-dynamics study of the velocity-autocorrelation function and the self-diffusion coefficient in multicomponent mixtures. *Phys. Rev. A* **45,** 8559–8565 (1992).

11. Daivis, P. J. & Evans, D. J. Comparison of constant pressure and constant volume nonequilibrium simulations of sheared model decane. *J. Chem. Phys.* **100,** 541 (1994).